An Analysis of Two Years of Nimbus 6 Earth Radiation Budget Observations: July 1975 to June 1977

by
G.G. Campbell and T.H. Vonder Haar

Department of Atmospheric Science
Colorado State University
Fort Collins, Colorado

Department of Atmospheric Science

Paper No. 320

AN ANALYSIS OF TWO YEARS OF NIMBUS 6 EARTH RADIATION BUDGET OBSERVATIONS: JULY 1975 TO JUNE 1977

by

G. G. Campbell and T. H. Vonder Haar

Department of Atmospheric Science
Colorado State University
Fort Collins, Colorado 80523

May 1980

Atmospheric Science Paper No. 320

ABSTRACT

An independent analysis of Nimbus 6 Earth Radiation Budget measurements is presented for July 1975 to June 1977. Monthly mean maps of albedo, emitted exitance and net radiation were constructed from the individual satellite irradiance measurements from the wide field of view sensors. A recalibration was performed with reference to Nimbus 7 ERB, day-night comparisons, and removal of the trend in reflected data. Also, a resolution enhance scheme was used to improve the details in the maps, both on the emitted exitance and albedo estimates. The maps are then discussed in terms of zonal averages, land averages, ocean averages and variance emphasizing the year to year differences. For instance, substantial changes in emitted and albedo appear around the intertropical convergence zone for these two years. The largest variance in net radiation occurred along the north coast of the Pacific.

INTRODUCTION

Variation over the earth of the net radiation is the fundamental driving force of the atmosphere. It is a manifestation of the latitude variation of incident flux from the sun with more incident in the equatorial regions than the polar. The other fundamental fact is that the atmosphere-ocean-earth system is not in local radiative equilibrium either in space or time. The system's circulation is such that large transports of energy occur giving the weather we see around us. Near balance between the thermal emission and the absorbed energy occurs only on an annual and global average, resulting in the strong similarity between one year's weather and the next.

Early estimates were made of the radiation terms (London, 1954) but only in the era of artificial satellites have moderately accurate measurements been made by various systems (Table 1). Vonder Haar and Ellis (1974) have summarized the measurements of the 1960's in Atlas of Radiation Budget Measurements from Satellites. The companion report, Climatology of Radiation Budget Measurements by Satellites by Campbell and Vonder Haar (1980) and Stephens et al. (1980) discuss this in some detail. Figure 1 shows the climatology of the annual cycle of the zonal average emitted and net fluxes and the albedo.

A small seasonal variation appears in the albedo caused partly by the sun-earth geometry and by changes in cloudiness, Ellis (1978). The emitted exitance matches the temperature changes except near the equator where clouds produce the dip. Finally the net radiation leads the temperature cycle, an indication of the heat capacity of the atmosphere-ocean system.

The major difficulties with the measurements in this climatology result from the many changes of instruments and non-continuity of the time series. Few overlaps in time are available to check the sensor calibrations and standardize the measurements. The variation in the resolution has smoothed out some features. Also the local time of measurement changed improving the representativeness of the mean but making comparisons difficult.

A new radiation budget experiment began in July 1975 with the Nimbus 6 Earth Radiation Budget experiment (Smith et al., 1977). Here we present an analysis of two years of these measurements (7/75-6/77). This is the first continuous record over more than one year from one instrument. Measurements have been recorded up to October 1978 from Nimbus 6 followed by a similar experiment on Nimbus 7 continuing to the present. These two experiments and their successors, Earth Radiation Budget Experiment, promise long term observations which will monitor the mean weather and perhaps detect systematic climate changes.

Our primary purpose here is to discuss the analysis scheme used in the production of the Nimbus 6 radiation budget estimates. The flow chart summarizes the steps discussed below. Only a few interpretations will be presented. We are presently involved with comparing these maps with mean weather for the concurrent times (Campbell, 1980).

ERB INSTRUMENT

The Earth Radiation Budget experiment of Nimbus 6 (and Nimbus 7) contains three principle components: 1) a multi-spectral solar observing instrument to monitor the sun, 2) a multi-axis scanning device to measure the angular reflection and emission characteristics of the earth radiance fields and obtain a medium resolution (500 km) budget and 3) wide field of

Table 1. Chronological list of earth orbiting satellites from which present radiation measurements were taken. The approximate local time at which each satellite crossed the equator during daylight hours appears in parenthesis. EX - experimental, N2 - Nimbus 2, N3 - Nimbus 3, N6 - Nimbus 6, E3 - Essa 3 and E7 - Essa 7.

Month	1964	1965	1966	1968	1969	1970	1975	1976	1977	Sample Size
Jan		Ex(10:30)			E7	N3		N6	N6	5
Feb		Ex(10:35)			E7			.	N6	4
Mar		Ex(10:40)			E7			.	N6	4
Apr					N3(11:30)*			.	N6	3
May					N3			.	N6	3
Jun			N2(11:30)*		N3			.	N6	4
Jul	Ex(8:30)				N3		N6(11:45)*	.		4
Aug	Ex(8:55)				N3		N6	.		4
Sep	Ex(9:15)						N6	.		3
Oct	Ex(9:40)			E7(14:30)	N3		N6	.		5
Nov	Ex(10:05)			E7			N6	.		4
Dec	Ex(10:30)		E3(14:40)	E7			N6	.		5
Annual	6	3	2	3	9	1	6	12	6	48

Resolution ≈ Half Power Diameter

Experimental	1280 km, 11.5°
ESSA3	
Nimbus 2	Averaged to 10° grid
ESSA7	2200 km, 20°
Nimbus 3	Averaged to 10° grid
Nimbus 6	1100 km, 10° (analyzed from 16°

*Albedo corrected for diurnal variation of reflection with directional reflectance model.

Figure 1a.

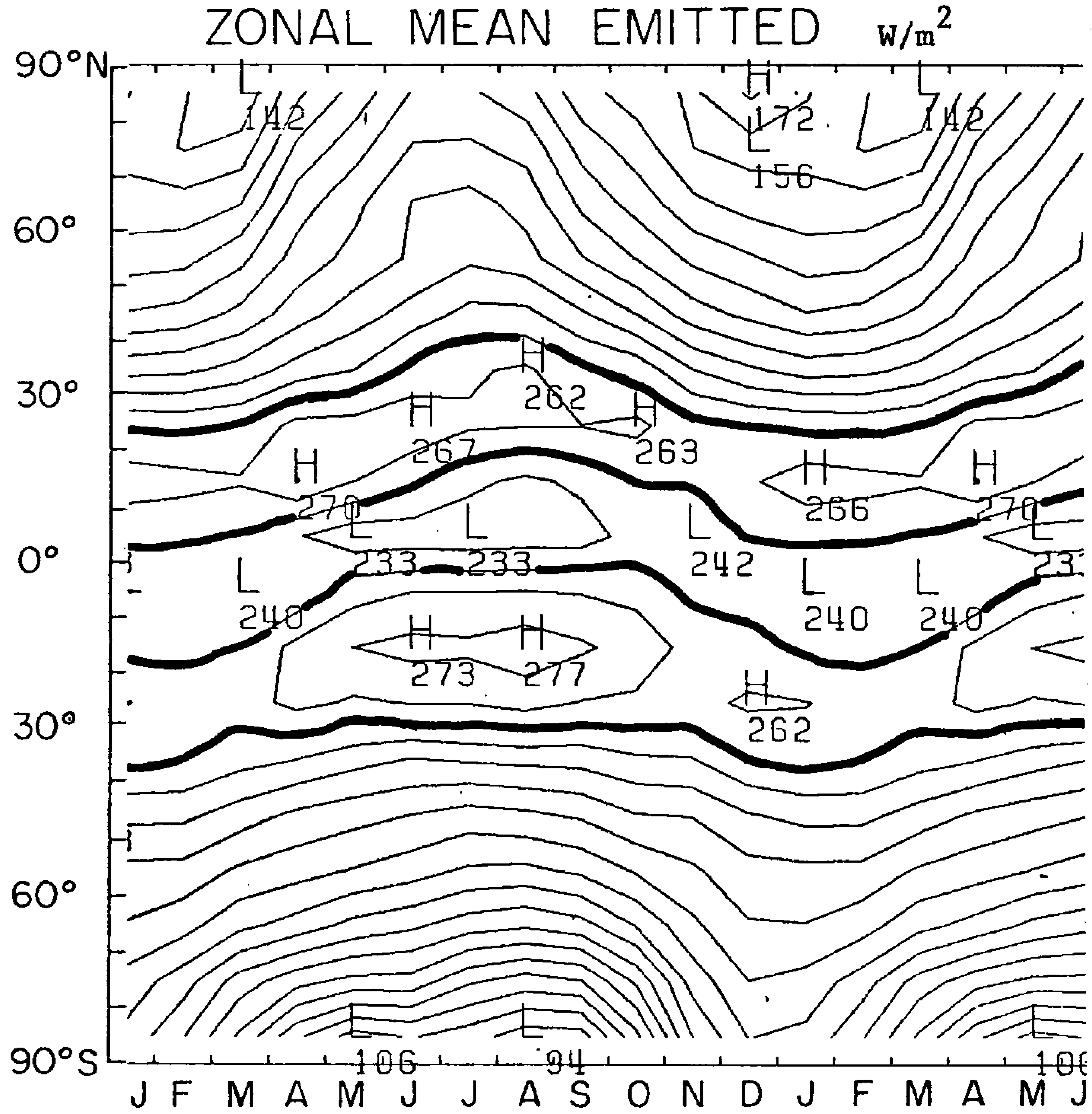

Contour Interval 10 W/m^2

Heavy line at 250 W/m^2

Figure 1b.

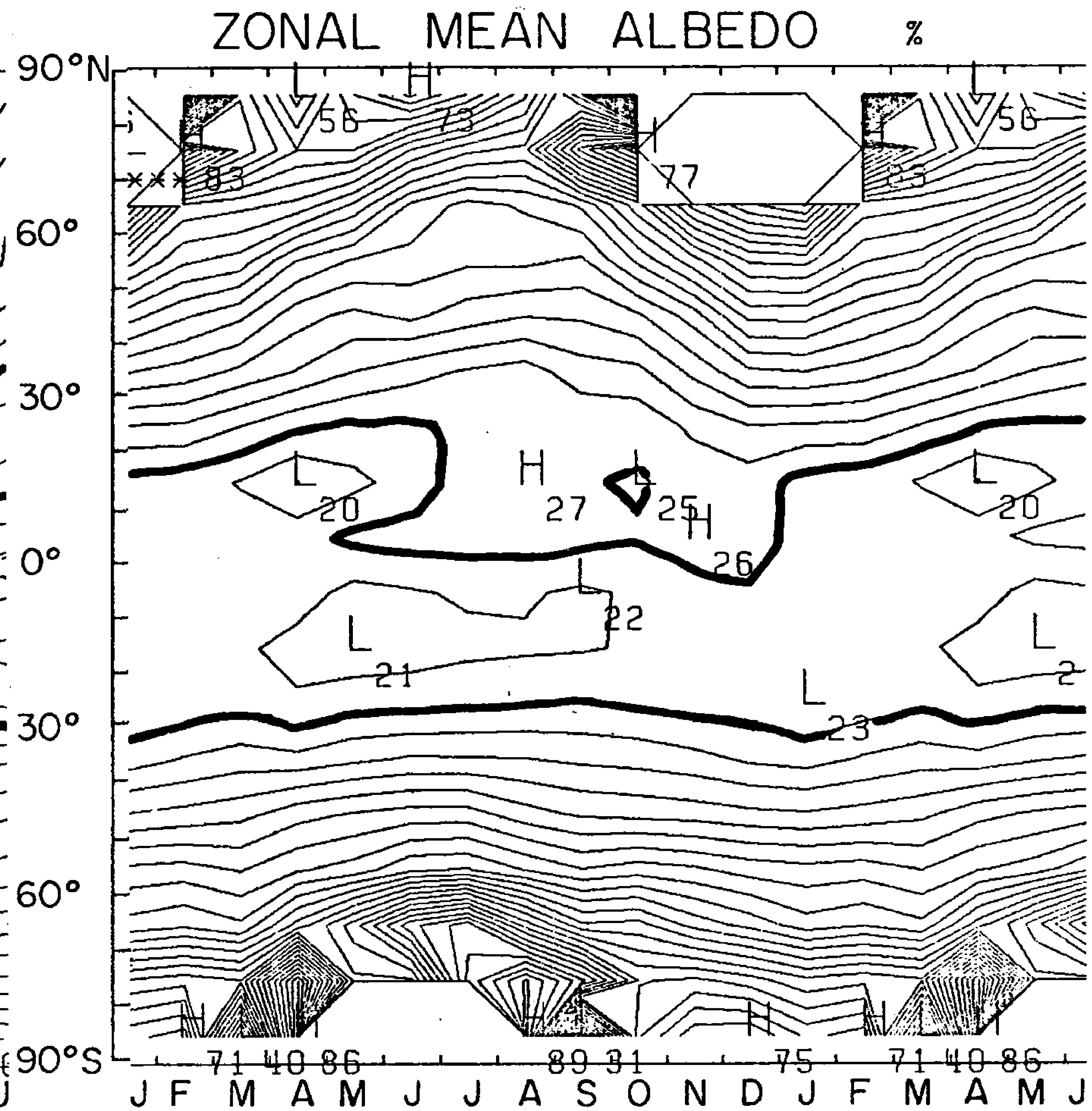

Contour Interval 2.5%

Heavy line at 25%

TIME VARIATION

The time variation of the zonal means shows the seasonal change following the solar declination. 18 months are shown, 13-18 being a repetition of 1-6.

Figure 1c.

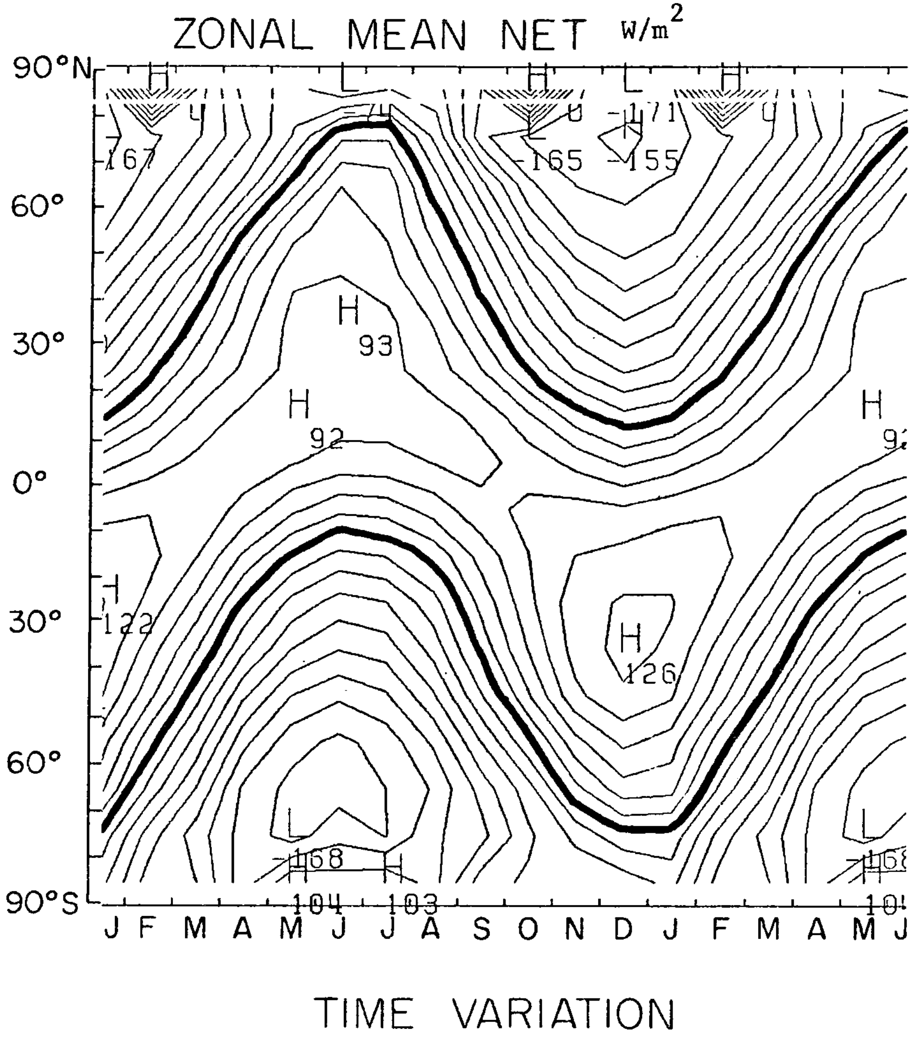

Contour Interval 20 W/m^2

Heavy line at 0 W/m^2

FLOW CHART OF DATA PROCESSING OF NIMBUS 6 ERB

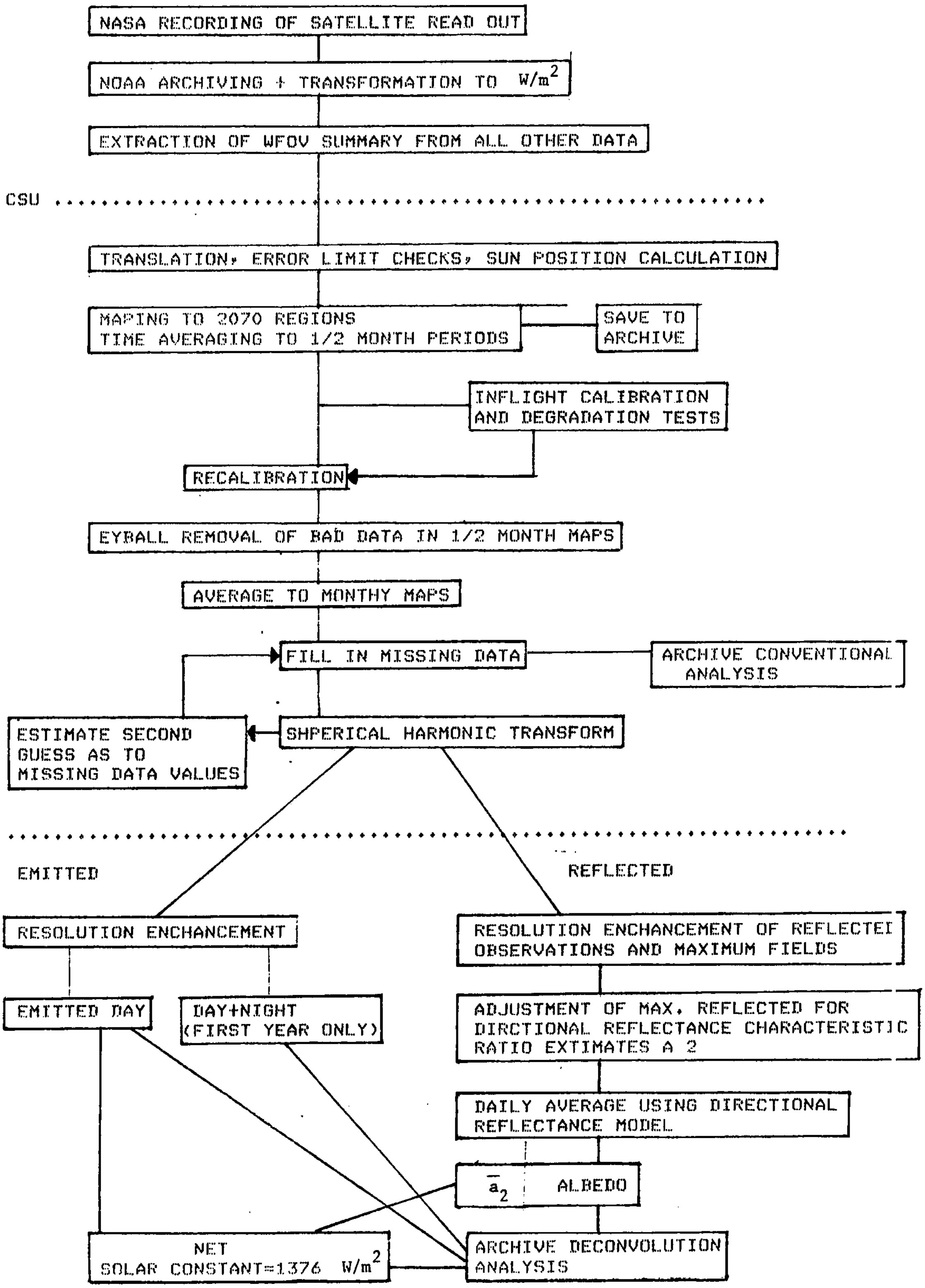

view (WFOV) integrating sensors to measure low resolution, 200 km, fluxes and the global integral budgets. We will discuss results from the WFOV detectors of the earth fluxes. Results from the other systems have been discussed elsewhere (Hickey et al., 1977; Jacobowitz et al., 1979). Perhaps the most interesting result is the stability of the solar constant with no variations detected to the instrument accuracy ($\pm$ .5%) over 4 years (Hickey, 1980).

Instrument measurements by the WFOV sensors were made by flat plate thermopile detectors. The instruments have been described by Hickey et al. (1974) but here we discuss them briefly as it will explain the calibration procedure used. The total channel (#12) was a black painted detector with a field of view stop slightly bigger than the earth's disc as seen at 1100 km altitude. This detector responded to all radiation, both emitted and reflected from the earth (as well as the sun when it is near the earth's edge). The thermopile voltage was converted to irradiance by equation 1.

$$\Delta\ (\text{Irradiance}) = \frac{V - V_o}{S} = \int_{\text{angle subtended by earth}} E(\alpha,\beta)\cos\alpha\, d\cos\alpha\, d\beta$$

$$+ \epsilon_s[1 - F_D(\alpha)]T_s^4 - \epsilon_D\ \sigma T_D^4 \qquad (1)$$

$$+ \epsilon_D(1-\epsilon_s)\sigma T_D^4\ (1-F_D)$$

V = thermopile voltage

V_o = offset voltage

s = sensitivity

E = source radiance field (space contributes zero)

$\epsilon_s[1-F_D]T_s^4$ = radiation emitted by the field stop to the detector (close to zero)

$\epsilon_D \sigma T_D^4$ = emitted flux from detector

$_D$ = detector emissivity = .977

T_D = detector temperature (changed very little during orbit)

$\epsilon_D(1-\epsilon_s)\ T_D^2[1-F_D]$ = radiance reflected from field stop

F_D = size of the whole in field stop

ϵ_s = the polished aluminum field stop reflected all radiation so this is essentially zero.

A calibration was used to measure the sensitivity, s. The entire field of view was filled with a constant temperature black body and V was recorded for several temperatures. Essentially E = $\sigma T_{BB}^4/\pi$ for all angles and so equation 1 becomes 2.

$$\frac{V - V_o}{S} = \sigma T_{BB}^4\ F_D - \epsilon_D \sigma T_D^4 F_D \qquad (2)$$

This calibration is not a measure of s but really a measure of s times F_D. Originally F_D was calculated from the geometry.

This problem was discovered when disagreement was found between the total channel and the long wave scan channel measurements in space. For the Nimbus 7 experiment the field of view, F_D, was measured in the pre-flight calibration and has been confirmed by comparisons between the systems on Nimbus 7. We have chosen to use the measured Nimbus 7 field of view in our analysis of the Nimbus 6 data since the instruments were built to be identical. This results in the factor, F = 1.068, which is the ratio of measured to calculated fields of view, eq. 4.

A separate shuttered channel with the same design as the total channel was included to measure the time change of sensitivity of #12. This channel was open approximately once a month and, to the measurement accuracy, it showed no change in the sensitivity of #12 for two years (Jacobowitz, 1979).

The reflected WFOV detector was a similar thermopile with two Supersil W dome filters outside the field stop to absorb infrared radiation and transmit the solar spectrum. Figure 2 shows the transmission curve. Figure 3 shows a sample time series of raw data covering more than two orbits. The rapid changes are the sun blip caused by direct solar illumination. During the ascending part of the orbit, channel 12 responds to changes in reflected as well as emitted exitance. Similarly, channel 13 follows the reflected term. On the descending part of the orbit #12 responds only to the emitted and ideally #13 should read zero. In the original NOAA analysis a constant offset was added to the #13 results to eliminate negative reading at night. This appeared because the filter dome temperatures were lower in space than in the ground calibration. Basically this means the V_o for 13 should be changed. Also the exponential change in the #13 reading after the sun blip may imply that the offset varies in time. House and Giannola have discussed this extensively in various Nimbus 7 ERB NET project reports. We experimented with the inclusion of this effect but since it is still unsubstantiated we have not included this potential correction in the analysis. A detailed comparison of integrated scanning channel emitted measurements with the colocated WFOV measurements might substantiate these results.

During the sun blip, the difference between 12 and 13 should be the emitted radiance exitance. Because the angular response of the two channels is not the same near the field of view limiters, this is not true. We have discarded all the data for these periods in the construction of the maps. This has resulted in substantial missing data regions in

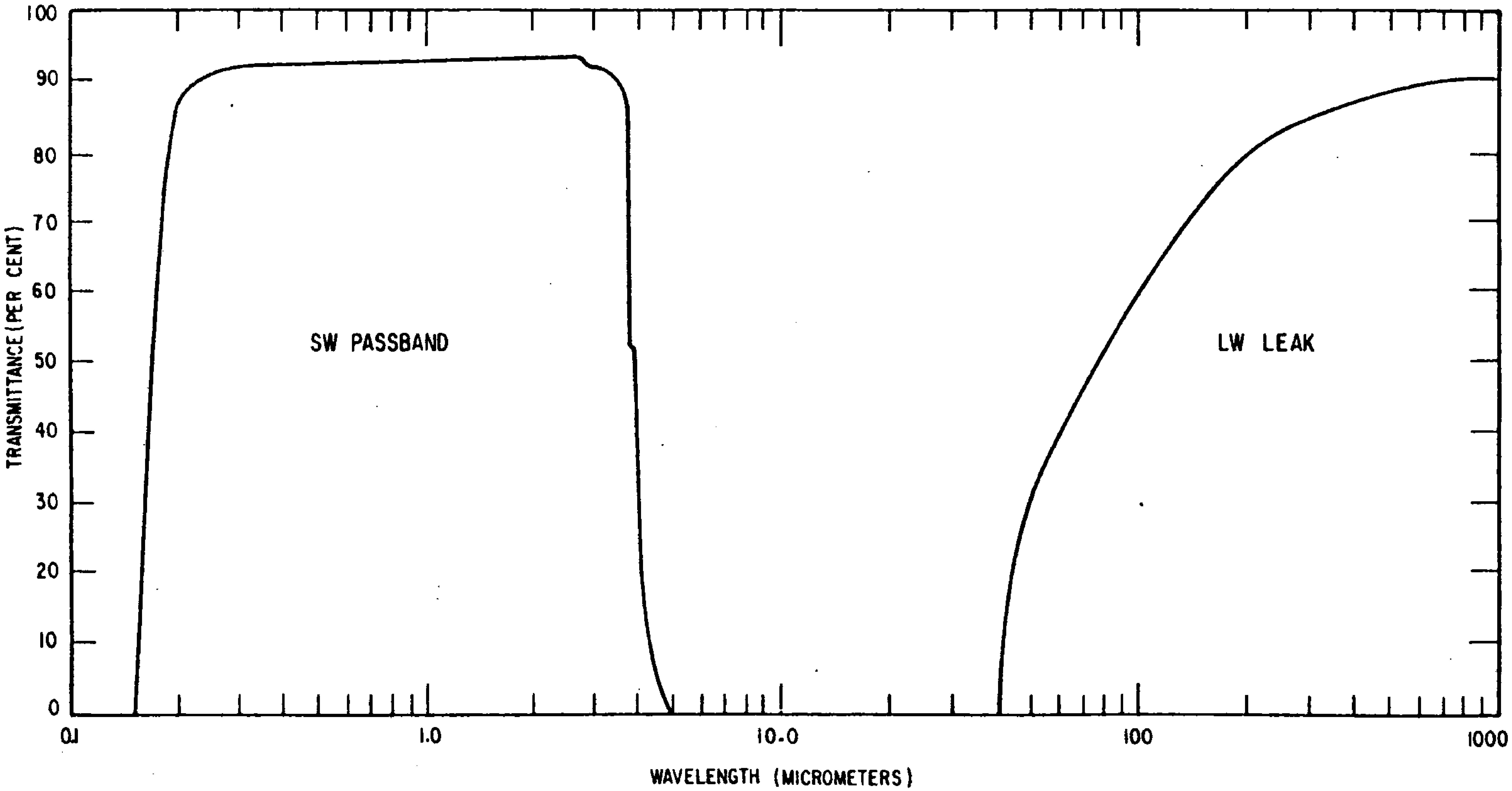

Fig. 2. Transmittance of Supersil W fused quartz filters, channel 13.
Nimbus 6 User's Guide, 1975.

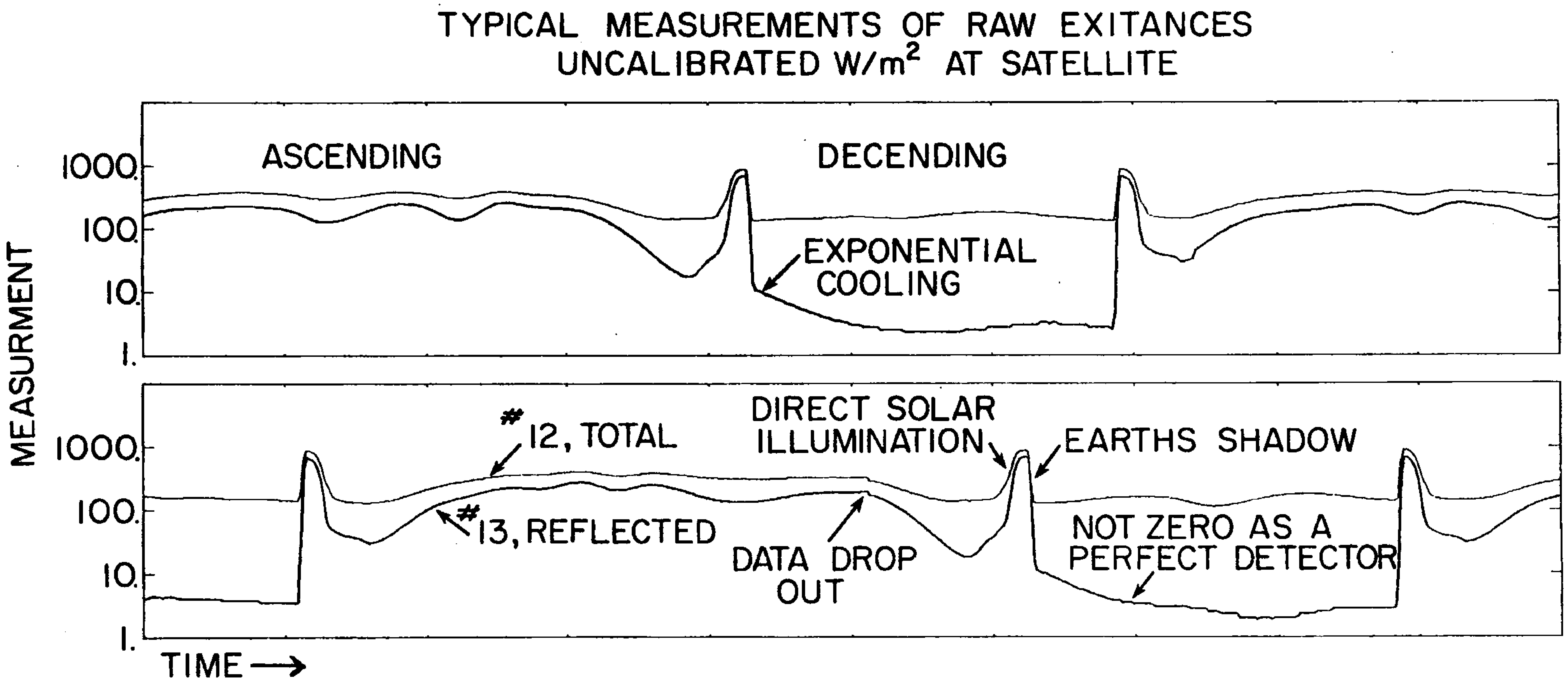

Fig. 3. Sample plot of time series of measurements for two orbits.

the analyzed fields especially on the night or descending half of the orbit. The peak of the sun blip can provide an estiamte of the solar constant if the exact angular response of the detector were accurately known. More importantly, though, it provides a measure of the time variation of the sensitivity which can be changed by degradation of filter transmission or change in absorbtivity of the detector thermopile.

Several inconsistent results have been found from the measurements of this detector. First albedo calculations showed results much lower than the climatology. The solar flux estimates when the sun was at the edge of the field of view was correct (in comparison to the solar channels). The emitted flux at night (the total measurement) was larger than the daytime (total minus reflected) over oceanic regions, an unlikely situation. The reflected measurements on the dark side of the earth were negative. The solar flux estimate shows a linear decrease of 6%/year from this channel on day to night and 0%/year change on night to day blip indicating a decrease in transmissivity of the domes (Jacobowitz, 1978).

All these observations lead us to an inflight calibration procedure. Equations 3 and 4 are the transformations from the data we received and those corrected exitances used in the production of this atlas.

$$\text{Reflected} = s*R_r*\,(1 + d(t-t_o)) = R_c \qquad (3)$$

$$\text{Emitted} \quad E_c = T_r*f - R_c \;.\;.\;.\; \text{day side} \qquad (4)$$

$$= T_r*f \;.\;.\;.\; \text{night side}$$

R_r = Recorded reflected radiant exitance

T_r = Recorded total exitance

f = field of view adjustment = 1.068 = measured/ calculated

s = scaling of reflected = .97 *f(± .01*f)

d = time decay of transmission = .025/year (± .002/year)

t_o = time of first data (7/76)

t = time

The scaling of the reflected flux, s, was estimated by requiring that the emitted measurement be the same (in the least squares sense) day and night over the mid Pacific (Fig. 4) for the region 180°E to 225°E and 27°N to 27°S. Only ten months of data were available for this test, because of pausity of measurements at night caused by a mechanical failure of the satellite tape recorder. The decay of dome transmission, d, was estimated by requiring the annual cycle of average emitted flux to be the same for the two years of daytime measurements (Fig. 5). Since there was consistency in the estimates of d for several regions we feel justified in using it. It does not agree with the 6% change in solar measurement by the WFOV channels, but this could be evidence of non-uniform transmission change over the domes. All of these adjustments destroy any absolute calibration of the results but relative changes are still detected. Also, it removed any year to year change in the annual global mean fluxes.

ERROR ESTIMATE

A quantitative error estimate is difficult because only a few other measurements can be compared and some of these are used in the calibration adjustments. The initial measurement digitization error is .1 W/M^2. The absolute electrical calibrations of the thermopiles is ±2% (Hickey, et al., 1978). The measurement of the field of view, F_v, is accurate to ±1%.

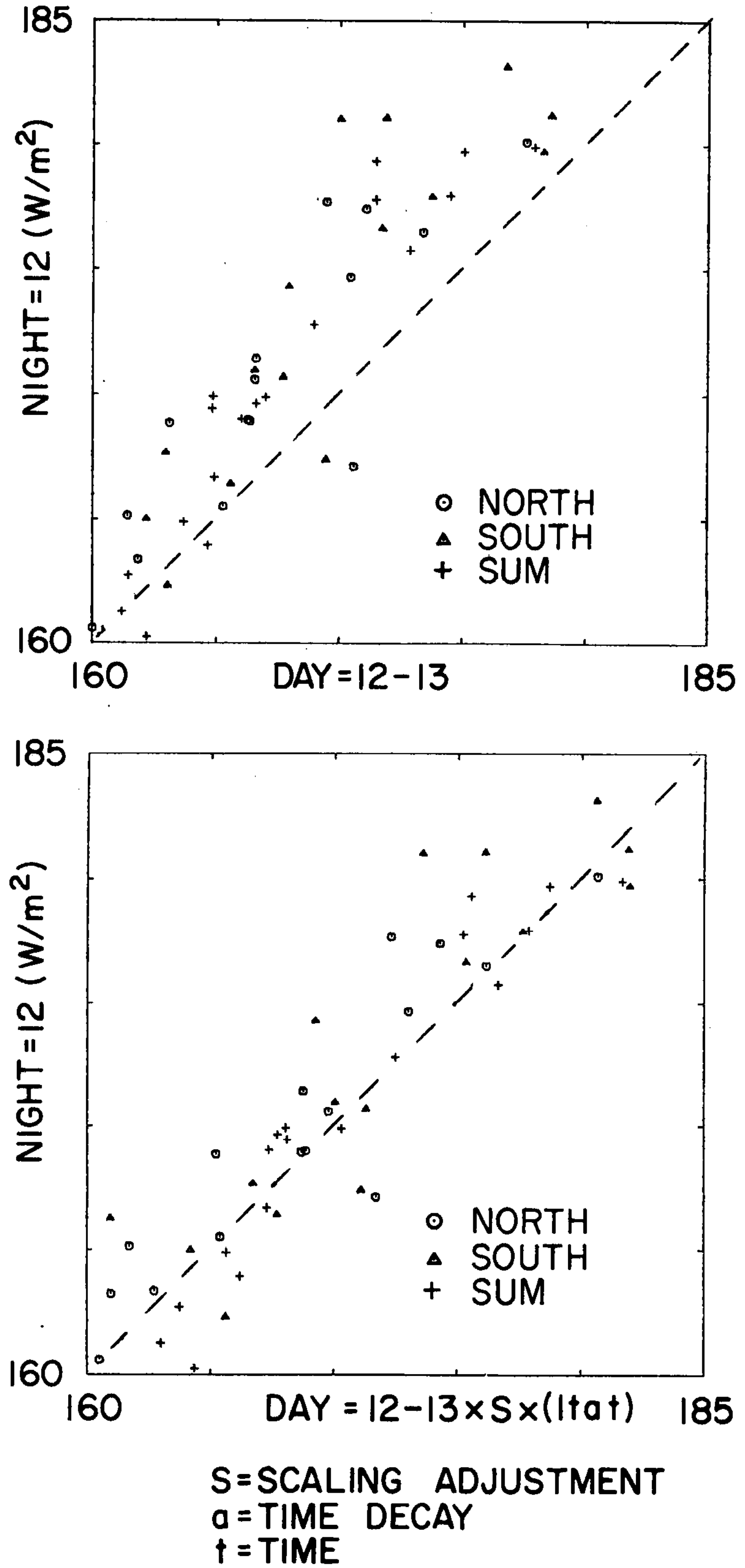

Fig. 4. Scatter diagram of uncorrected and corrected mid-Pacific area averages. This was used to derive the empirical scaling adjustment s = .97*f ($\pm$ .01*f).

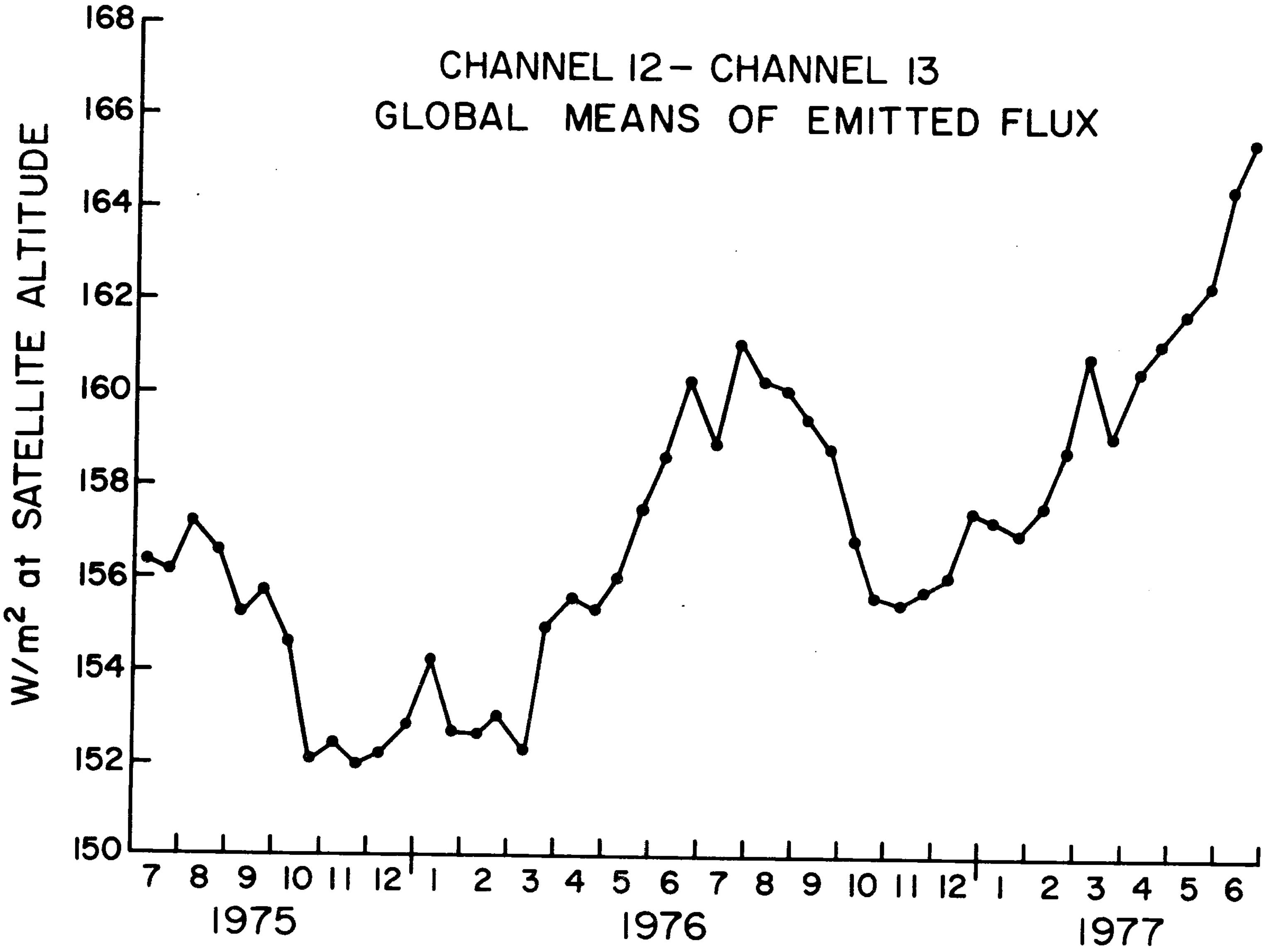

Fig. 5a. Time series of two week orbital means for two years. The trend in reflected and emitted was removed by fitting the first year observations to the second. This assumed a linear decline in transmission of the channel #13 filter produced the trend.

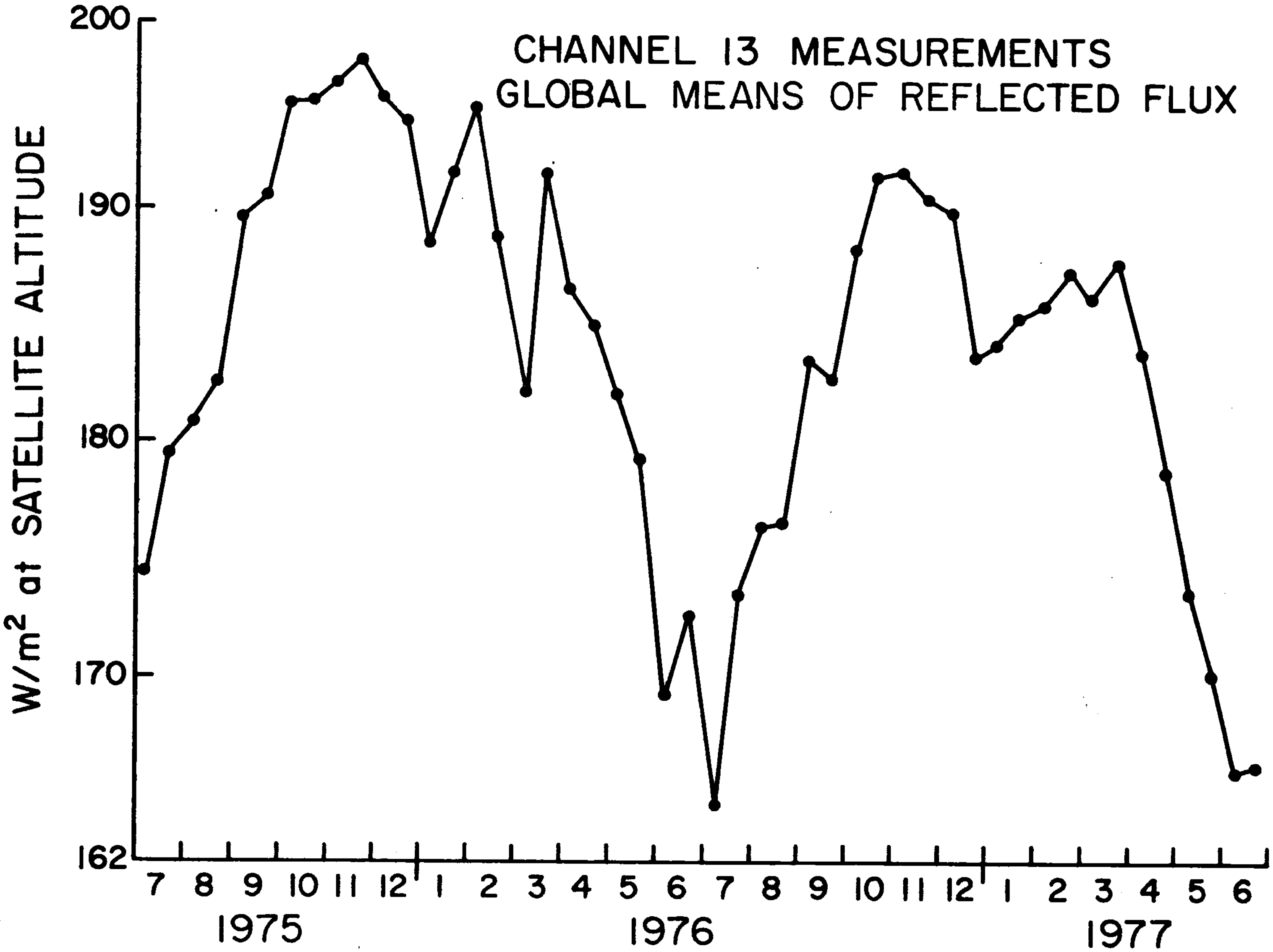
CHANNEL 13 MEASUREMENTS
GLOBAL MEANS OF REFLECTED FLUX
W/m² at SATELLITE ALTITUDE
200
190
180
170
162
7 8 9 10 11 12 1 2 3 4 5 6 7 8 9 10 11 12 1 2 3 4 5 6
1975
1976
1977

Fig. 5b.

The largest uncretainty appears in the scaling adjustments, ($\pm$2%) because a complete physical explanation is not available.

THE ANALYSIS PROCEDURE

The original data was recorded at 4 second intervals, but the data we processed were 16 second averages. All the second data values were mapped onto 2070 equal area regions over the earth. These areas are approximately 4.50 by 4.50 great circle arc. Maps were made for the emitted exitance, E_c, and reflected, R_c, and maximum diffuse reflected exitance for ascending and descending halves of the orbits (6 maps). Data was rejected for those times when the sun shone into the detectors, about 15% of each orbit, sun zenith angles from 96° to 123°. These maps of the radiant exitance through the sphere with radius 7478 km at near local noon or midnight.

A zero order estimate of the earth albedo is the reflected measurement divided by the maximum. Similarly, the zero order emitted radiant exitance at the top of the atmosphere (TOAM) is just the distance corrected map (orbit radius/earth radius)**2. A spherical earth was assumed with a radius 6378 km. These estimates are substantially smoother than atmosphere fields. A realistic resolution is the size of the half power region, $1600^2 km^2$ or a circle 15.8°arc in diameter.[1] Incidentally, these procedures were used in the earlier radiation budget experiments except the Nimbus 2 and 3 scanning analyses. We have chosen a more

[1] The half power region is the circular cap on the earth centered at the sub-satellite point which contributes half the total power incident on the detector. For this one assumes a unit source function and thus total power on the flatplate detector is r_e^2/r_s^2 or 0.727. The total power area has a diameter of 63° circular arc. As an interesting sidelight, the edge of the half power area occurs at the observation zenith angle of 45°.

complex approach which removes some of the smoothing and includes the systematic diurnal effects.

RESOLUTION ENHANCEMENT

A measurement at satellite altitude is an integral over the field of view of the radiance leaving the TOAM toward the detector (Eq. 5).

$$m(\vec{r}_s) = \int s(\vec{r}_e \cdot \vec{r})\ g(\hat{r}_e \cdot \hat{r}_s,\ \vec{r}_e \cdot \vec{r}_s)\ d\Omega \qquad (5)$$

s = source radiance dependent on position, view point and time

g = weighting dependent on sensor geometry

$= \dfrac{(\hat{r}_c \cdot \vec{r})\ (\vec{r} \cdot \hat{r}_s)}{r^2}$ for flat plate detector

$\vec{r}_e$ = vector to source point at TOAM

$\vec{r}_s$ = satellite position

$\vec{r} = \vec{r}_s - \vec{r}_e$ = observation vector

$d\Omega = d\cos\theta\ d\phi$

(θ,ϕ) = colatitude, longitude earth coordinates

The weighting function, g, depends on the angular properties of the source, radiance and the view position. If the function g depends only on the relative position of observer and source the equation has a simple solution.

EMITTED FLUX

For the emitted radiance, a diffuse emission model is quite good at the TOAM so Equation 5 becomes 6 for the flat plate detectors.

$s = E(r_e)$ = emitted radiant exitance at TOAM $\qquad (6)$

$$E_c(\vec{r}_s) = \int E(\vec{r}_e) g\ d\ \Omega$$

It can be shown that spherical harmonics are eigen functions of this simplified equation with the spherical harmonic addition theorem (Smith et al., 1975) Thus equation 7 follows.

$$m = \sum_{n=0}^{N} \sum_{l=0}^{n} m_n^l Y_n^l(\theta_s, \phi_s) \tag{7}$$

$$s = \sum_{n=0}^{N} \sum_{l=0}^{n} s_n^l Y_n^l(\theta_s, \phi_s)$$

$$\int Y_n^l (\theta_e, \phi_e) \; g \; d\,\Omega = \lambda_n \; Y_n^l \; (\theta_s, \phi_s)$$

Thus

$$s_n^l = m_n^l / \lambda_n$$

where

Y = spherical harmonics

(θ_e, ϕ_e) = colatitude, longitude of earth point

(θ_s, ϕ_s) = colatitude and longitude of observation point

The eigen values, λ, depend only on the order of the term, n. Table 2 shows the values of λ for the Nimbus 6 orbit. Since λ decreases with increasing resolution (increasing n) noise will be amplified as one extends the series. The coefficients at satellite altitude were determined by numerically integrating the maps times the spherical harmonics and using the orthonormal properties of these functions.

The series was truncated at order 15. Also, terms with l greater than 13 were set to zero because these terms were excited by the orbit sampling. Approximately 13 orbits occurred each day leading to an artificial east-west wave number about 13. Truncating the series and deleting terms set the resolution of the final maps without introducing excessive amounts of noise.

Table 2. Eigen values of measurement operator, λ

Order	λ	Order	λ
0	.727	10	.312
1	.714	11	.273
2	.689	12	.240
3	.654	13	.209
4	.610	14	.184
5	.560	15	.161
6	.508	16	.141
7	.455	17	.124
8	.404	18	.108
9	.356	20	.094

The final resolution should delineate about (n+1)**2 regions giving a size of 1000^2 km^2 or 10^o arc diameter half power areas.[2] We feel that this procedure improves the specificity of the results and makes the size of the highs and lows more representative of the radiation budget at the top of the atmosphere. This resolution means that points separated by 1100 km are still highly correlated. Independence is not obtained until about 1500 km ($\sqrt{2}$ x 1100 km). This same statement is true of the conventional analysis except the respective sizes are 1700 km and about 2400 km. One should then be very cautious when discussing small scale features.

REFLECTED EXITANCE; ALBEDO

Calculation of daily average albedo from any measurement or a group of measurements requires several assumptions. First to convert a set of radiance measurements into flux (the integral of radiance of all up angles) one must assume some form of the angular pattern of reflection. Incidently the prime purpose of the scanning component of the Nimbus ERB experiment systmes is to measure this function. From a small set of scanner measurements from Nimbus 6, Campbell and Vonder Haar (1978) showed that a diffuse reflection pattern is reasonably accurate for large scale wide field of view measurements. One can then estimate a zero order albedo at the time of measurement by calculating the maximum reflected diffuse flux, R_{max}, at the sensor, Eq. 8.

---

[2] In analogy with the half power region calculated above, the 250 coefficients $[(15+1)^2-6]$ specify 250 regions. Half the area of these correspond to the half power resolution of the enhanced resolution analysis.

$$R_{max}\ (\vec{r}_s \cdot \hat{r}_{sun}) = \int I\ \hat{r}_e \cdot \hat{r}_{sun}\ g\ d\Omega \qquad (8)$$

where the integration is carried out over all points in the field of view.

I = solar constant adjusted for earth sun distance.

Thus $a_o = R_c/R_{max}$

R_{max} depends on the satellite altitude (the g function) and the sun zenith angle (local noon) at the subsatellite point. The solar constant was chosen to be 1376 W/m^2 from Hickey et al. (1980).

This method neglects the systematic change of albedo with sun angle during the day. This is especially important for the Nimbus 6 analysis because of the near noon orbit (11:45 local). Measurements of most surfaces show the lowest albedo at the highest zenith angle. Figure 6 shows some observations and models of this variation from the analysis of the Nimbus 3 experiment (Raschke et al., 1973). We have chosen to use the land-cloud model from the N-3 analysis in two ways. First, the maximum reflected flux is adjusted with the inclusion of the model, Eq. 9.

$$R^m_{max}\ (\vec{r}_s \cdot \vec{r}_{sun}) = \int I\ \hat{r}_e \cdot \hat{r}_{sun}\ f(\hat{r}_e \cdot \hat{r}_{sun})\ g\ d\Omega \qquad (9)$$

$f\ (\hat{r}_e \cdot \hat{r}_{sun})$ = directional reflectance function

thus

$a_1\ (t_{local}) = R_c/R^m_{max}$

t_{local} = local time of measurement

Since the local time is near noon, R_{max} is generally larger than the diffuse model maximum implying a lower noon time albedo than the diffuse assumption for ERB. Second, though, one must convert the near noon albedo to the daily average again using the model, Eq. 10.

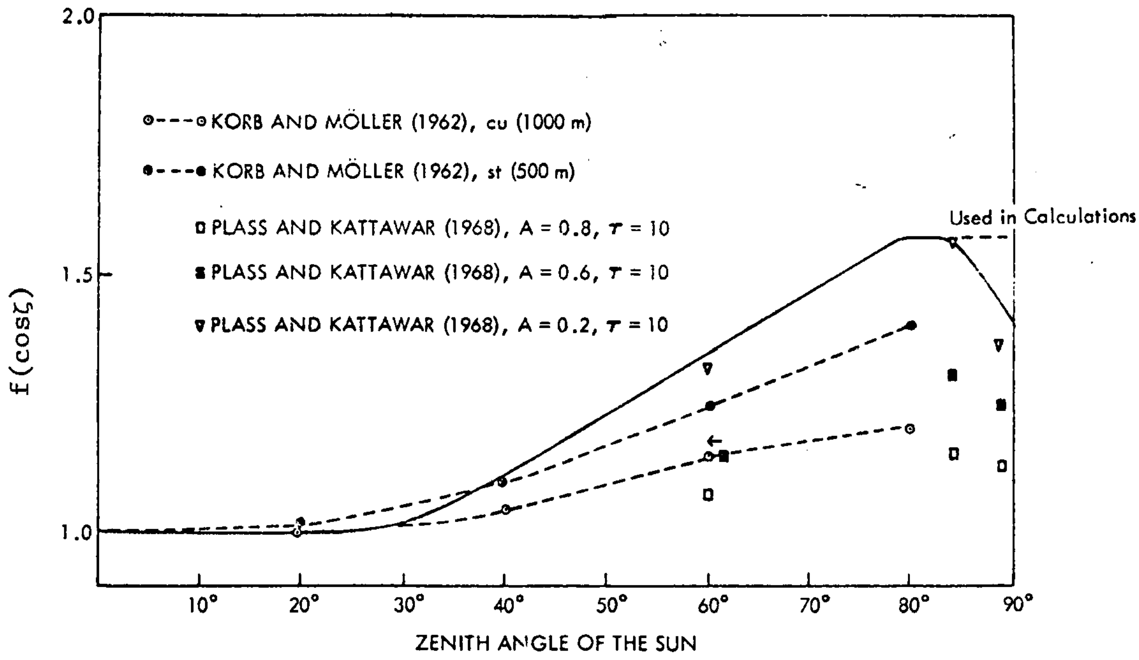

Fig. 6. Direction reflectance function from Raschke et al. (1973).

$$\bar{a}_1 = \frac{\int_{day} a_1\ (t_{local})\ \hat{r}_e \cdot \hat{r}_{sun}\ f\ (t_{local})\ d\ t_{local}}{\int \hat{r}_e \cdot \hat{r}_{sun}\ d\ t_{local}} \qquad (10)$$

One can call this a first order daily average albedo estimate.

Figure 7 shows the daily average albedos of a cloud like surface over the whole globe for different times of year. This is the result of substituting .3 for a_1 in equation 8 and plotting $\bar{a}_1$. One sees quite large changes with changing illumination conditions.

Another important effect is the smoothing of the reflected flux field occurring because the measurements are made at 1100 km rather than at the top of the atmosphere. In analogy with the resolution enhancement of the emitted flux the measurement field $R_c\ (\hat{r}_s)$ and the maximum R_{max} $(\hat{r}_s)$ have been expanded in spherical harmonic coefficients. These coefficients were amplified by the eigen values of the diffuse model and then a higher resolution reflected flux and maximum fields were reconstructed (Eq. 11, 12, 13).

$$R(\hat{r}_e) = \sum_{n=0}^{N} \sum_{1=0}^{n} r_n^1\ Y_n^1\ (\theta_e, \phi_e) \qquad (11)$$

$$R_c(r_s) = \sum_{n,1} r_{cn}^1\ Y_n^1\ (\theta_s, \phi_s)$$

$$r_n^1 = r_{cn}^1 / \lambda_n$$

$$R_{max}(\hat{r}_e) = \sum_{n,1} r_{mn}^1\ Y_n^1 \qquad (12)$$

$$R_{max}(r_s) = \sum_{n,1} r_{sn}^1\ Y_n^1$$

$$r_{mn}^1 = r_{sn}^1 / \lambda_n$$

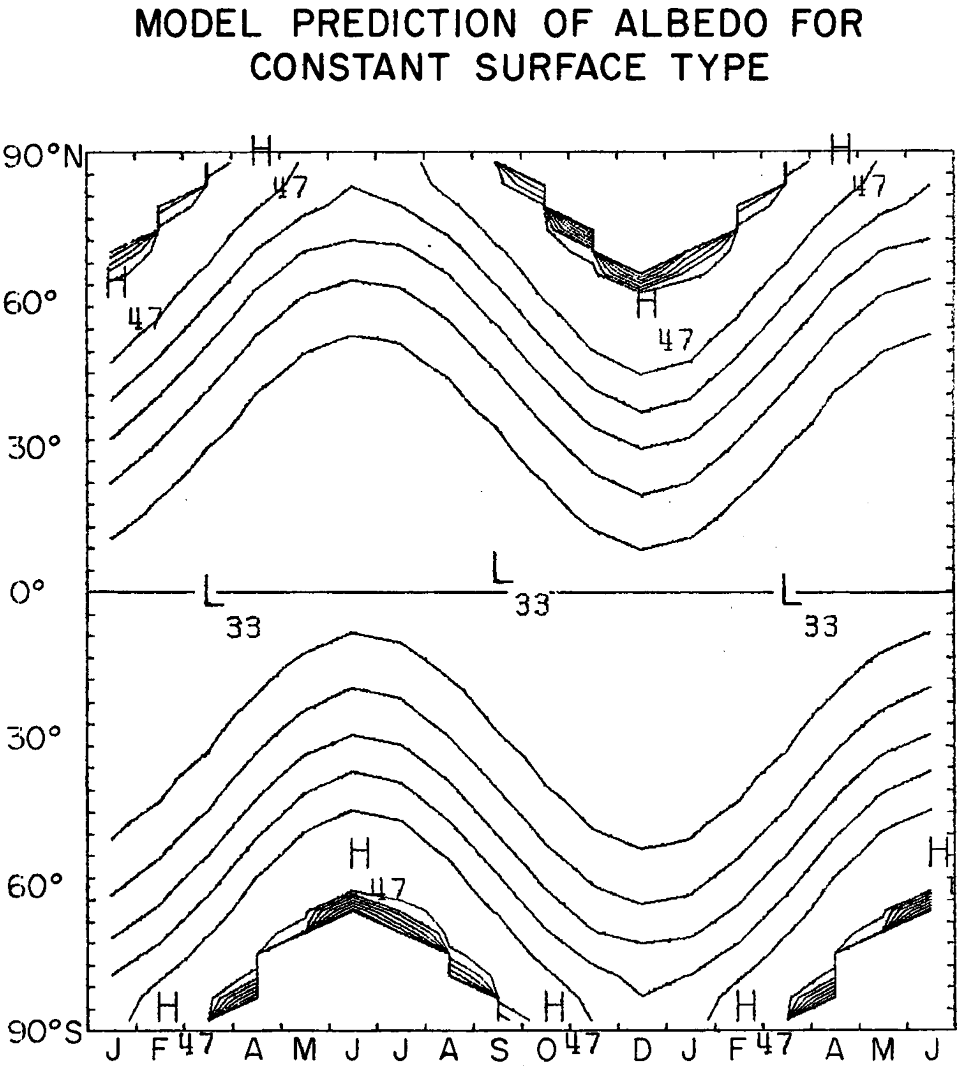

Fig. 7. Model predicted albedo for a surface with 33% albedo at the equator on the equinox. Based on the Nimbus land-cloud model (Raschke et al., 1973)
Contour interval is 2.5%.

Then a second order local time albedo is the ratio of these higher resolution fields, (Eq. 13).

$$a_2\ (\hat{r}_e) = R_c(\hat{r}_e)/R_{max}(\hat{r}_e) \tag{13}$$

Finally the daily average albedo is estimated via equation 13 to include the systematic diurnal variation.

$$\bar{a}_2 = \int a_2\ \hat{r}_e \cdot \hat{r}_{sun}\ d\ t_{local} / \int\ \hat{r}_e \cdot \hat{r}_{sun}\ d\ t_{local} \tag{14}$$

These final resolution enhancement steps are justified by examining the resultant albedo maps. Certain expected features like the bright intertropical convergence zone, the bright Sahara and the contrast between land and ocean are better resolved as displayed in the before and after maps (Fig. 8). The analysis of the Nimbus 7 scanner data compared to the WFOV may confirm or deny the utility of these steps. The final accuracy is difficult to estimate without independent high resolution measurements. The models are known to perhaps $\pm$ 10% for particular source fields, and the combination into a single earth field presents more problems. The adjustment with the model changes the albedo by about 10% so the effect of this unknown is perhaps $\pm$ 1%. The combined error estimate for the monthly average albedo is then $\pm$ 4%.

Figures 8a, b and c show an example of the transformations. The first of each pair of plots shows the results of the conventional analysis scheme with just a distance correction. The noisy looking plots results from the mapping of the data in the relatively small regions (500 km x 500 km). This noise arises from uneven space and time sampling. One should bin the data in regions about the size of the half power for the final presentation. The same thing could be accomplished with a spatial smoothing filter.

EMITTED EXITANCE (W/m^2)

Ascending Measurements Only

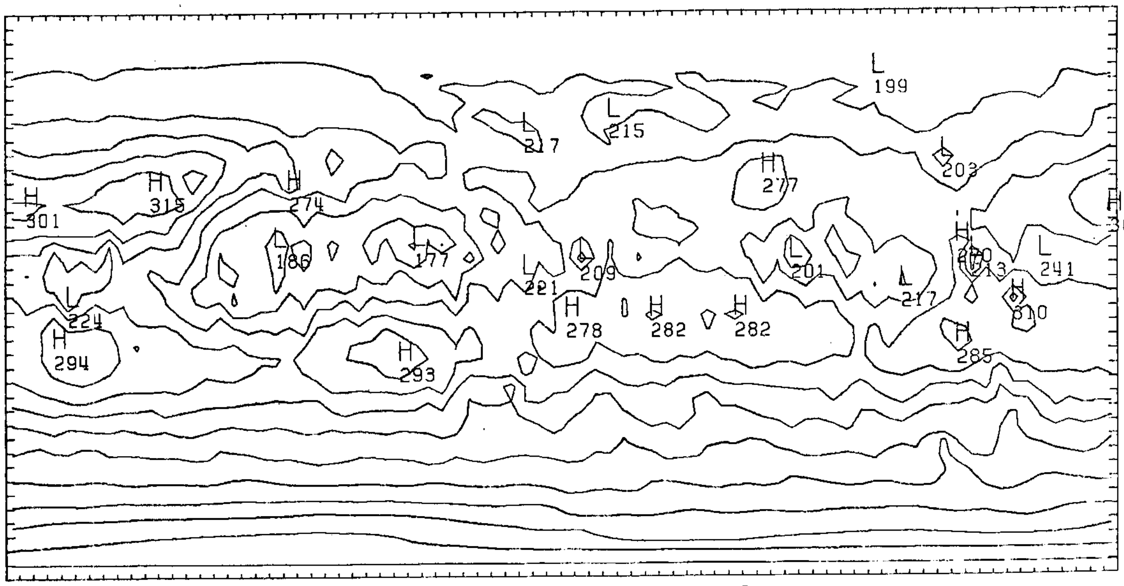

Distance Corrected $(R_s{}^2/R_e{}^2)$

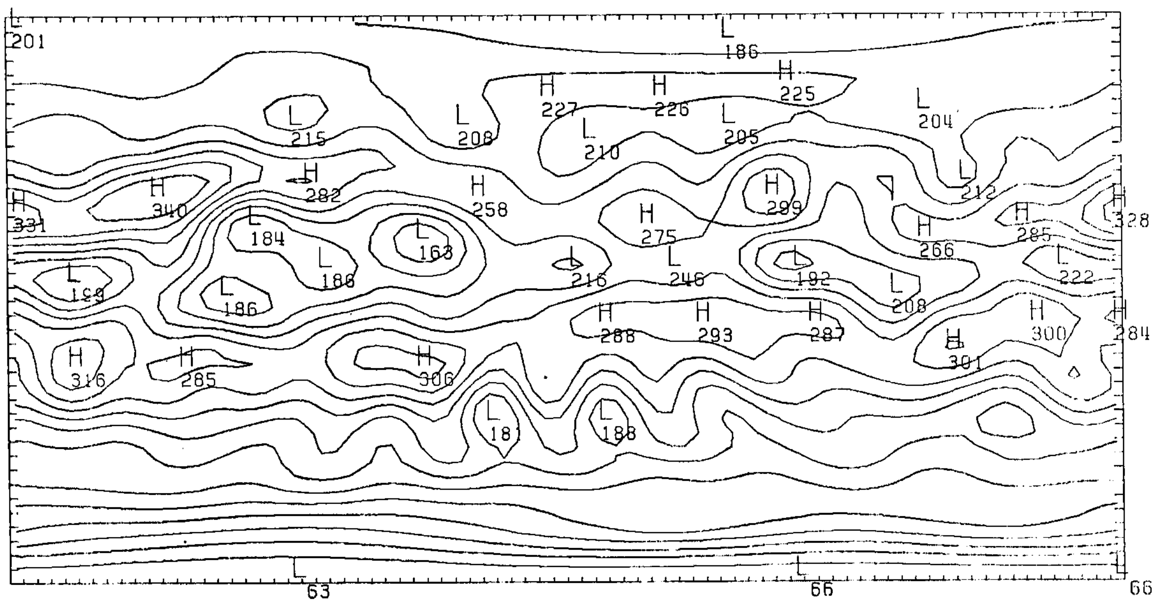

Resolution Enhancement

Contour Interval 20 W/m^2

Fig 8a. Comparison of August 1975 emitted exitance with conventional analysis and the resolution enhancement analysis scheme. Only data from the ascending half of the orbit (day time) was included.

EMITTED EXITANCE (W/m^2)

Ascending and Descending Measurements

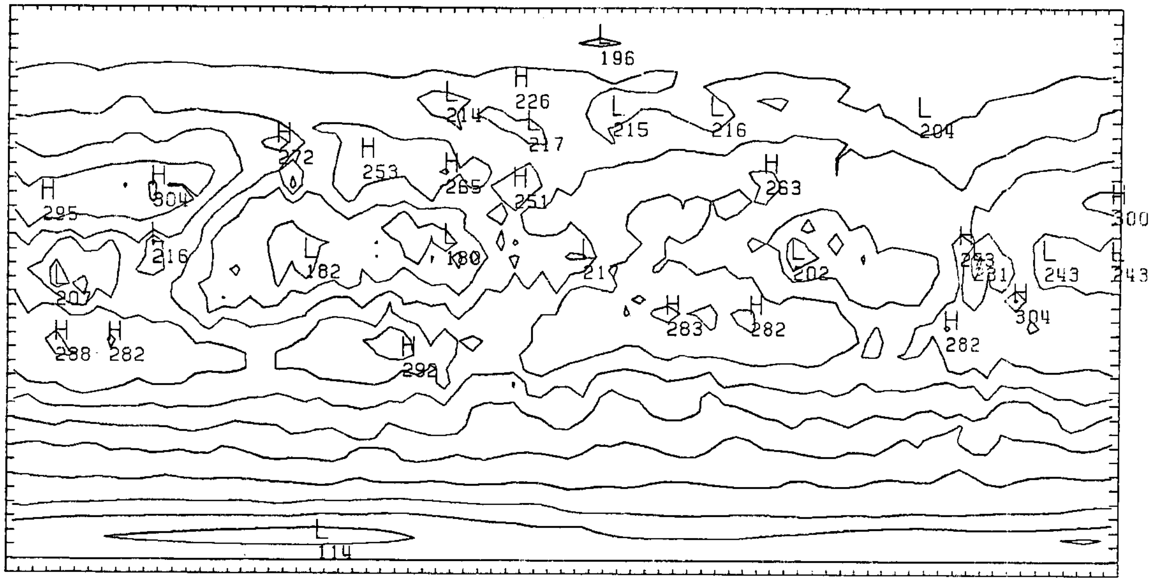

Distance Corrected (R_s^2/R_e^2)

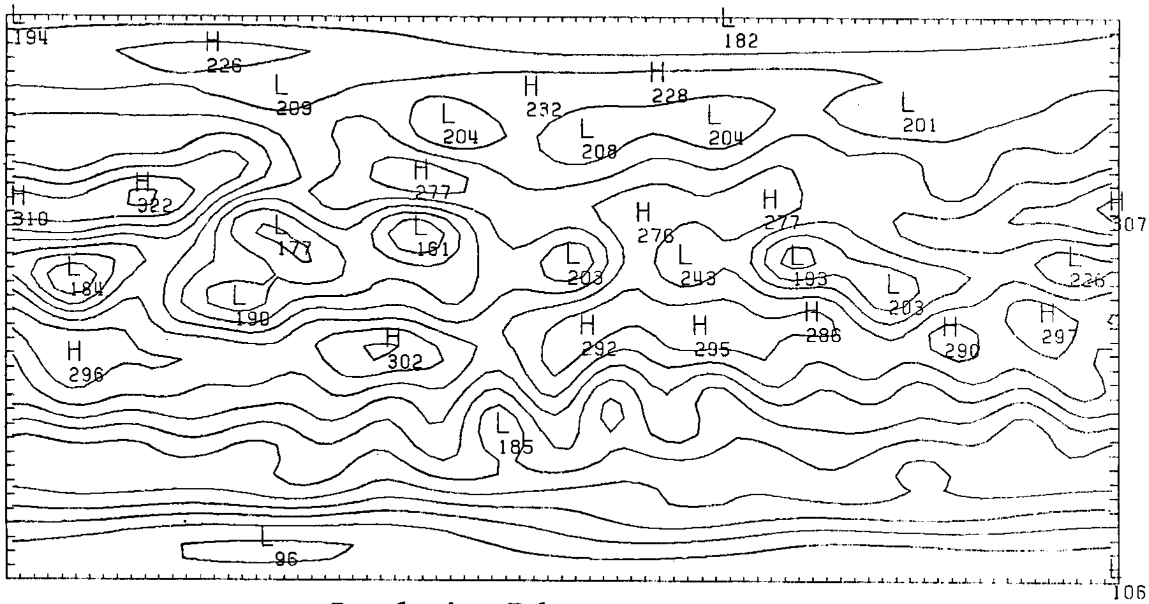

Resolution Enhancement

Contour Interval 20 W/m^2

Fig 8b. Comparison of August 1975 emitted exitance with conventional analysis and the resolution enhancement analysis scheme.

ALBEDO (%)

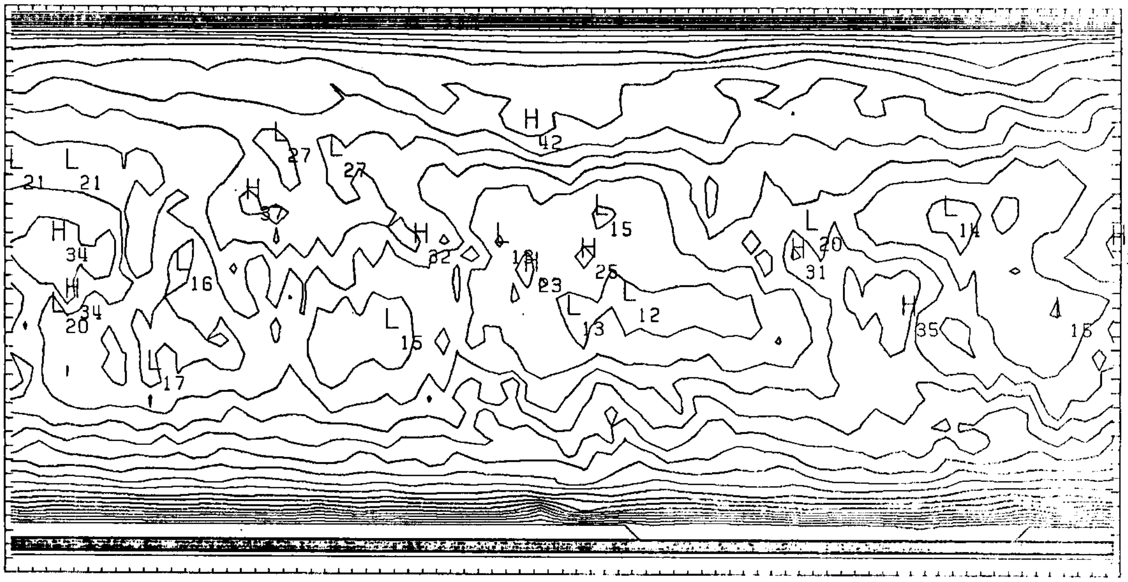

Reflected / Max. Reflected , a_o

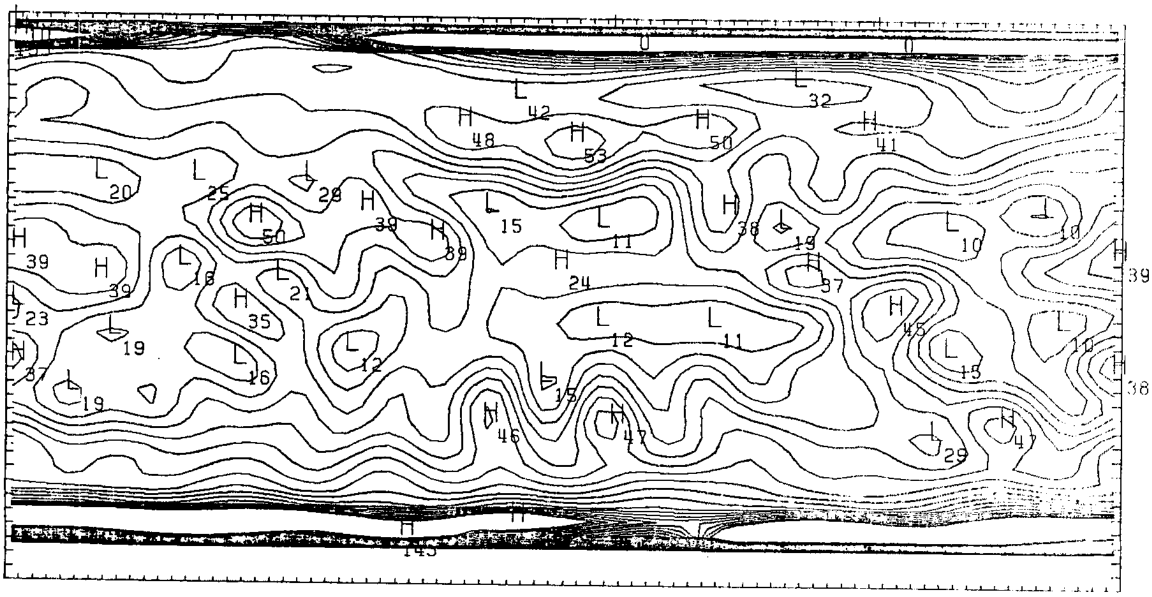

Resolution Enhanced, $\bar{a}_2$

Contour Interval 5%

Fig 8c. Comparison of August 1975 albedo with conventional analysis and the resolution enhancement scheme.

The integration times the spherical harmonics performs this smoothing of the very small scale noise. The intermediate scale (1500 km) variations are amplified.

The differences between the ascending or day side emitted exitance and the combined ascending and descending observations are significant especially over land. We have chosen to present only the daytime observation in the 24 monthly maps because only about 8 months of descending observations with good global coverage are available. This of course leads to systematic errors, but the consistency of time makes comparisons between years more reasonable.

RESULTS

There are three maps presented for each month from July 1975 to June 1977; 1) the emitted flux based on the daytime half of the orbits is presented, the sum of day and night is not used as there is no night data for the second year, 2) the daily average albedo including land cloud model and resolution enhancement, 3) and the derived field, the net radiation at the top of the atmosphere (Eq. 15).

$$\text{Net} = \overline{I}(1 - \overline{a}_2(\hat{r}_e)) - E(\hat{r}_e) \qquad (15)$$

$\overline{I}$ = daily mean incident = I $\hat{r}_e \cdot \hat{r}_{sun}$ d t_{local}/24 hours

I = solar constant at this day of year

Transparent overlays have been provided showing the scale and geography for the maps. Also, various summary plots are presented as the discussion unfolds.

GLOBAL AVERAGES

Table 3 shows the two years of global average radiation budget estimates. The seasonal variation agrees with the climatology and results discussed by Ellis et al. (1978). The interannual differences have been suppressed by the calibration scheme but some differences are still evident. The fact that each year shows a net radiation gain is probably an indication of systematic errors. A small change in the ratio of the measured to calculated field of views, $f = F_m/F_D$, equations 3 and 4, would bring the globe into balance. If f were 1.1 rather than 1.068 both the emitted exitance and albedo would increase by 3% giving net equal to zero ($\pm$ 1 W/m^2). It may be that the Nimbus 6 instrument is slightly different than Nimbus 7. Some detailed studies of the overlap tiem period after launch of 7 might resolve this. An alternate calibration method might be to force the annual net to be zero, for instance Campbell and Vonder Haar (1980b) use this in energetics studies.

ZONAL FIELDS

Because of the strong zonal symmetry of the average weather, a similar symmetry appears in the radiation maps. Much of the annual variation can be seen in the zonal mean plots, Fig. 10, Table 3. This can be compared to Fig. 1, the climatology. One sees immediately more variation of the maximum and minima. Some of the differences between old and new are caused by the weather but much is caused by the resolution changes. The albedo estimates of Nimbus 6 appear to be artificially high near the terminator due to the analysis scheme. Albedo estimates are quite difficult when part of the scene is dark. Also when measurements are attempted outside the high sun angle situations (beyond

Fig. 9a

ZONAL AVERAGE EMITTED EXITANCE (W/m²)

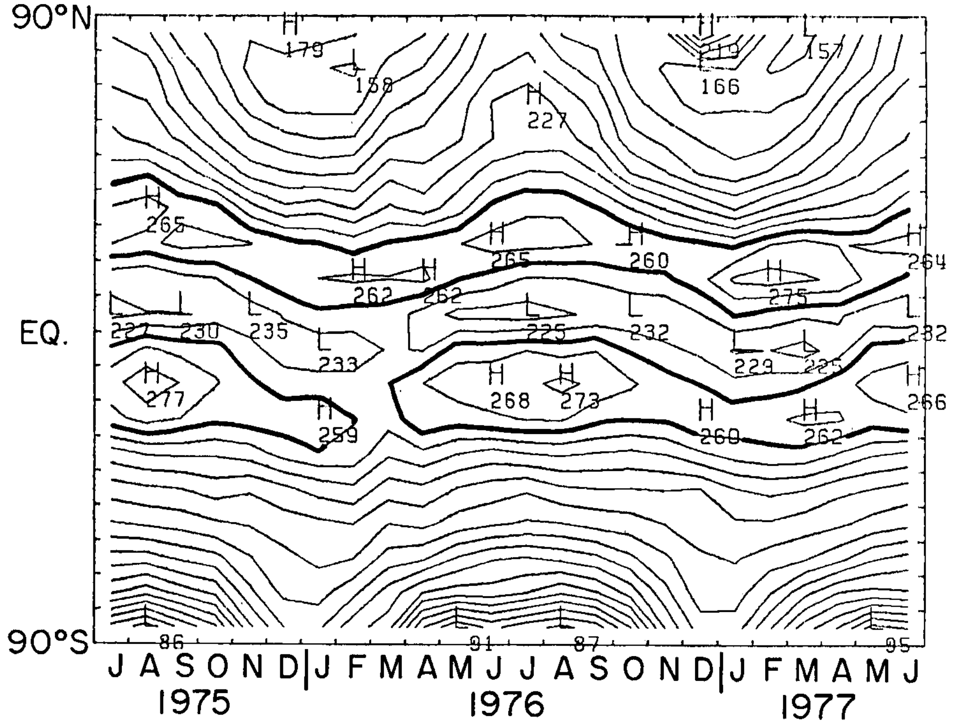

Fig. 9b

ZONAL AVERAGE ALBEDO (%)

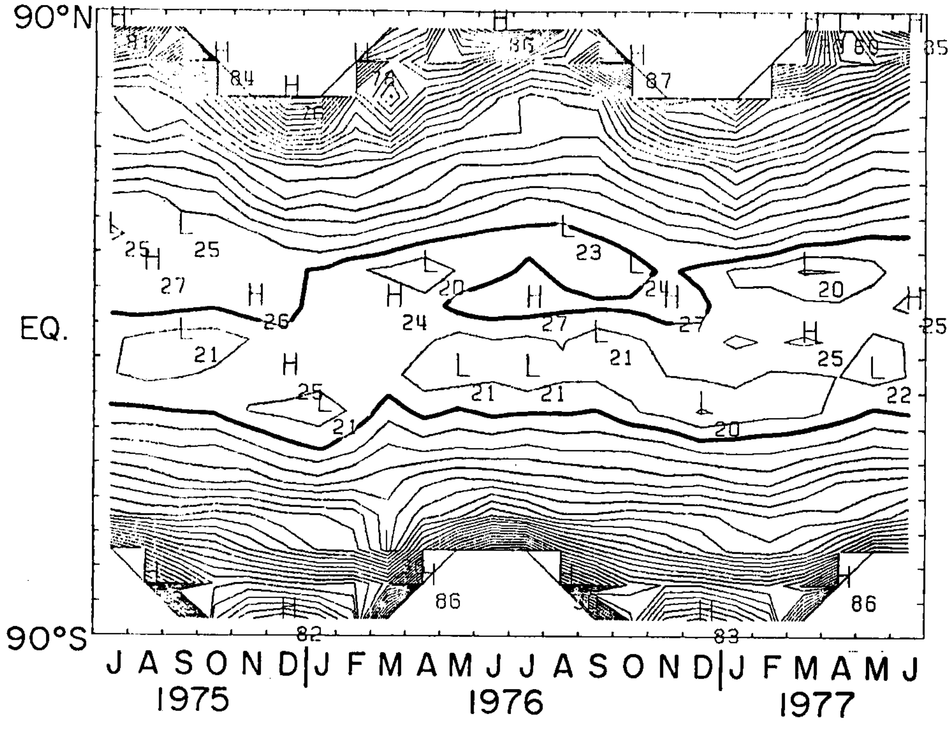

Fig. 9. Contour plots of time variation of zonal mean exitance, albedo and net radiation for 2 years.

Fig. 9c

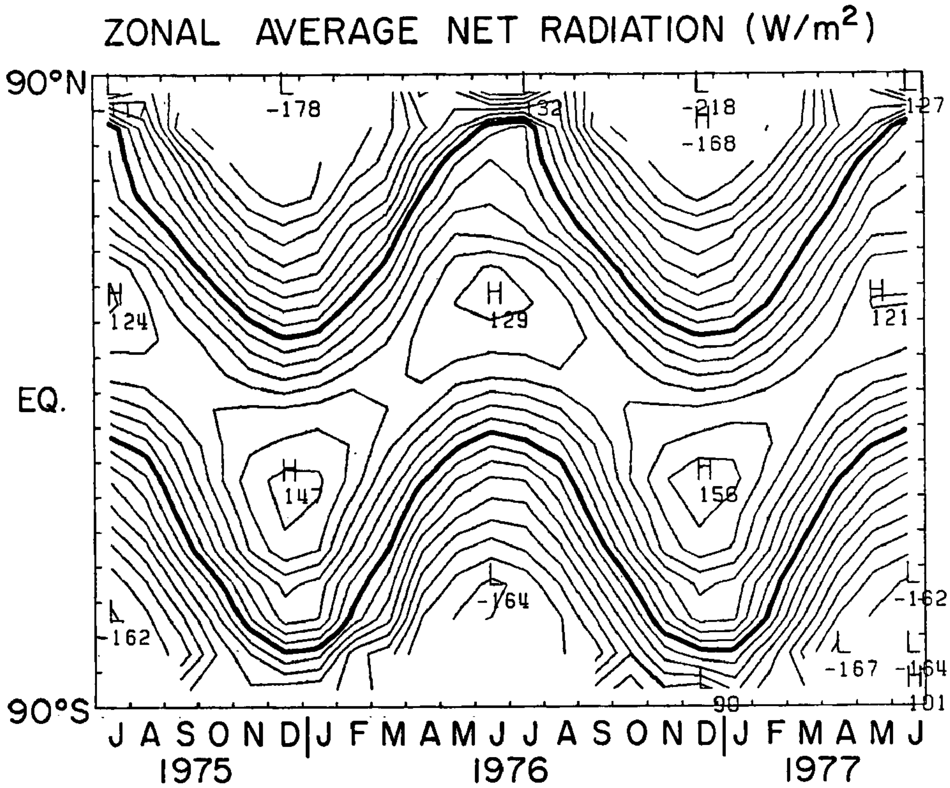
ZONAL AVERAGE NET RADIATION (W/m²)
90°N
EQ.
90°S
-178
-218
-168
124
129
121
147
156
-164
-162
-162
-167
J A S O N D J F M A M J J A S O N D J F M A M J
1975
1976
1977

Table 3a.

ALL GLOBE ZONAL AVERAGE EMITTED EXITANCE W/m^2

ZONE	7/75	8/75	9/75	10/75	11/75	12/75	1/76	2/76	3/76	4/76	5/76	6/76	YEAR 1
1	210.	202.	185.	178.	171.	179.	174.	170.	162.	170.	184.	204.	182.
2	214.	215.	196.	182.	167.	164.	161.	158.	174.	181.	195.	209.	185.
3	225.	220.	203.	191.	174.	165.	166.	165.	186.	194.	205.	221.	193.
4	232.	226.	218.	202.	190.	184.	179.	181.	200.	204.	209.	220.	204.
5	244.	248.	236.	222.	205.	201.	198.	200.	217.	213.	224.	235.	220.
6	261.	265.	257.	254.	234.	222.	226.	219.	232.	225.	236.	253.	240.
7	260.	257.	264.	262.	260.	254.	250.	245.	252.	255.	259.	265.	257.
8	234.	231.	237.	240.	250.	259.	260.	262.	260.	262.	251.	246.	249.
9	227.	230.	230.	235.	235.	241.	248.	246.	246.	236.	227.	226.	235.
10	253.	261.	257.	254.	243.	235.	233.	234.	241.	239.	256.	256.	247.
11	266.	277.	270.	261.	252.	244.	244.	243.	249.	260.	266.	268.	258.
12	257.	265.	260.	252.	255.	256.	259.	251.	244.	258.	254.	258.	256.
13	226.	231.	232.	232.	235.	244.	249.	247.	232.	238.	230.	226.	235.
14	206.	209.	211.	216.	212.	218.	225.	228.	215.	218.	210.	206.	214.
15	190.	192.	195.	199.	201.	205.	208.	210.	200.	203.	196.	192.	199.
16	167.	167.	173.	177.	190.	198.	203.	201.	186.	182.	169.	161.	181.
17	144.	135.	145.	154.	178.	193.	194.	184.	166.	151.	146.	146.	161.
18	97.	86.	103.	119.	158.	180.	183.	164.	155.	111.	91.	103.	129.
0	228.	226.	228.	229.	230.	233.	233.	236.	233.	230.	227.	227.	230.

ALL GLOBE ZONAL AVERAGE EMITTED EXITANCE W/m^2

ZONE	7/76	8/76	9/76	10/76	11/76	12/76	1/77	2/77	3/77	4/77	5/77	6/77	YEAR 2
1	206.	189.	187.	175.	176.	219.	197.	166.	157.	167.	186.	203.	186.
2	214.	203.	194.	176.	169.	166.	170.	159.	162.	178.	191.	207.	182.
3	227.	216.	206.	184.	174.	167.	169.	168.	173.	192.	207.	218.	192.
4	224.	225.	213.	194.	187.	179.	174.	176.	188.	200.	214.	221.	200.
5	241.	241.	230.	210.	201.	189.	185.	192.	202.	215.	223.	231.	213.
6	259.	259.	251.	240.	229.	219.	209.	221.	229.	233.	236.	249.	236.
7	263.	263.	260.	260.	257.	253.	248.	260.	265.	260.	261.	264.	259.
8	239.	239.	241.	246.	248.	256.	272.	275.	271.	269.	256.	246.	255.
9	225.	229.	232.	232.	232.	239.	250.	245.	241.	241.	234.	232.	236.
10	260.	256.	260.	249.	243.	238.	229.	230.	225.	236.	254.	257.	245.
11	267.	273.	267.	262.	254.	250.	243.	245.	248.	256.	264.	266.	258.
12	261.	261.	253.	250.	251.	260.	257.	258.	262.	261.	255.	258.	257.
13	230.	231.	229.	227.	230.	238.	244.	247.	246.	239.	230.	227.	235.
14	202.	208.	210.	210.	211.	210.	220.	223.	221.	213.	210.	206.	212.
15	189.	190.	193.	196.	200.	206.	208.	209.	205.	202.	196.	192.	199.
16	159.	163.	168.	178.	188.	198.	201.	195.	191.	183.	171.	166.	180.
17	141.	132.	139.	154.	177.	195.	195.	181.	163.	149.	147.	149.	160.
18	94.	87.	94.	119.	160.	185.	185.	161.	134.	119.	95.	100.	128.
0	226.	228.	228.	230.	231.	233.	233.	234.	231.	227.	225.	226.	229.

Table 3b.

ALL GLOBE ZONAL AVERAGE ALBEDO W/m^2

ZONE	7/75	8/75	9/75	10/75	11/75	12/75	1/76	2/76	3/76	4/76	5/76	6/76	YEAR 1
1	.809	.642	.428	I	I	I	I	I	.491	.536	.754	.861	.731
2	.506	.484	.668	.835	I	I	I	.780	.584	.654	.652	.570	.584
3	.400	.407	.438	.515	.623	.762	.755	.552	.654	.546	.503	.428	.475
4	.382	.402	.382	.430	.507	.599	.587	.492	.545	.434	.416	.403	.431
5	.338	.329	.331	.349	.398	.423	.428	.416	.399	.373	.347	.348	.362
6	.263	.260	.286	.288	.339	.374	.356	.371	.351	.338	.306	.284	.310
7	.246	.257	.253	.259	.268	.290	.303	.300	.279	.260	.249	.243	.264
8	.266	.275	.255	.256	.257	.251	.250	.227	.220	.205	.228	.242	.244
9	.257	.264	.259	.254	.264	.262	.237	.229	.239	.236	.264	.266	.253
10	.228	.219	.212	.213	.226	.243	.246	.235	.237	.230	.213	.224	.227
11	.227	.217	.222	.228	.238	.247	.238	.231	.232	.212	.212	.221	.228
12	.254	.253	.248	.244	.223	.217	.210	.229	.263	.242	.255	.242	.237
13	.307	.304	.296	.299	.279	.255	.243	.264	.301	.285	.295	.292	.280
14	.385	.370	.349	.337	.343	.317	.307	.324	.336	.366	.380	.377	.338
15	.458	.444	.445	.462	.453	.432	.427	.416	.361	.411	.437	.501	.432
16	.743	.666	.591	.571	.522	.482	.447	.437	.359	.547	.698	.795	.495
17	I	.868	.773	.668	.679	.659	.646	.654	.591	.861	I	I	.665
18	I	I	.295	.718	.796	.822	.792	.714	.331	I	I	I	.757
0	.303	.298	.301	.297	.304	.303	.297	.292	.291	.300	.312	.314	.301

ALL GLOBE ZONAL AVERAGE ALBEDO W/m^2

ZONE	7/76	8/76	9/76	10/76	11/76	12/76	1/77	2/77	3/77	4/77	5/77	6/77	YEAR 2
1	.847	.595	.458	I	I	I	I	I	.890	.596	.756	.855	.748
2	.498	.508	.658	.874	I	I	I	.880	.804	.658	.650	.556	.593
3	.387	.404	.410	.559	.648	.626	.719	.595	.577	.546	.490	.426	.465
4	.399	.380	.380	.457	.524	.564	.571	.533	.496	.442	.399	.395	.427
5	.345	.337	.337	.378	.397	.413	.458	.426	.410	.370	.350	.356	.369
6	.266	.275	.287	.309	.340	.354	.395	.348	.339	.324	.306	.292	.311
7	.242	.235	.250	.259	.277	.283	.304	.290	.264	.260	.245	.249	.260
8	.255	.244	.241	.239	.254	.242	.219	.214	.197	.200	.215	.244	.230
9	.267	.256	.253	.254	.266	.257	.232	.238	.232	.229	.245	.254	.248
10	.218	.227	.209	.220	.232	.241	.255	.248	.254	.247	.218	.226	.233
11	.206	.220	.220	.218	.225	.228	.233	.221	.221	.225	.216	.226	.222
12	.249	.247	.252	.228	.217	.197	.208	.217	.217	.233	.254	.249	.227
13	.303	.293	.293	.292	.282	.263	.263	.266	.275	.286	.303	.298	.281
14	.361	.357	.347	.344	.333	.340	.322	.315	.343	.375	.382	.388	.342
15	.475	.431	.432	.445	.440	.433	.418	.400	.414	.406	.432	.470	.427
16	.804	.647	.581	.545	.510	.478	.440	.435	.461	.540	.658	.647	.494
17	I	.900	.800	.688	.673	.671	.640	.627	.680	.861	I	I	.670
18	I	I	.303	.641	.808	.834	.790	.720	.462	I	I	I	.760
0	.305	.294	.295	.298	.300	.304	.294	.286	.287	.298	.310	.309	.298

Table 3c.

ALL GLOBE ZONAL AVERAGE NET RADIATION W/m^2

ZONE	7/75	8/75	9/75	10/75	11/75	12/75	1/76	2/76	3/76	4/76	5/76	6/76	YEAR 1
1	-118.	-90.	-130.	-210.	-171.	-179.	-174.	-178.	-138.	-56.	-77.	-132.	-138.
2	15.	-52.	-146.	-176.	-167.	-164.	-168.	-154.	-130.	-89.	-47.	7.	-106.
3	45.	-16.	-82.	-142.	-163.	-162.	-161.	-130.	-125.	-53.	5.	55.	-77.
4	52.	3.	-49.	-105.	-146.	-160.	-148.	-107.	-90.	-3.	49.	68.	-53.
5	68.	30.	-16.	-67.	-109.	-128.	-115.	-74.	-35.	35.	76.	82.	-21.
6	88.	57.	10.	-41.	-81.	-98.	-87.	-42.	-2.	55.	89.	94.	4.
7	91.	73.	38.	-2.	-44.	-64.	-52.	-8.	32.	70.	89.	92.	26.
8	94.	90.	79.	52.	13.	-10.	-1.	36.	68.	91.	96.	93.	59.
9	82.	85.	91.	81.	62.	47.	56.	80.	88.	97.	85.	77.	77.
10	35.	50.	80.	95.	100.	98.	102.	110.	95.	80.	46.	28.	77.
11	-17.	5.	49.	85.	105.	115.	119.	112.	81.	40.	-2.	-25.	56.
12	-60.	-31.	25.	81.	121.	136.	133.	104.	56.	-2.	-46.	-68.	37.
13	-87.	-53.	6.	63.	116.	140.	132.	82.	29.	-34.	-77.	-94.	18.
14	-124.	-88.	-24.	42.	101.	135.	121.	56.	1.	-77.	-117.	-132.	-9.
15	-153.	-123.	-69.	-13.	49.	86.	70.	13.	-29.	-112.	-149.	-165.	-50.
16	-162.	-146.	-107.	-51.	18.	68.	59.	-10.	-54.	-142.	-162.	-159.	-71.
17	-130.	-133.	-125.	-73.	-39.	-10.	-23.	-80.	-109.	-147.	-126.	-146.	-95.
18	-97.	-120.	-78.	-58.	-67.	-82.	-79.	-81.	-101.	-151.	-91.	-103.	-92.
0	20.	21.	15.	11.	5.	0.	2.	2.	9.	12.	15.	17.	11.

ALL GLOBE ZONAL AVERAGE NET RADIATION W/m^2

ZONE	7/76	8/76	9/76	10/76	11/76	12/76	1/77	2/77	3/77	4/77	5/77	6/77	YEAR 2
1	-133.	-63.	-135.	-203.	-176.	-219.	-197.	-176.	-152.	-68.	-79.	-128.	-144.
2	18.	-48.	-143.	-171.	-169.	-166.	-180.	-156.	-141.	-87.	-42.	17.	-106.
3	48.	-11.	-80.	-139.	-163.	-163.	-164.	-137.	-99.	-52.	9.	59.	-74.
4	52.	12.	-43.	-102.	-144.	-154.	-141.	-107.	-66.	-2.	52.	71.	-48.
5	68.	34.	-12.	-63.	-104.	-115.	-106.	-68.	-24.	34.	75.	82.	-17.
6	89.	56.	15.	-34.	-77.	-91.	-78.	-38.	4.	54.	89.	94.	7.
7	90.	78.	44.	-0.	-43.	-60.	-50.	-20.	25.	66.	90.	90.	26.
8	94.	95.	82.	53.	16.	-4.	-2.	28.	68.	87.	97.	92.	59.
9	80.	89.	92.	84.	64.	51.	57.	78.	95.	95.	86.	76.	79.
10	31.	52.	79.	96.	97.	96.	102.	108.	104.	76.	46.	26.	76.
11	-12.	9.	52.	89.	109.	118.	122.	114.	88.	39.	-1.	-25.	58.
12	-63.	-26.	31.	90.	128.	143.	136.	103.	57.	-2.	-47.	-70.	40.
13	-90.	-50.	10.	71.	119.	142.	127.	81.	24.	-36.	-79.	-97.	18.
14	-117.	-85.	-23.	44.	107.	132.	118.	65.	-7.	-74.	-117.	-134.	-8.
15	-153.	-119.	-65.	-5.	56.	85.	74.	21.	-47.	-110.	-149.	-163.	-48.
16	-156.	-142.	-100.	-44.	25.	69.	64.	-3.	-80.	-142.	-162.	-162.	-69.
17	-125.	-130.	-121.	-78.	-35.	-20.	-21.	-69.	-119.	-145.	-128.	-149.	-95.
18	-94.	-119.	-70.	-42.	-75.	-93.	-80.	-80.	-91.	-148.	-95.	-100.	-91.
0	21.	21.	17.	10.	5.	-0.	2.	6.	12.	17.	18.	20.	13.

9:00 to 15:00 local), the results are more model sensitive. Both these problems occur with N-6 near the poles. One concludes that more measurements are needed to get more accuracy in these regions of low sun angles.

These results are very similar to Jacobowitz et al. (1978) except that we show larger gradients and higher peaks. This of course is produced by the analysis scheme. The variation of the albedo is significantly different in some details, Fig. 10. Our albedo estimate shows more variation in the tropical region, 30^oN to 30^oS, although this may be due to the contour interval chosen. This is evident in June and July, 1975 where we estimate the albedo at 5^oN to be 27% and this feature is missed by the Jacobowitz et al. analysis.

The analysis by Winston et al., 1979 also covers this time period. Their results are from high resolution scanning instruments with narrow spectral responses. We have not done a detailed comparison with their results but Fig. 11 shows their estimate of net radiation. Of course the basic pattern is synchronized with the sun, but the net radiation gained in the tropics is less and more is lost in the polar regions. This corresponds to the reported global and time average net radiation loss to space, whereas our results are biased the other way. A detailed comparison of the maps would be very interesting to determine if the differences are just systematic over the whole globe or whether the differences are concentrated in particular regions and perhaps caused by the spectral response differences. Ramanathan and Breigleib (1980) at NCAR are undertaking a study of this kind.

ZONAL REGIONS

Campbell and Vonder Haar (1980b) showed from the climatology that a fruitful first regional separation is the averages over land and ocean

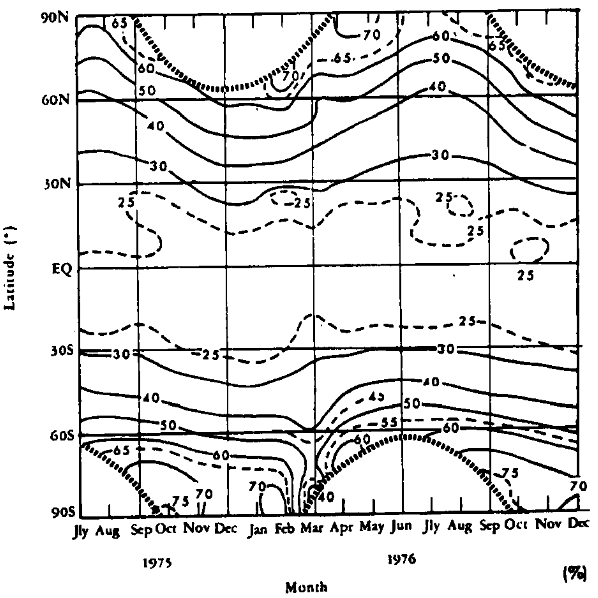

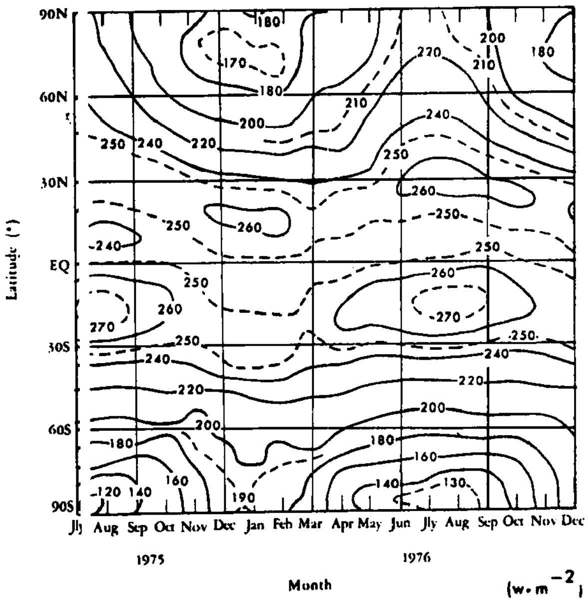

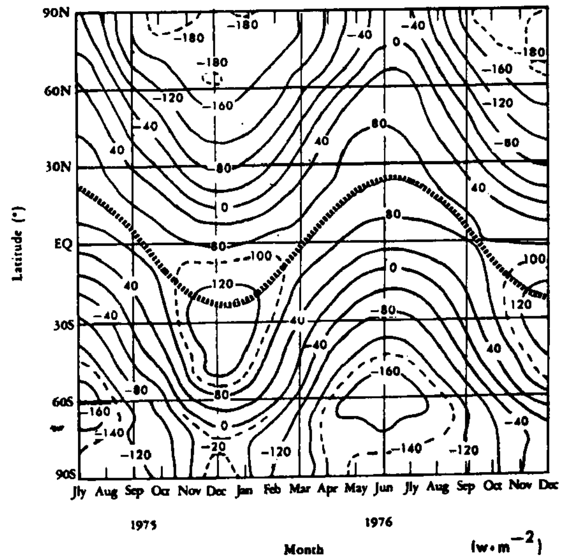

Fig. 10. Estimates from Jacobowitz et al., 1979 of the 18 months of zonal mean albedo, emitted exitance and net radiation.

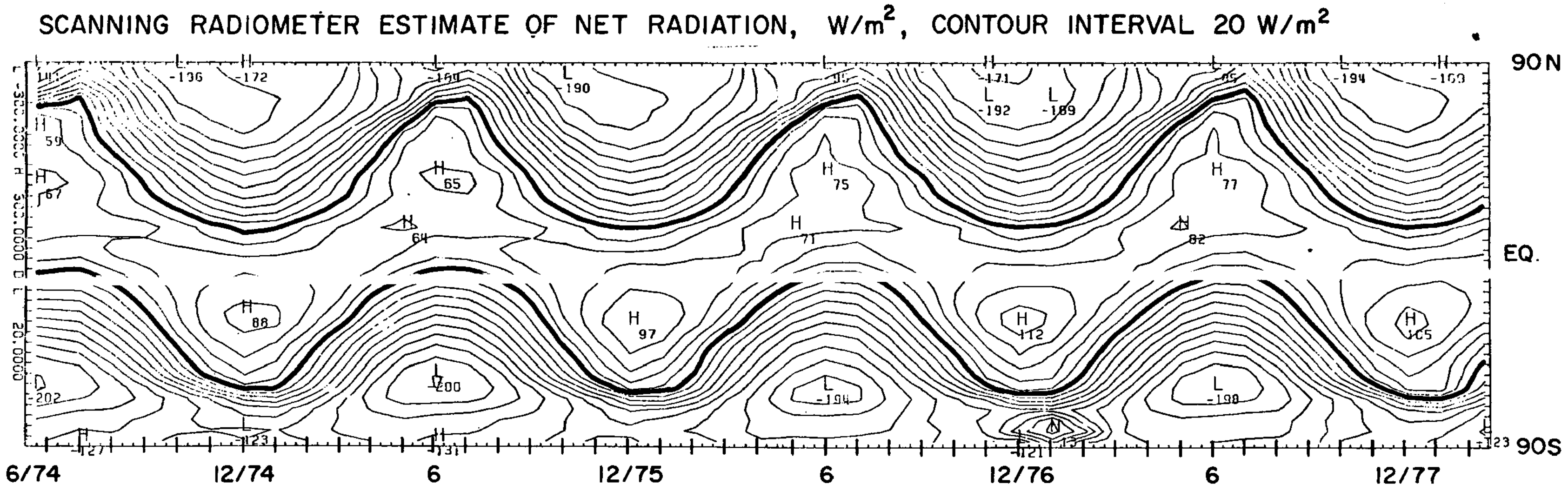

Fig. 11. Scanning radiometer estimates of zonal average net radiation. This data set overlaps with the Nimbus 6 observations.

surfaces. Figures 12 and 13 a, b, and c and Tables 4 and 5 show the two year time sequence of emitted and reflected exitance and net radiation. The annual cycle synchronized with the sun is obvious. As seen in the climatology the variation of seasonal changes over land generally has a higher amplitude than over ocean as one would expect from the differences in heat capacity. In fact, the emitted component over the ocean shows a very weak seasonal change south of the equator from 0^{o}S to 50^{o}S. The northern tropical oceans (0-30^{o}N) show bigger changes but are rather disorganized. North of 30^{o}N and south of 50^{o}S one sees the seasonal change with matching changes in sea and air temperature. In contrast the seasonal wave in emitted is clear in all land regions.

The time change in albedo from 45^{o}N to 45^{o}S is partly modulated by solar illumination angle and mean weather changes. Again one sees bigger changes over the land than ocean. The patterns though are rather disorganized. In the polar regions (45^{o} and poleward) the time change is dominated by the directional reflectance effect. Snow may cause the increase in albedo in spring over fall but this resolution data does not allow observation of a snow line.

The net flux shows very large seasonal change of course produced by changes in daily average solar insolation. The near symmetry in the ocean pattern shows that the southern and northern ocean climates are very similar. In fact, most of the difference between the southern maxima (147 + 151)/2 = 151 and northern (129 + 124)/2 = 126 can be explained by earth sun distance changes (7%*solar constant * (1-albedo) ≈ 19 W/m^2). In contrast, the land zonal averages are much different because the ocean like climate dominates the small amount of land south of 35^{o}S.

Also presented are the year to year differences (Fig. 14). If one compares individual points, the difference from year to year of the fields

Fig. 12a

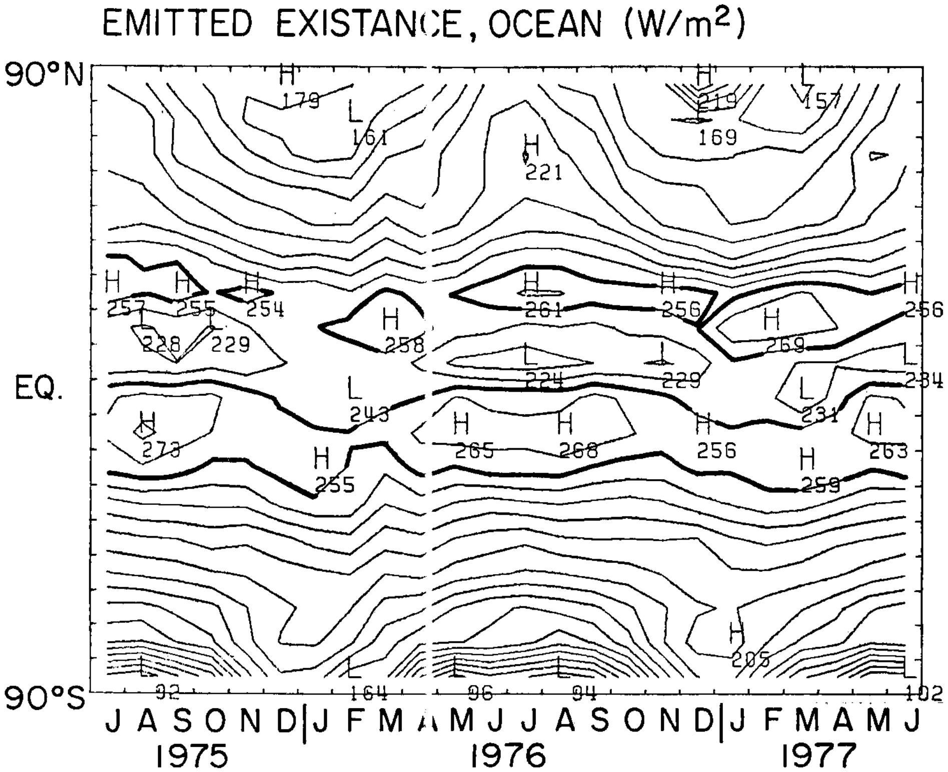

Fig. 13a

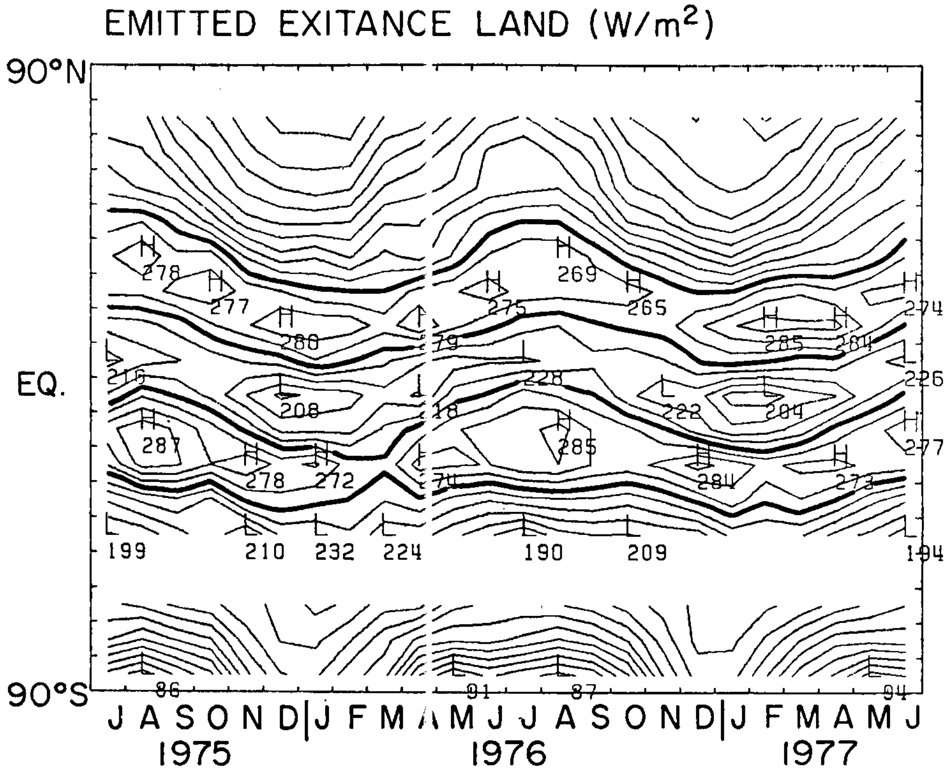

Fig. 12. Zonal average of exitance, albedo and net for just ocean regions.

Fig. 12b

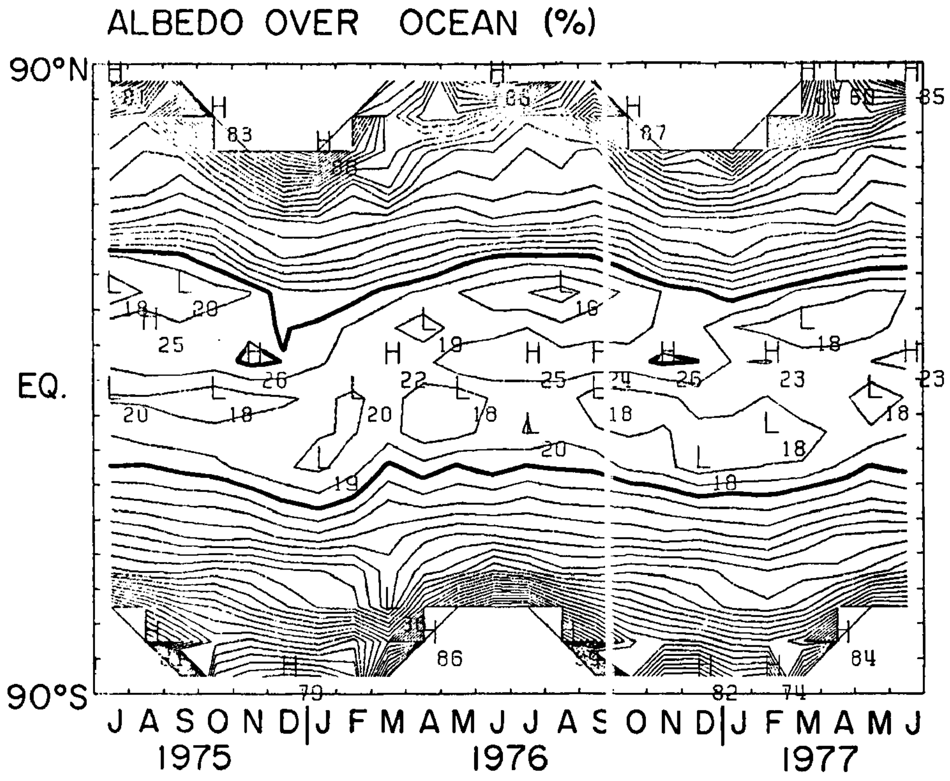

Fig. 13b

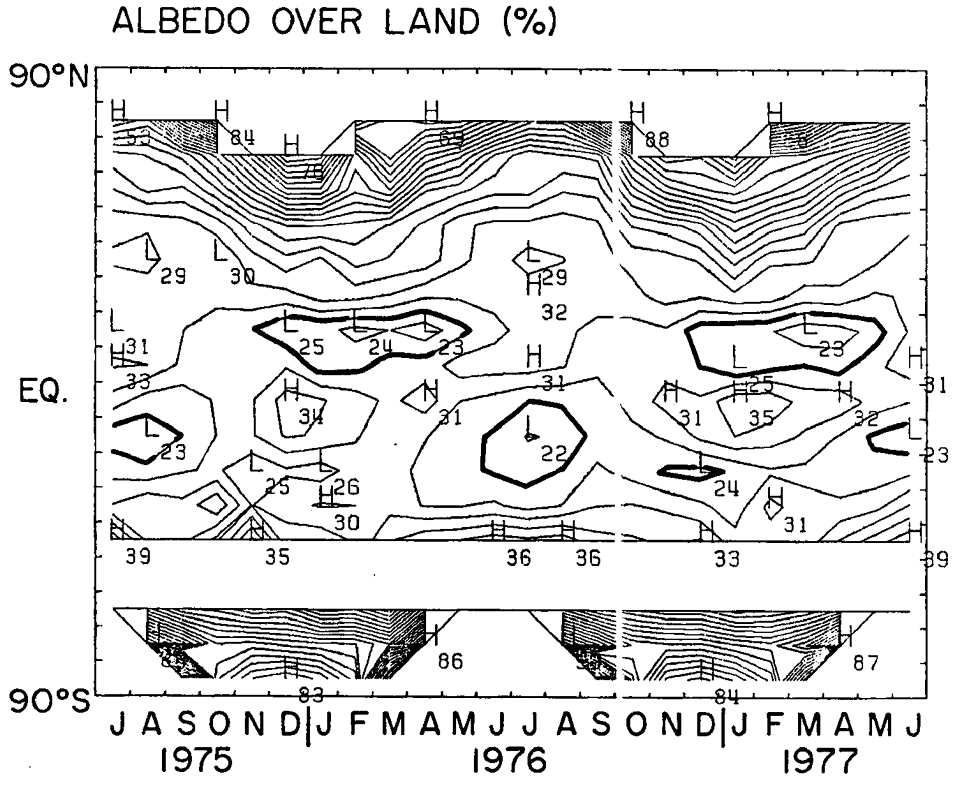

Fig. 13. Zonal average of exitanc: albedo and net for just land regions.

Fig. 12c

NET OVER OCEAN (W/m2)

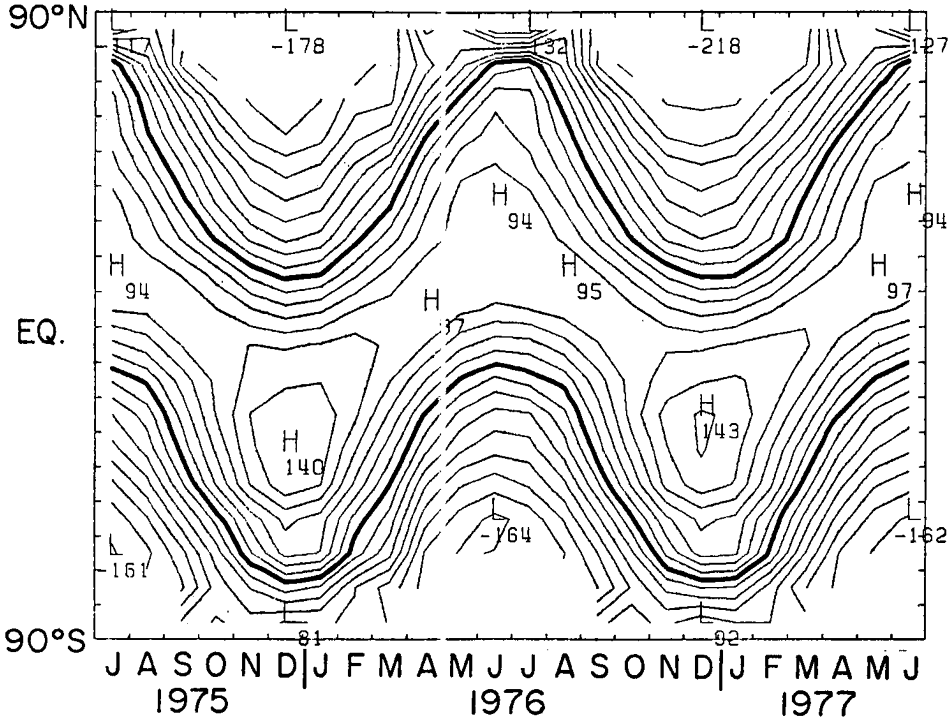

Fig. 13c

NET OVER LAND (W/m2)

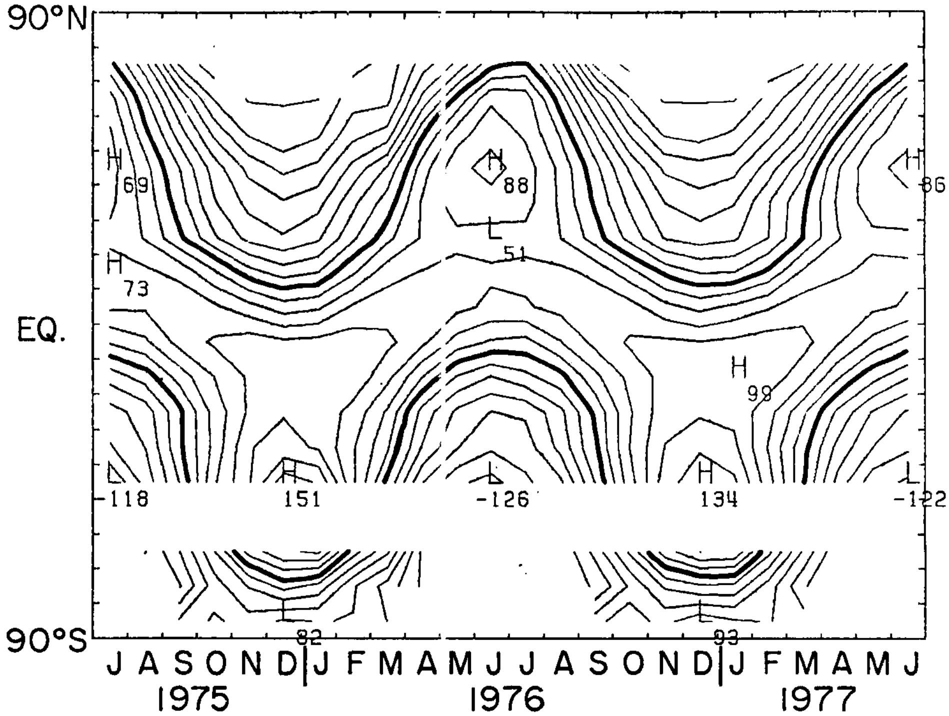

Table 4a.

OCEAN ZONAL AVERAGE EMITTED EXITANCE W/m^2

ZONE	7/75	8/75	9/75	10/75	11/75	12/75	1/76	2/76	3/76	4/76	5/76	6/76	YEAR 1
1	210.	202.	185.	178.	171.	179.	174.	170.	162.	170.	184.	204.	182.
2	214.	215.	198.	184.	168.	167.	163.	161.	176.	183.	196.	211.	186.
3	216.	216.	197.	193.	182.	173.	164.	168.	189.	192.	207.	211.	192.
4	224.	221.	210.	203.	197.	192.	190.	186.	198.	197.	203.	212.	203.
5	225.	230.	222.	215.	208.	205.	199.	199.	213.	202.	209.	220.	212.
6	251.	249.	249.	239.	228.	221.	223.	219.	231.	223.	229.	242.	234.
7	257.	251.	255.	249.	254.	249.	249.	241.	252.	248.	251.	255.	251.
8	233.	228.	234.	229.	239.	247.	250.	253.	258.	253.	244.	242.	243.
9	231.	232.	230.	235.	232.	239.	244.	245.	247.	238.	227.	225.	235.
10	259.	263.	261.	263.	254.	249.	243.	243.	248.	250.	261.	257.	254.
11	261.	273.	266.	260.	255.	252.	251.	251.	253.	263.	265.	264.	259.
12	255.	259.	254.	247.	249.	253.	255.	249.	242.	254.	249.	255.	252.
13	226.	231.	231.	232.	233.	242.	249.	247.	230.	236.	229.	225.	234.
14	206.	209.	210.	215.	212.	218.	224.	228.	215.	218.	210.	206.	214.
15	190.	192.	195.	199.	201.	205.	208.	210.	200.	203.	196.	192.	199.
16	167.	167.	173.	177.	190.	198.	203.	201.	186.	182.	170.	161.	181.
17	152.	150.	161.	168.	187.	201.	202.	192.	174.	163.	160.	159.	172.
18	98.	92.	109.	126.	166.	188.	186.	164.	165.	120.	96.	108.	135.
0	228.	227.	228.	228.	227.	229.	231.	232.	230.	228.	226.	228.	229.

OCEAN ZONAL AVERAGE EMITTED EXITANCE W/m^2

ZONE	7/76	8/76	9/76	10/76	11/76	12/76	1/77	2/77	3/77	4/77	5/77	6/77	YEAR 2
1	206.	189.	187.	175.	176.	219.	197.	166.	157.	167.	186.	203.	186.
2	215.	205.	196.	178.	170.	169.	171.	164.	163.	178.	195.	208.	184.
3	221.	211.	208.	186.	179.	177.	180.	185.	181.	192.	211.	209.	195.
4	218.	215.	210.	198.	193.	191.	184.	183.	190.	193.	206.	211.	199.
5	225.	225.	221.	211.	199.	193.	190.	192.	197.	202.	212.	217.	207.
6	247.	247.	241.	236.	224.	218.	209.	217.	226.	230.	228.	236.	230.
7	261.	261.	256.	256.	256.	255.	246.	257.	261.	257.	251.	256.	256.
8	237.	239.	237.	242.	244.	250.	268.	269.	265.	260.	250.	245.	250.
9	224.	227.	230.	231.	229.	235.	248.	242.	240.	240.	234.	234.	234.
10	256.	255.	264.	258.	253.	245.	241.	243.	231.	244.	262.	259.	251.
11	264.	268.	267.	261.	256.	256.	252.	254.	253.	258.	263.	262.	259.
12	256.	256.	248.	246.	245.	253.	251.	255.	259.	258.	251.	256.	253.
13	229.	230.	228.	226.	229.	236.	241.	246.	244.	237.	230.	228.	234.
14	202.	209.	210.	210.	210.	210.	219.	223.	220.	213.	210.	207.	212.
15	189.	190.	193.	196.	200.	206.	208.	209.	205.	202.	196.	192.	199.
16	159.	163.	168.	178.	189.	199.	201.	195.	191.	183.	171.	166.	180.
17	154.	143.	151.	166.	189.	205.	205.	191.	178.	173.	161.	165.	173.
18	101.	94.	100.	127.	165.	190.	193.	168.	142.	132.	102.	102.	135.
0	228.	229.	228.	229.	229.	230.	230.	230.	229.	226.	225.	227.	228.

Table 4b.

OCEAN ZONAL AVERAGE ALBEDO W/m^2

ZONE	7/75	8/75	9/75	10/75	11/75	12/75	1/76	2/76	3/76	4/76	5/76	6/76	YEAR 1
1	.808	.640	.427	I	I	I	I	I	.491	.535	.754	.861	.730
2	.498	.480	.661	.832	I	I	I	.804	.551	.640	.639	.556	.572
3	.473	.450	.458	.561	.682	.803	.885	.655	.567	.507	.469	.476	.494
4	.445	.443	.409	.443	.511	.606	.574	.464	.534	.447	.436	.444	.456
5	.383	.367	.356	.370	.406	.417	.427	.412	.399	.379	.373	.396	.385
6	.222	.229	.240	.270	.341	.380	.369	.353	.325	.304	.275	.248	.283
7	.181	.201	.200	.212	.223	.265	.271	.266	.237	.219	.200	.186	.217
8	.241	.248	.230	.241	.246	.251	.245	.218	.203	.188	.207	.213	.226
9	.230	.241	.245	.238	.257	.249	.228	.217	.221	.217	.245	.249	.236
10	.197	.197	.188	.181	.190	.196	.205	.196	.209	.188	.182	.203	.194
11	.223	.210	.210	.207	.212	.211	.201	.199	.210	.184	.190	.210	.206
12	.251	.253	.241	.234	.214	.202	.195	.213	.257	.234	.254	.240	.229
13	.308	.302	.295	.293	.279	.251	.235	.259	.302	.287	.297	.294	.278
14	.385	.373	.351	.341	.342	.320	.309	.326	.337	.368	.382	.378	.340
15	.458	.444	.445	.462	.453	.432	.427	.416	.361	.411	.437	.501	.432
16	.746	.668	.593	.573	.524	.480	.447	.437	.357	.546	.698	.797	.495
17	I	.808	.731	.640	.661	.630	.612	.663	.551	.864	I	I	.641
18	I	I	.307	.733	.769	.786	.778	.727	.363	I	I	I	.743
0	0.	0.	0.	0.	0.	0.	0.	0.	0.	0.	0.	0.	0.

OCEAN ZONAL AVERAGE ALBEDO W/m^2

ZONE	7/76	8/76	9/76	10/76	11/76	12/76	1/77	2/77	3/77	4/77	5/77	6/77	YEAR 2
1	.847	.597	.461	I	I	I	I	I	.890	.597	.755	.855	.749
2	.482	.497	.648	.874	I	I	I	.882	.795	.645	.640	.538	.580
3	.447	.463	.435	.569	.671	.618	.751	.577	.521	.504	.456	.474	.480
4	.431	.438	.425	.450	.510	.553	.548	.498	.462	.460	.421	.426	.446
5	.389	.380	.365	.381	.410	.412	.411	.403	.405	.417	.377	.396	.392
6	.238	.246	.249	.282	.345	.356	.379	.344	.323	.299	.278	.275	.290
7	.175	.162	.187	.205	.226	.242	.269	.246	.219	.209	.199	.199	.207
8	.225	.207	.215	.211	.231	.231	.201	.192	.178	.180	.189	.210	.205
9	.249	.239	.241	.241	.256	.251	.224	.227	.215	.216	.225	.232	.234
10	.203	.213	.184	.187	.194	.209	.208	.199	.223	.211	.181	.202	.201
11	.198	.216	.203	.197	.202	.194	.192	.182	.188	.205	.204	.223	.199
12	.253	.246	.244	.217	.209	.184	.195	.201	.202	.226	.253	.242	.218
13	.307	.295	.292	.291	.281	.260	.264	.260	.274	.287	.304	.294	.280
14	.361	.357	.347	.345	.334	.341	.324	.317	.347	.378	.383	.388	.343
15	.475	.431	.432	.445	.440	.433	.418	.400	.414	.406	.432	.470	.427
16	.805	.648	.582	.545	.510	.476	.438	.432	.458	.538	.660	.651	.493
17	I	.900	.778	.654	.631	.626	.586	.578	.617	.839	I	I	.625
18	I	I	.318	.630	.814	.821	.720	.739	.457	I	I	I	.743
0	0.	0.	0.	0.	0.	0.	0.	0.	0.	0.	0.	0.	0.

Table 4c.

OCEAN ZONAL AVERAGE NET RADIATION W/m^2

ZONE	7/75	8/75	9/75	10/75	11/75	12/75	1/76	2/76	3/76	4/76	5/76	6/76	YEAR 1
1	-118.	-90.	-130.	-207.	-171.	-179.	-174.	-172.	-138.	-56.	-77.	-132.	-137.
2	18.	-51.	-147.	-178.	-172.	-167.	-168.	-157.	-128.	-88.	-43.	13.	-106.
3	21.	-26.	-81.	-148.	-172.	-171.	-162.	-141.	-113.	-40.	18.	42.	-81.
4	31.	-8.	-48.	-108.	-153.	-169.	-158.	-108.	-86.	-1.	46.	56.	-59.
5	66.	32.	-11.	-65.	-112.	-132.	-116.	-73.	-31.	43.	79.	74.	-21.
6	117.	87.	34.	-20.	-76.	-98.	-86.	-37.	8.	72.	111.	123.	19.
7	124.	104.	69.	27.	-25.	-52.	-42.	7.	47.	96.	121.	129.	50.
8	105.	104.	94.	69.	28.	2.	11.	49.	78.	108.	112.	110.	72.
9	89.	93.	97.	88.	67.	53.	64.	87.	94.	104.	92.	85.	84.
10	41.	58.	87.	100.	105.	104.	110.	119.	100.	86.	53.	34.	63.
11	-11.	12.	58.	95.	115.	124.	129.	119.	87.	48.	7.	-18.	64.
12	-58.	-25.	34.	90.	132.	147.	144.	113.	61.	5.	-41.	-64.	45.
13	-88.	-52.	7.	65.	118.	144.	136.	84.	29.	-34.	-77.	-94.	20.
14	-125.	-88.	-25.	41.	101.	135.	120.	55.	1.	-77.	-117.	-132.	-9.
15	-153.	-123.	-69.	-13.	49.	86.	70.	13.	-29.	-112.	-149.	-165.	-50.
16	-163.	-146.	-108.	-51.	18.	69.	59.	-10.	-54.	-142.	-162.	-160.	-71.
17	-130.	-147.	-136.	-80.	-40.	-3.	-14.	-91.	-112.	-159.	-129.	-159.	-100.
18	-98.	-148.	-85.	-68.	-63.	-70.	-75.	-85.	-114.	-175.	-96.	-108.	-99.
0	25.	26.	21.	19.	13.	7.	7.	9.	17.	20.	20.	22.	18.

OCEAN ZONAL AVERAGE NET RADIATION W/m^2

ZONE	7/76	8/76	9/76	10/76	11/76	12/76	1/77	2/77	3/77	4/77	5/77	6/77	YEAR 2
1	-133.	-64.	-136.	-205.	-176.	-219.	-197.	-170.	-152.	-68.	-80.	-128.	-144.
2	24.	-47.	-143.	-174.	-173.	-169.	-186.	-161.	-141.	-85.	-42.	25.	-106.
3	28.	-26.	-86.	-142.	-169.	-174.	-175.	-152.	-97.	-39.	20.	44.	-81.
4	43.	0.	-52.	-105.	-148.	-165.	-150.	-110.	-61.	-2.	50.	65.	-53.
5	63.	32.	-13.	-64.	-105.	-119.	-105.	-63.	-18.	28.	75.	77.	-18.
6	114.	82.	39.	-21.	-73.	-90.	-74.	-32.	13.	67.	109.	115.	21.
7	123.	112.	74.	23.	-27.	-52.	-38.	-1.	46.	91.	121.	121.	49.
8	109.	112.	97.	68.	28.	6.	8.	43.	82.	104.	114.	108.	73.
9	88.	98.	99.	91.	71.	57.	62.	85.	104.	103.	94.	83.	86.
10	41.	59.	85.	102.	104.	103.	111.	117.	112.	83.	52.	32.	83.
11	-5.	15.	60.	99.	119.	128.	133.	124.	96.	45.	4.	-20.	66.
12	-59.	-20.	39.	99.	138.	156.	148.	112.	66.	4.	-43.	-66.	48.
13	-90.	-50.	12.	72.	121.	145.	130.	84.	26.	-35.	-79.	-97.	20.
14	-118.	-85.	-23.	44.	107.	132.	118.	65.	-8.	-74.	-118.	-134.	-8.
15	-153.	-119.	-65.	-5.	56.	85.	74.	21.	-47.	-110.	-149.	-163.	-48.
16	-156.	-142.	-101.	-44.	24.	70.	65.	-2.	-80.	-143.	-162.	-163.	-69.
17	-128.	-141.	-130.	-82.	-29.	-5.	-5.	-64.	-125.	-168.	-132.	-165.	-98.
18	-101.	-141.	-76.	-47.	-82.	-91.	-54.	-93.	-98.	-194.	-102.	-102.	-98.
0	26.	27.	24.	16.	13.	5.	9.	13.	19.	23.	23.	24.	19.

Table 5a.

LAND ZONAL AVERAGE EMITTED EXITANCE W/m^2

ZONE	7/75	8/75	9/75	10/75	11/75	12/75	1/76	2/76	3/76	4/76	5/76	6/76	YEAR 1
1	I	I	I	I	I	I	I	I	I	I	I	I	I
2	212.	213.	190.	179.	165.	157.	155.	152.	170.	174.	192.	205.	180.
3	226.	221.	203.	191.	173.	164.	166.	164.	185.	194.	205.	222.	193.
4	236.	228.	222.	202.	187.	179.	174.	179.	201.	207.	212.	224.	204.
5	256.	260.	245.	227.	204.	198.	197.	200.	219.	219.	233.	245.	225.
6	268.	278.	263.	266.	239.	223.	229.	219.	232.	227.	241.	261.	245.
7	263.	264.	274.	277.	267.	260.	252.	249.	251.	264.	269.	275.	264.
8	234.	236.	244.	259.	268.	280.	278.	277.	265.	279.	263.	253.	261.
9	216.	225.	229.	234.	241.	245.	260.	250.	242.	232.	225.	229.	236.
10	241.	258.	249.	237.	220.	208.	212.	216.	226.	218.	246.	252.	232.
11	277.	287.	278.	264.	247.	226.	227.	226.	242.	254.	268.	276.	256.
12	262.	285.	282.	270.	278.	267.	272.	255.	253.	274.	272.	270.	270.
13	222.	233.	239.	228.	254.	258.	253.	250.	241.	248.	236.	231.	241.
14	199.	204.	217.	227.	210.	233.	232.	239.	224.	225.	213.	202.	219.
15	I	I	I	I	I	I	I	I	I	I	I	I	I
16	158.	163.	172.	177.	188.	192.	203.	198.	184.	183.	162.	158.	178.
17	142.	131.	142.	150.	175.	191.	193.	181.	164.	148.	142.	143.	159.
18	97.	86.	102.	118.	157.	179.	182.	164.	154.	110.	91.	102.	129.
0	230.	227.	230.	233.	236.	240.	235.	242.	241.	237.	232.	229.	234.

LAND ZONAL AVERAGE EMITTED EXITANCE W/m^2

ZONE	7/76	8/76	9/76	10/76	11/76	12/76	1/77	2/77	3/77	4/77	5/77	6/77	YEAR 2
1	I	I	I	I	I	I	I	I	I	I	I	I	I
2	211.	199.	191.	170.	165.	159.	166.	148.	160.	176.	182.	206.	178.
3	228.	217.	206.	184.	173.	165.	168.	166.	172.	192.	207.	219.	191.
4	227.	230.	215.	192.	185.	173.	168.	172.	187.	203.	218.	225.	200.
5	251.	250.	236.	210.	202.	186.	181.	193.	205.	223.	231.	240.	217.
6	269.	269.	259.	244.	233.	220.	210.	224.	232.	235.	242.	260.	241.
7	266.	265.	264.	265.	258.	250.	250.	264.	269.	262.	272.	274.	263.
8	243.	240.	249.	252.	255.	268.	279.	285.	282.	284.	266.	249.	263.
9	228.	232.	237.	234.	239.	249.	255.	252.	246.	246.	233.	226.	240.
10	267.	259.	252.	233.	222.	224.	205.	204.	215.	219.	238.	252.	233.
11	276.	285.	269.	263.	252.	235.	223.	226.	235.	254.	265.	277.	255.
12	278.	280.	269.	266.	273.	284.	276.	267.	273.	273.	268.	265.	273.
13	237.	239.	238.	233.	241.	253.	266.	251.	260.	250.	233.	221.	244.
14	190.	206.	210.	209.	213.	215.	233.	231.	231.	216.	207.	194.	213.
15	I	I	I	I	I	I	I	I	I	I	I	I	I
16	156.	159.	164.	174.	183.	193.	196.	191.	186.	175.	168.	160.	176.
17	137.	129.	136.	151.	174.	193.	192.	178.	159.	144.	143.	145.	157.
18	93.	87.	94.	119.	160.	185.	184.	161.	133.	118.	94.	100.	127.
0	228.	228.	232.	235.	236.	237.	241.	241.	237.	230.	228.	229.	233.

Table 5b.

LAND ZONAL AVERAGE ALBEDO W/m^2

ZONE	7/75	8/75	9/75	10/75	11/75	12/75	1/76	2/76	3/76	4/76	5/76	6/76	YEAR 1
1	I	I	I	I	I	I	I	I	I	I	I	I	I
2	.525	.492	.684	.844	I	I	I	.725	.658	.685	.681	.604	.609
3	.391	.402	.436	.510	.615	.756	.739	.539	.665	.551	.507	.422	.473
4	.350	.382	.369	.423	.505	.595	.593	.506	.550	.428	.406	.383	.418
5	.309	.305	.315	.335	.392	.428	.429	.419	.398	.370	.331	.318	.347
6	.295	.286	.323	.303	.338	.368	.346	.385	.372	.306	.331	.312	.331
7	.318	.320	.313	.312	.319	.318	.339	.338	.326	.306	.304	.308	.317
8	.311	.322	.301	.282	.276	.251	.258	.243	.250	.235	.265	.293	.275
9	.328	.325	.296	.297	.283	.296	.260	.262	.286	.286	.312	.311	.295
10	.291	.262	.260	.278	.297	.336	.327	.314	.293	.314	.276	.266	.294
11	.236	.232	.250	.276	.297	.329	.321	.303	.283	.277	.261	.246	.280
12	.265	.254	.272	.279	.255	.271	.262	.286	.288	.267	.256	.247	.268
13	.300	.323	.307	.348	.274	.291	.303	.300	.292	.273	.274	.279	.298
14	.391	.318	.309	.268	.354	.258	.259	.279	.322	.343	.350	.364	.303
15	I	I	I	I	I	I	I	I	I	I	I	I	I
16	.685	.634	.552	.542	.504	.513	.438	.448	.381	.564	.691	.762	.493
17	I	.882	.783	.675	.683	.666	.655	.652	.600	.860	I	I	.670
18	I	I	.294	.716	.799	.826	.793	.713	.328	I	I	I	.758
0	0.	0.	0.	0.	0.	0.	0.	0.	0.	0.	0.	0.	0.

LAND ZONAL AVERAGE ALBEDO W/m^2

ZONE	7/76	8/76	9/76	10/76	11/76	12/76	1/77	2/77	3/77	4/77	5/77	6/77	YEAR 2
1	I	I	I	I	I	I	I	I	I	I	I	I	I
2	.534	.534	.682	.876	I	I	I	.877	.824	.686	.671	.595	.623
3	.380	.397	.407	.557	.646	.627	.715	.597	.584	.552	.494	.420	.463
4	.383	.351	.357	.461	.531	.569	.582	.550	.513	.434	.388	.379	.417
5	.317	.310	.320	.376	.388	.414	.488	.440	.413	.341	.333	.331	.354
6	.289	.299	.317	.331	.336	.352	.408	.352	.352	.343	.328	.305	.328
7	.316	.316	.320	.319	.334	.328	.344	.338	.314	.317	.296	.304	.318
8	.309	.310	.286	.289	.296	.261	.253	.253	.230	.236	.262	.302	.274
9	.312	.302	.283	.288	.293	.274	.251	.268	.277	.265	.295	.312	.285
10	.250	.254	.257	.286	.308	.305	.347	.346	.314	.318	.290	.275	.297
11	.223	.229	.260	.266	.278	.305	.325	.311	.296	.271	.243	.232	.274
12	.237	.251	.280	.266	.246	.242	.253	.271	.268	.259	.260	.270	.258
13	.266	.277	.300	.302	.296	.281	.261	.309	.285	.281	.292	.330	.289
14	.355	.364	.334	.329	.320	.328	.284	.285	.284	.328	.365	.395	.319
15	I	I	I	I	I	I	I	I	I	I	I	I	I
16	.788	.630	.555	.532	.507	.507	.466	.477	.505	.563	.632	.589	.509
17	I	.900	.805	.696	.683	.682	.653	.639	.696	.866	I	I	.681
18	I	I	.302	.642	.808	.835	.796	.718	.462	I	I	I	.762
0	0.	0.	0.	0.	0.	0.	0.	0.	0.	0.	0.	0.	0.

Table 5c.

LAND ZONAL AVERAGE NET RADIATION W/m^2

ZONE	7/75	8/75	9/75	10/75	11/75	12/75	1/76	2/76	3/76	4/76	5/76	6/76	YEAR 1
1	I	I	I	I	I	I	I	I	I	I	I	I	I
2	8.	-53.	-143.	-173.	I	-157.	I	-147.	-134.	-91.	-56.	-6.	-95.
3	48.	-14.	-82.	-141.	-162.	-161.	-161.	-128.	-127.	-55.	3.	57.	-77.
4	63.	8.	-49.	-103.	-142.	-156.	-144.	-107.	-93.	-4.	51.	74.	-50.
5	69.	28.	-20.	-69.	-106.	-126.	-115.	-74.	-38.	30.	74.	88.	-22.
6	65.	33.	-10.	-57.	-86.	-98.	-87.	-46.	-10.	42.	71.	72.	-9.
7	54.	39.	5.	-36.	-66.	-77.	-64.	-25.	14.	42.	54.	51.	-1.
8	73.	64.	53.	23.	-12.	-31.	-22.	15.	51.	61.	67.	63.	34.
9	64.	63.	76.	64.	47.	29.	36.	62.	71.	79.	66.	55.	59.
10	23.	36.	68.	83.	91.	84.	87.	92.	85.	66.	32.	17.	64.
11	-32.	-10.	29.	60.	83.	94.	96.	95.	67.	22.	-21.	-41.	37.
12	-68.	-51.	-5.	47.	83.	99.	94.	73.	37.	-27.	-64.	-81.	11.
13	-82.	-60.	-4.	46.	99.	107.	98.	63.	23.	-41.	-79.	-97.	6.
14	-119.	-73.	-19.	57.	98.	151.	138.	64.	-3.	-79.	-116.	-127.	-2.
15	I	I	I	I	I	I	I	I	I	I	I	I	I
16	-153.	-141.	-101.	-42.	28.	57.	63.	-10.	-57.	-145.	-154.	-156.	-67.
17	I	-130.	-122.	-71.	-38.	-12.	-26.	-77.	-108.	-144.	I	-143.	-87.
18	-97.	I	-77.	-57.	-68.	-83.	-79.	-81.	-100.	I	-91.	-102.	-84.
0	10.	12.	9.	5.	4.	-3.	5.	-2.	0.	1.	7.	3.	3.

LAND ZONAL AVERAGE NET RADIATION W/m^2

ZONE	7/76	8/76	9/76	10/76	11/76	12/76	1/77	2/77	3/77	4/77	5/77	6/77	YEAR 2
1	I	I	I	I	I	I	I	I	I	I	I	I	I
2	5.	-52.	-143.	-166.	I	-159.	I	-146.	-141.	-93.	-42.	-2.	-94.
3	51.	-9.	-79.	-138.	-162.	-161.	-162.	-135.	-99.	-53.	8.	61.	-73.
4	57.	18.	-39.	-100.	-142.	-148.	-137.	-106.	-69.	-2.	52.	74.	-45.
5	71.	35.	-12.	-62.	-104.	-112.	-107.	-72.	-27.	37.	75.	86.	-16.
6	68.	36.	-4.	-44.	-80.	-92.	-82.	-42.	-3.	43.	72.	76.	-4.
7	53.	40.	11.	-26.	-61.	-69.	-63.	-40.	1.	38.	54.	55.	-1.
8	66.	65.	55.	27.	-6.	-22.	-21.	3.	43.	56.	65.	64.	33.
9	58.	67.	74.	68.	46.	34.	44.	58.	71.	75.	65.	58.	60.
10	13.	39.	66.	83.	85.	81.	85.	90.	88.	63.	34.	13.	62.
11	-26.	-6.	35.	66.	87.	96.	99.	92.	68.	24.	-11.	-38.	40.
12	-77.	-46.	4.	57.	92.	96.	94.	68.	25.	-23.	-61.	-82.	12.
13	-90.	-53.	-1.	60.	101.	118.	105.	58.	7.	-46.	-80.	-97.	7.
14	-104.	-84.	-19.	51.	111.	134.	124.	69.	2.	-67.	-112.	-123.	-1.
15	I	I	I	I	I	I	I	I	I	I	I	I	I
16	-153.	-136.	-93.	-37.	31.	60.	57.	-14.	-84.	-137.	-158.	-156.	-68.
17	I	-128.	-118.	-77.	-37.	-23.	-25.	-70.	-117.	-140.	I	-145.	-88.
18	-93.	I	-69.	-41.	-75.	-94.	-83.	-79.	-90.	I	-94.	-100.	-82.
0	12.	8.	8.	6.	6.	-2.	3.	1.	4.	7.	10.	6.	5.

is just at their relative accuracy of $\pm$ 5 W/m^2 or $\pm$ 1% for the albedo. These differences, though, are organized over large areas in space and time, making them significant.

The largest differences appear in March and are probably caused by poor data sampling in one of the two years. In the rest of the year the period from July to December shows more energy gained in 1976 than 1975. In the other six months of the year, higher net appears in the first year primarily from 40°N to 40°S. This feature appears to be caused by changes more in the emitted than in the albedo. The albedo differences are very small so one could say that there is no change in albedo from one year to the next except along the equator where it was lower the first year than the second and at 10°N where it was higher the first year. This might have been a shift northward of the convergence zone and its associated clouds.

Over the ocean these bands of difference near the equator are more obvious in the emitted and albedo. It is not apparent in the net over the ocean indicating the cause, probably a cloudiness change, showed reciprocity between emitted and absorbed damping out the change in the net. The ocean net time variation pattern is much the same as the full latitude zone in the northern hemisphere. The southern hemisphere is mostly ocean so of course they match well there. Also of interest is the emission in the first year in the northern and southern mid-latitudes.

Over the land regions the changes in emitted are larger than over the ocean, although not as simply organized in time. Figures 15 and 16 show the persistence of some of the features in the annual zonal means.

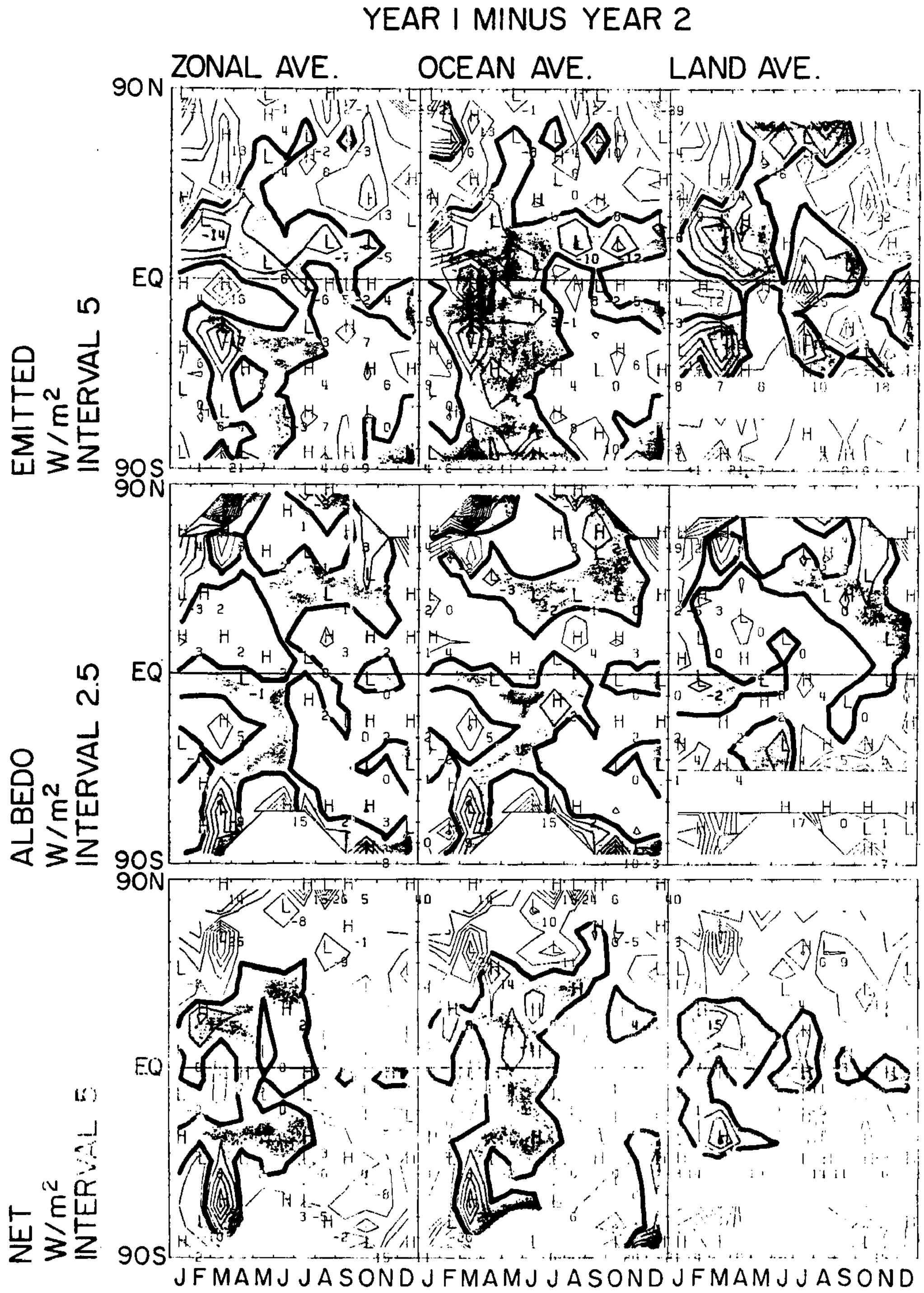

Fig. 14. Differences, year 1 minus year 2, of the zonal averages. Nine plots are presented for land, ocean and all latitude zone and for emitted, albedo and net radiation.

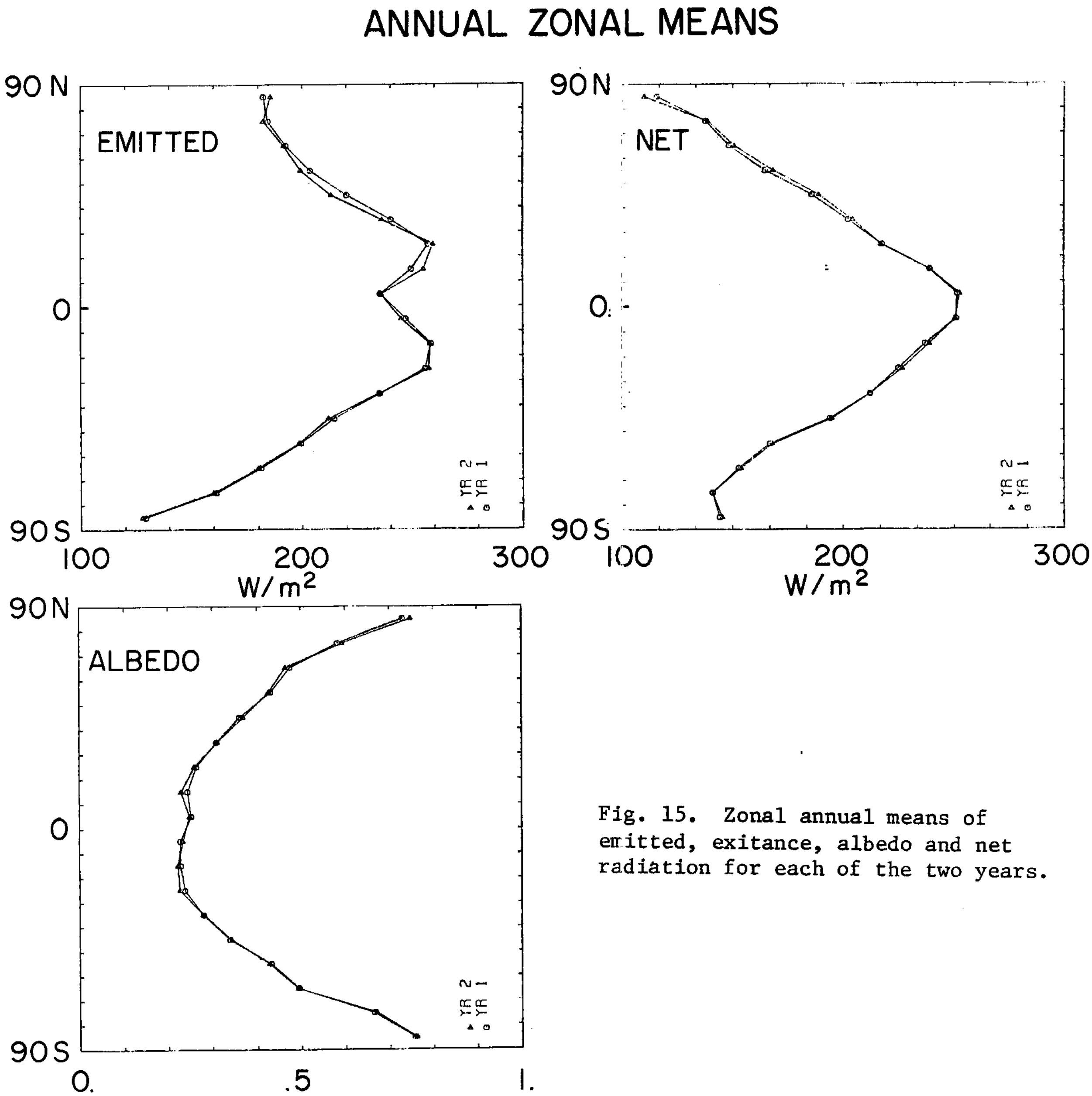

Fig. 15. Zonal annual means of emitted, exitance, albedo and net radiation for each of the two years.

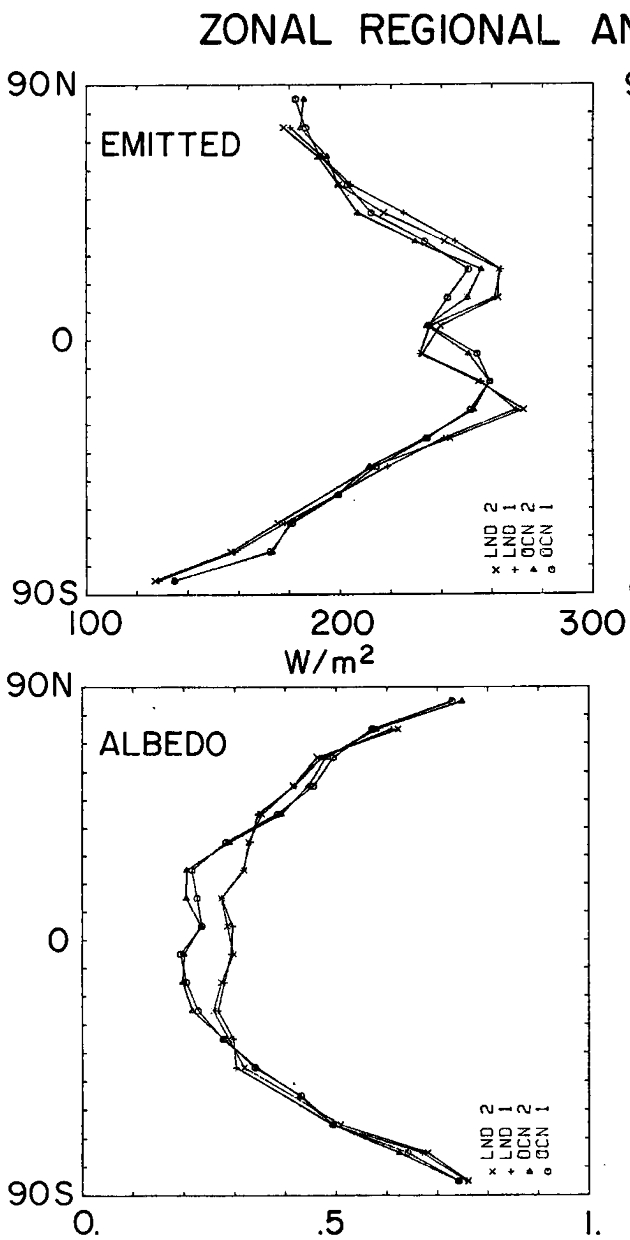

Fig. 16. Zonal annual means of emitted exitance, albedo, and net radiation for land and ocean regions for each of the two years.

VARIANCE

Another estimate of the year to year difference is presented in Figure 17. This is a map of the square root of the variance, eq. 16.

$$\sqrt{V} = \sqrt{\sum_{m=1}^{12} \left[N_1^m (\theta,\phi) - N_2^m (\theta,\phi) \right]^2 / 12} \qquad (16)$$

The most interesting feature is the arc of large variance along the north coast of the Pacific Ocean and in the south Pacific.

MONTHLY MAPS

The monthly maps, Appendix 1, show the emitted radiant exitance measured on the ascending portion of the orbit, near local noon. The albedo and derived net radiation are also presented. No sharp discontinuities appear in the maps because of the analysis by way of spherical harmonics. This produces the wave like patterns in the east west direction.

The orbit tracks went from bottom right to top left at about 80^{o} from the horizontal so features orientated at that angle are suspicious. For instance, February 1976 has a sampling problem especially in the Pacific. This problem occurs more often in the first year than the second because the instrument was being turned on and off to supply power to other Nimbus experiments. In the second year the data was nearly continuous in time except for drop outs in most descending orbit halves. From a qualitative examination of the maps, orbit tracks appear in July and October, 1975, February, March, June and July of 1976. The spherical harmonic coefficients could have been truncated further to smooth out the wiggles. But for studies with this data, features smaller than 1100 km are totally insignificant and only features at 2200 km are truly resolved, so we chose to ignore the problem.

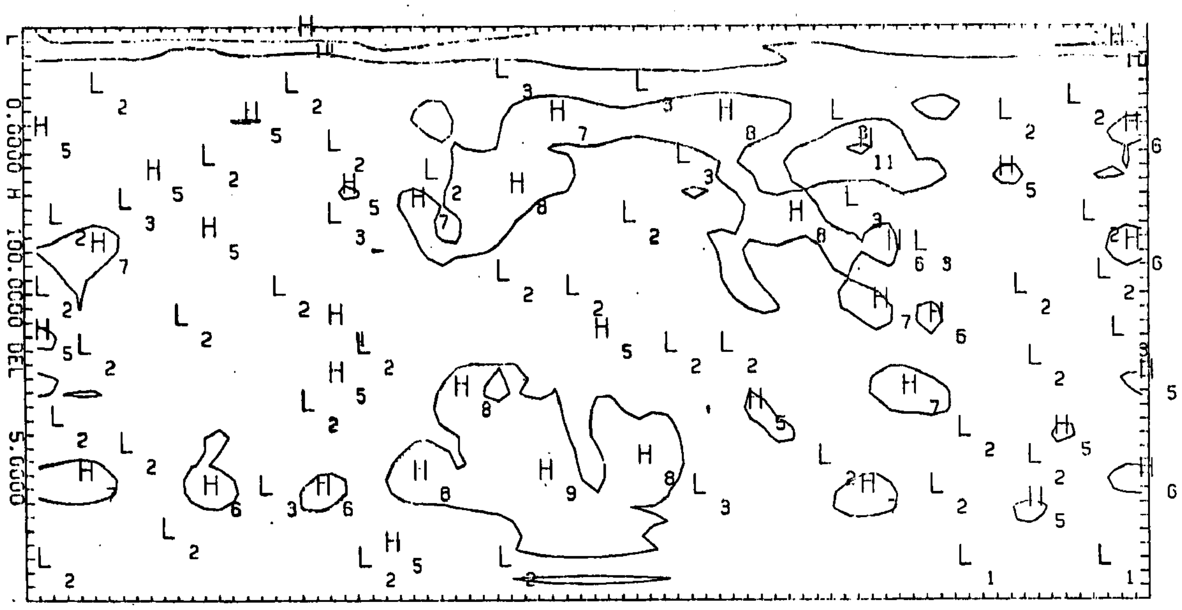

Fig. 17. Map of the square root of the variance of the net radiation, a summary of the large year to year differences, use overlay for locations.

We could now give qualitative descriptions of each month and in fact present year to year difference maps. This is not very fruitful without reference to simultaneous atmospheric events. That discussion will be deferred to Campbell, 1980.

CONCLUSION

This report is primarily descriptive of our analysis method and of the data fields derived. Because of the limitations in the instrument and calibration procedure we resorted to an inflight calibration. This depended on the Nimbus 7 calibration to adjust the total channel measurements. Second, the reflected channel was calibrated by comparing day and night in the Pacific. Third, the time decay of the reflected channel was estimated by comparing the second year to the first.

Some of these adjustments could be done better if detailed comparisons are made with the Nimbus 7 experiment results. Especially important is to resolve the contamination of the reflected channel result by the apparent dome temperature changes. The detailed comparison between channel 13 measurements and integrals of the scanning channel radiances could detect this effect. Finally, the time variation of the sensitivity can be determined by the recalibration by comparison at the Nimbus 7 launch.

Many tantalizing year to year differences have been described. The data show substantial changes in the emitted exitance and albedo around the intertropical convergence zone, probably due to systematic changes in the cloud features. The northern coast of the Pacific shows bigger year to year changes than other areas. The task remains to compare these variations with changes in monthly mean weather. Campbell (1980) will present these results.

ACKNOWLEDGEMENTS

We would like to thank Dr.'s H. Jacobowitz and W. Smith of NOAA for making the data available. Also, all the members of the Nimbus 7 Experiment Team contributed in the discussion and understanding of the calibration procedures. Without the efforts of this team it is likely that we would not have attempted the analysis project. Ms. L. Parkinson provided invaluable service in typing the manuscript and M. Howes assisted in the preparation of many of the figures. This effort was sponsored by the Nimbus 7 office of NASA, Contract NAS5-22959. Finally we would like to thank the Earth Radiation Budget Experiment of NASA for their continuing support.

REFERENCES

Campbell, G. G., 1980: Radiation Budget and the Mean Weather, Two Years of Observations. Ph.D. Thesis, Department of Atmospheric Science, Colorado State University, Ft. Collins, CO.

Campbell, G. G. and T. H. Vonder Haar, 1980a: Climatology of Radiation Budget Measurements from Satellites. Atmospheric Science Paper No. 323, Colorado State University, Ft. Collins, Colorado. 74 pp.

Campbell, G. G., and T. H. Vonder Haar, 1980b: Latitude Average Radiation Budget Over Land and Ocean from Satellite Observations and Some Implications for Energy Transport and Climate Modeling. Submitted to

Ellis, J., T. H. Vonder Haar, S. Levitus, and A. H. Oort, 1978: The Annual Variation in the Global Heat Balance of the Earth, _J. of Geophys. Res._, Vol. 83, #C4.

Hickey, J. R., and A. R. Karoli, 1974: Radiometric calibrations for the earth radiation budget experiment. _Appl. Opt._, Vol. 13, 523-533.

Hickey, J. R., F. J. Griffin, and H. B. Howel, 1977: Two years of solar measurements from the Nimbus 6 satellites. _Proc. Int. Solar Energy Society Solar World Conf._, Orlando, Vol. 1, pp. 14-36.

Hickey, J. R., L. L. Stowe, H. Jacobowitz, P. Pellegrino, R. H. Maschhoff, F. House, T. H. Vonder Haar, 1980: Initial Solar Irradiance Determination from Nimbus 7 Cavity Radiometer Measurements. _Science_, Vol. 208, pp. 281-283.

Jacobowitz, H., W. L. Smith, H. B. Howell, F. W. Nagle and J. R. Hickey, 1979: The first 18 months of planetary radiation budget measurements from Nimbus 6 ERB experiment. J. Atmos. Sci., Vol. 36, pp. 501-507.

London, J., 1954: A study of the atmospheric heat balance. Final Report, Contract # AF(122)-165, College of Engineering Research Div., New York University, 199 pp. (NTIS NO: PB115626).

Ramanathan, S., and B. Breigleib, 1980: Radiation budget estimate in different spectral intervals. In preparation.

Raschke, E., T. H. Vonder Haar, M. Pasternak and W. R. Bandeen, 1973: The radiation balance of the Earth-Atmosphere system from Nimbus 3 radiation measurements. NASA TN D-7247, April.

Smith, G. L., R. N. Greene and G. G. Campbell, 1975: A statistical interpretation technique for wide angle radiometer measurements of Earth energy budget. Proc. of 4th Conference on Probability and Statistics in Atmospheric Sciences, AMS, Tallahassee, FL.

Smith, W. L., D. T. Hilleary, H. Jacobowitz, H. B. Howell, J. R. Hickey, and A. J. Drummond, 1977: Nimbus-6 Earth Radiation Budget Experiment. Appl. Opt., Vol. 16, 306-318.

Stephens, G., G. G. Campbell and T. H. Vonder Haar, 1980: Earth Radiation Budget measurements from satellites and their interpretation for climate modeling and studies, submitted to J. of Geophys. Res.

Vonder Haar, T. H. and J. Ellis, 1974: Atlas of Radiation Budget Measurements from Satellites (1962-1970). Atmospheric Science Paper No. 231, Colorado State University, Ft. Collins, CO.

Winston, J., A. Gruber, T. Gray, M. Vernadore, C. Earnest and L. Mannello, 1979: The Earth Radiation Budget Analysis Derived from NOAA Satellite Data, June 1974 to February 1978. Vol. I and Vol. II, Meteorological Satellite Laboratory, Washington, D.C.

__________, 1977-1980: Earth Radiation Budget Nimbus 7 Science Team meeting minutes; Available Nimbus Project Office, NASA, Washington D.C.

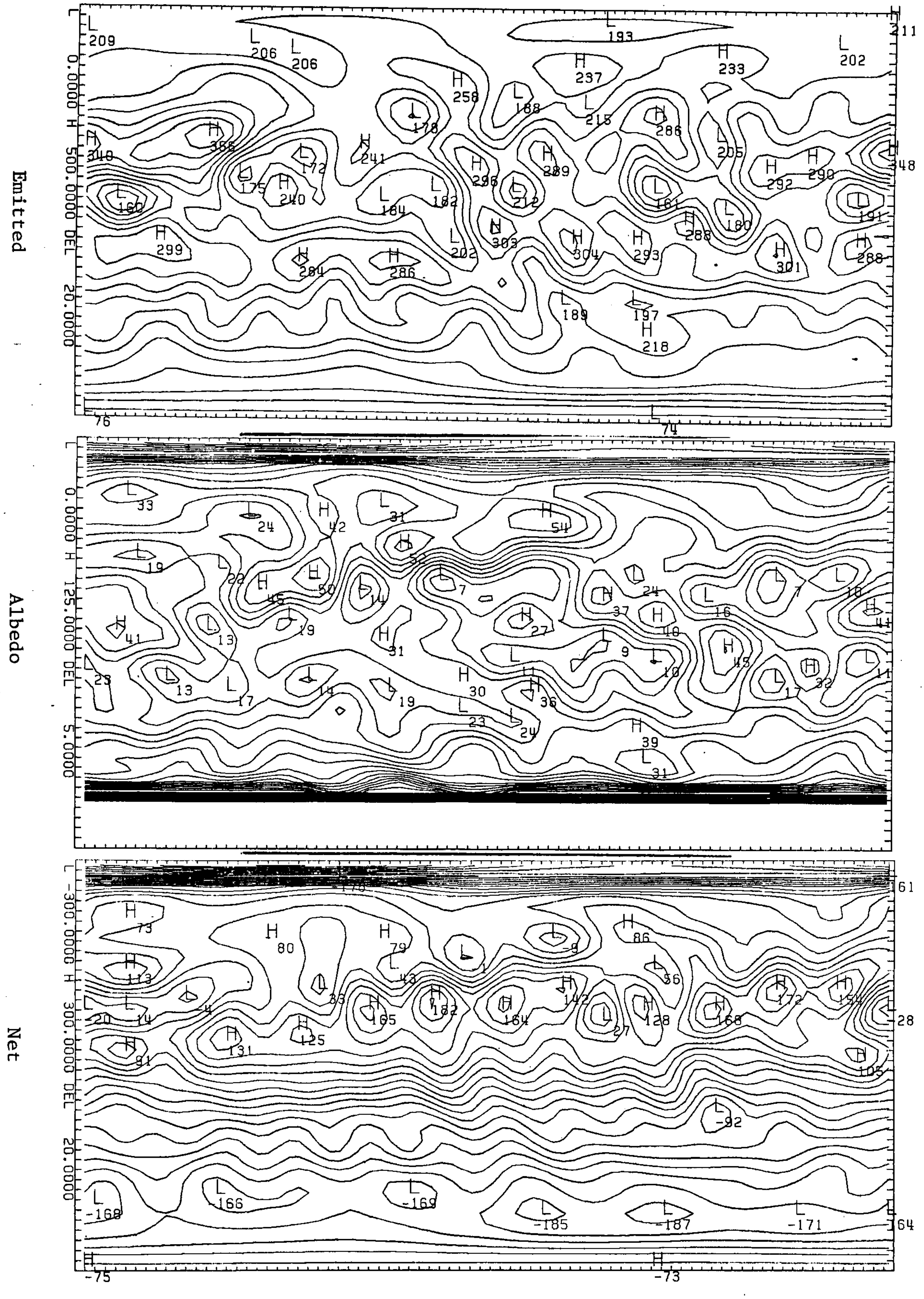
Emitted
0.0000 H 500.0000 DEL 20.0000
Albedo
0.0000 H 125.0000 DEL 5.0000
Net
-300.0000 H 300.0000 DEL 20.0000

7/ 75

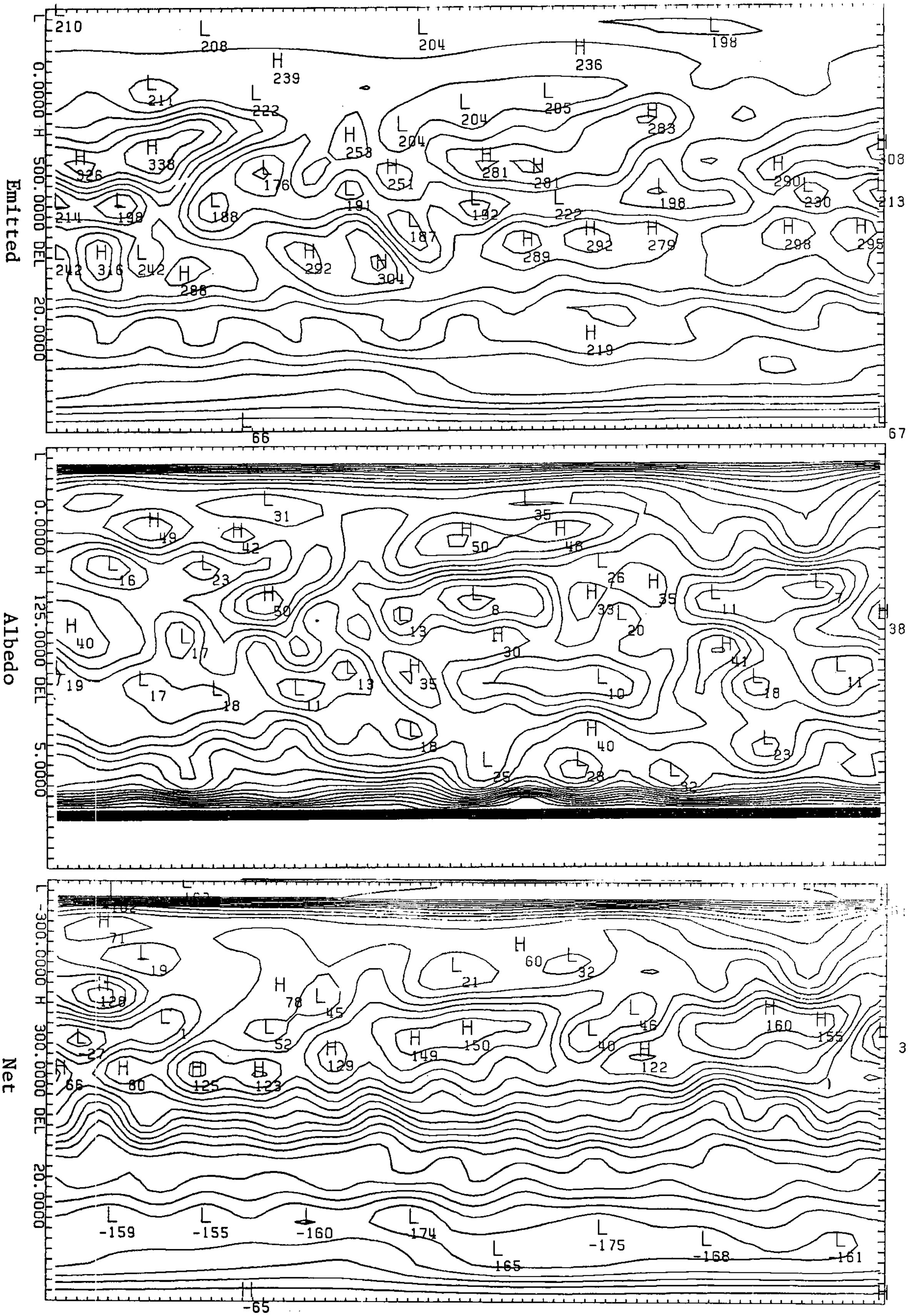
Emitted
0.0000 H 500.0000 DEL 20.0000
Albedo
0.0000 H 125.0000 DEL 5.0000
Net
-300.0000 H 300.0000 DEL 20.0000

7/ 76

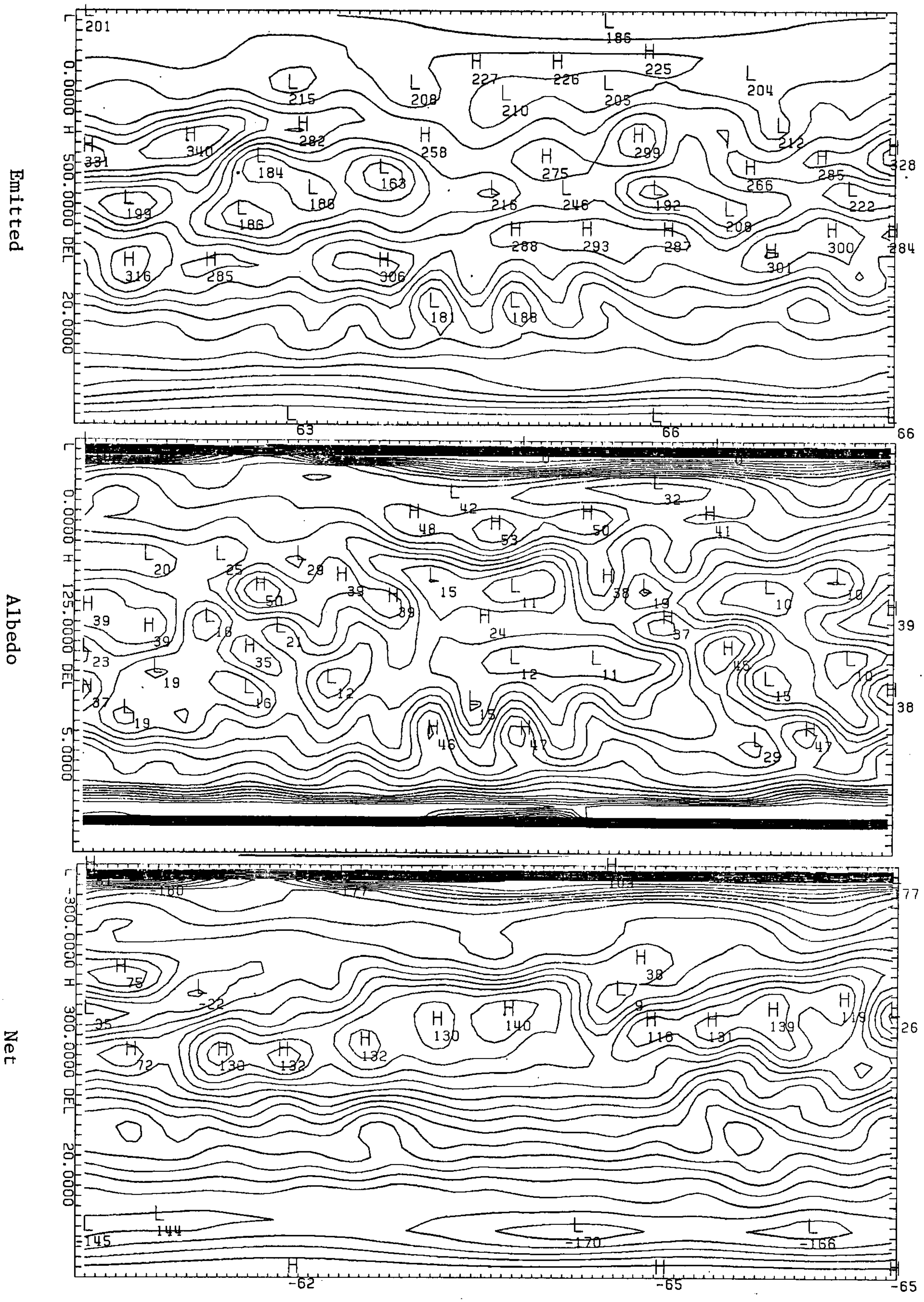
Emitted
0.0000 H 500.0000 DEL 20.0000
Albedo
0.0000 H 125.0000 DEL 5.0000
Net
-300.0000 H 300.0000 DEL 20.0000

8/ 75

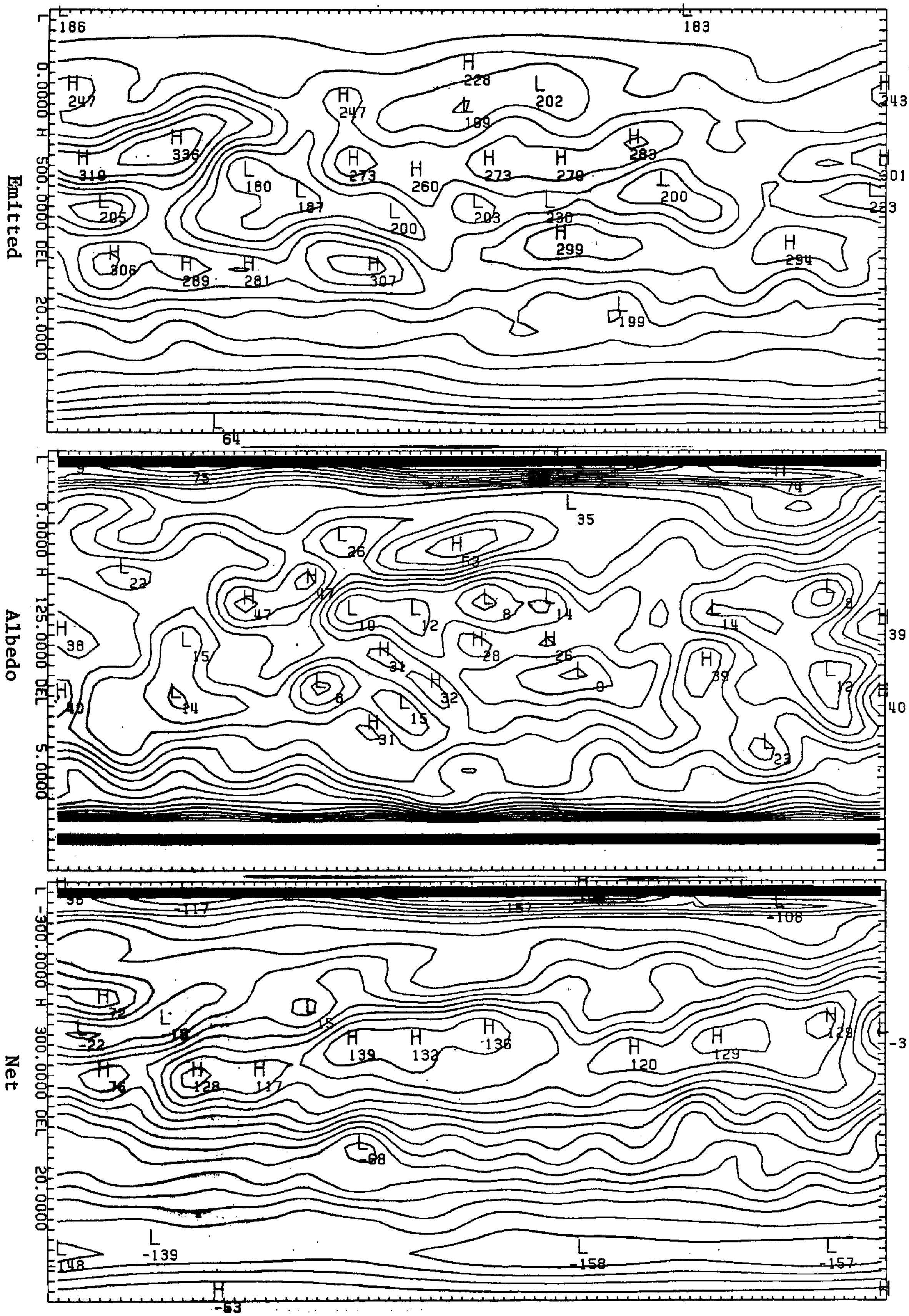
Emitted
0.0000 H 500.0000 DEL 20.0000
Albedo
0.0000 H 125.0000 DEL 5.0000
Net
-300.0000 H 300.0000 DEL 20.0000

8/ 76

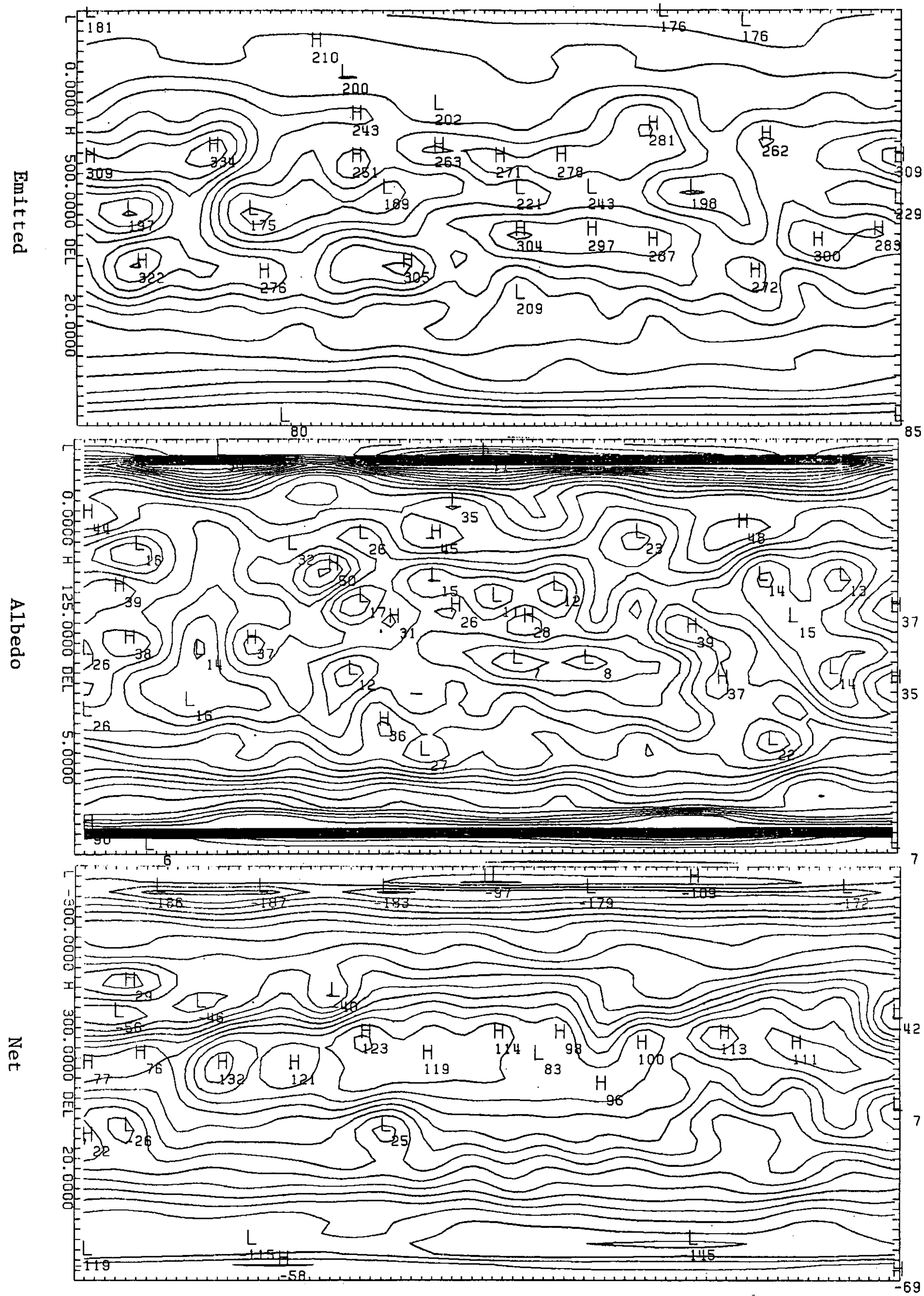

Emitted
0.0000 H 500.0000 DEL 20.0000
Albedo
0.0000 H 125.0000 DEL 5.0000
Net
-300.0000 H 300.0000 DEL 20.0000

9/ 75

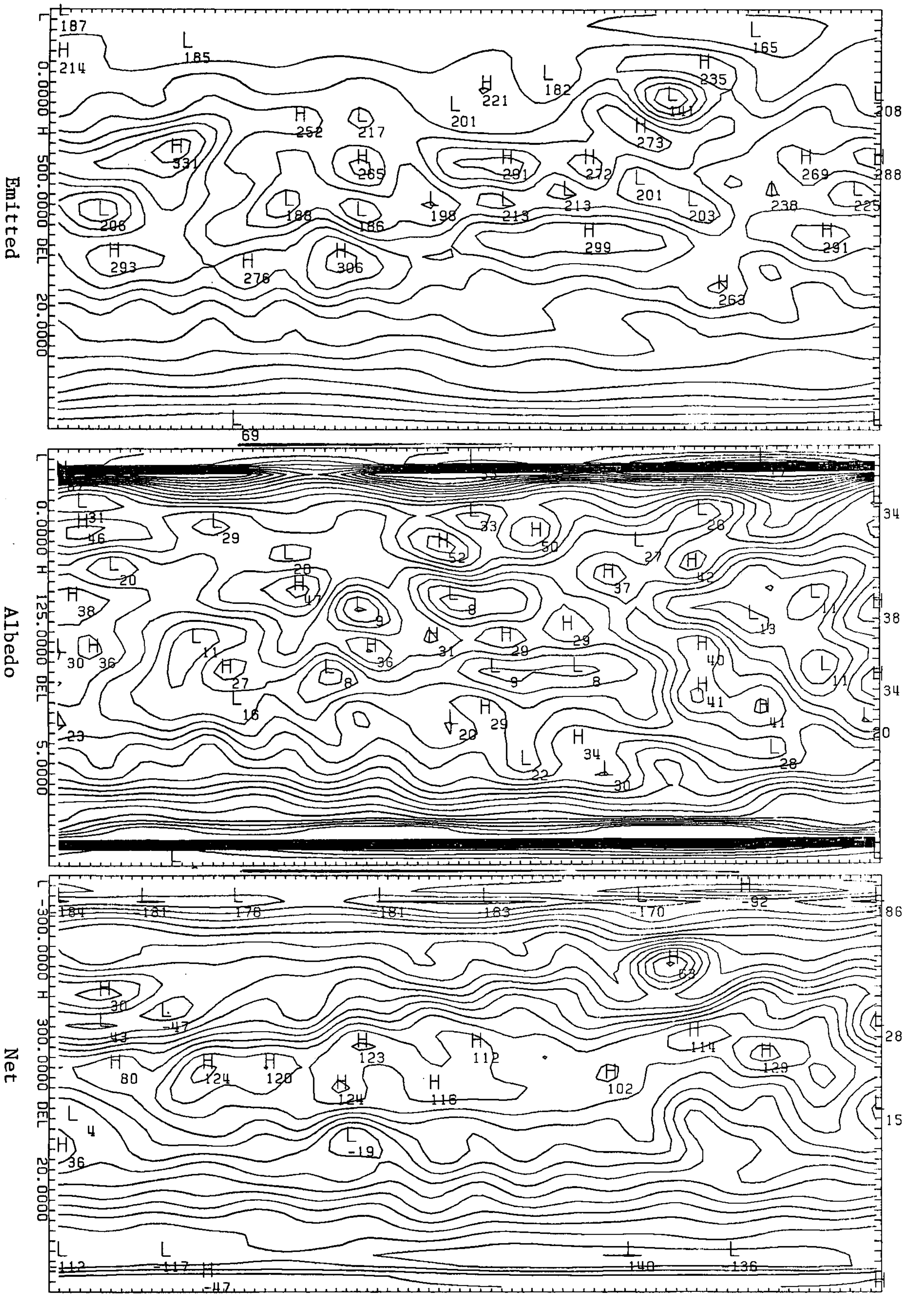
Emitted
0.0000 H 500.0000 DEL 20.0000
Albedo
0.0000 H 125.0000 DEL 5.0000
Net
-300.0000 H 300.0000 DEL 20.0000

9/ 76

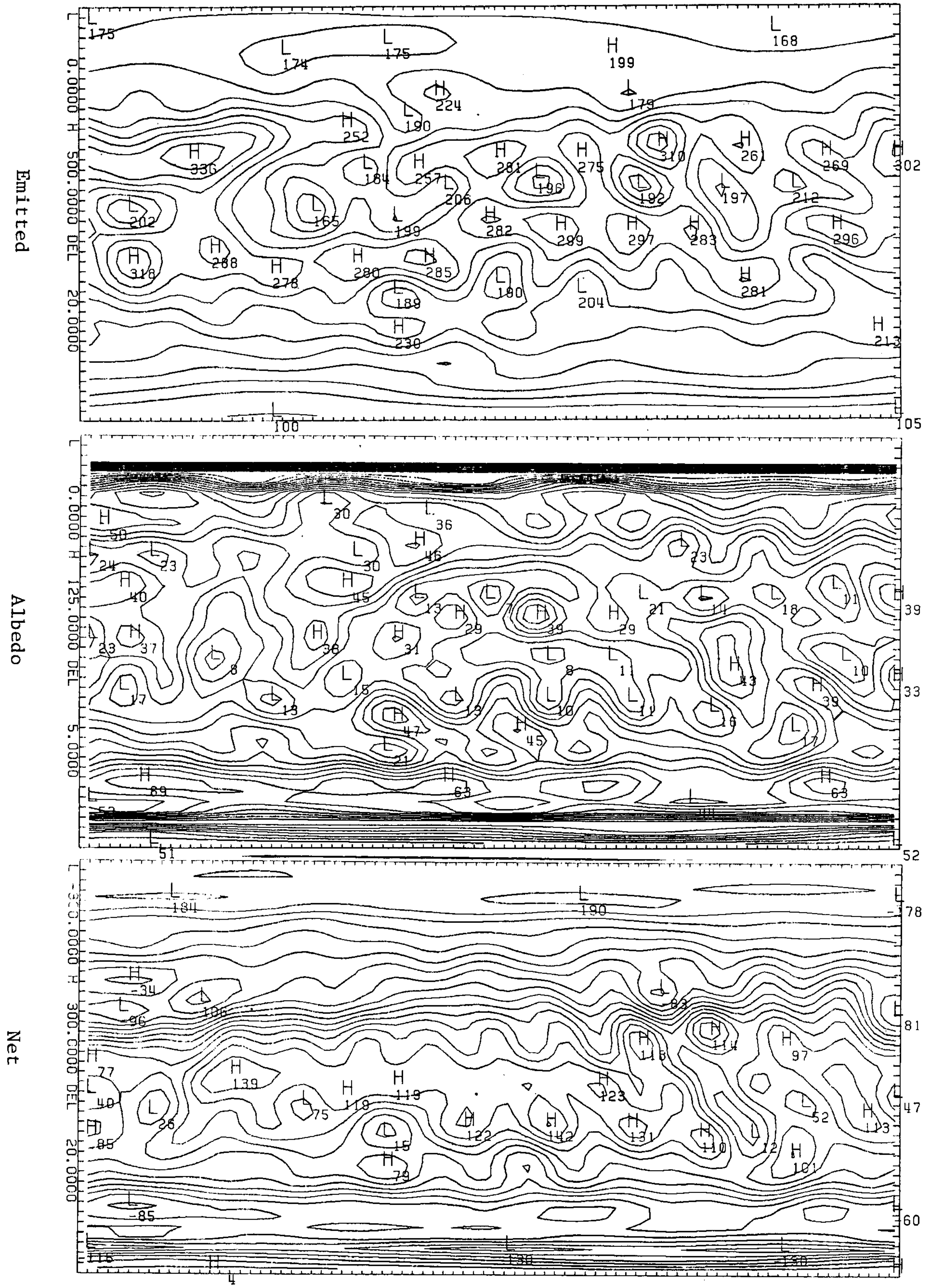
Emitted
0.0000 H 500.0000 DEL 20.0000
Albedo
0.0000 H 125.0000 DEL 5.0000
Net
-300.0000 H 300.0000 DEL 20.0000

10/ 75

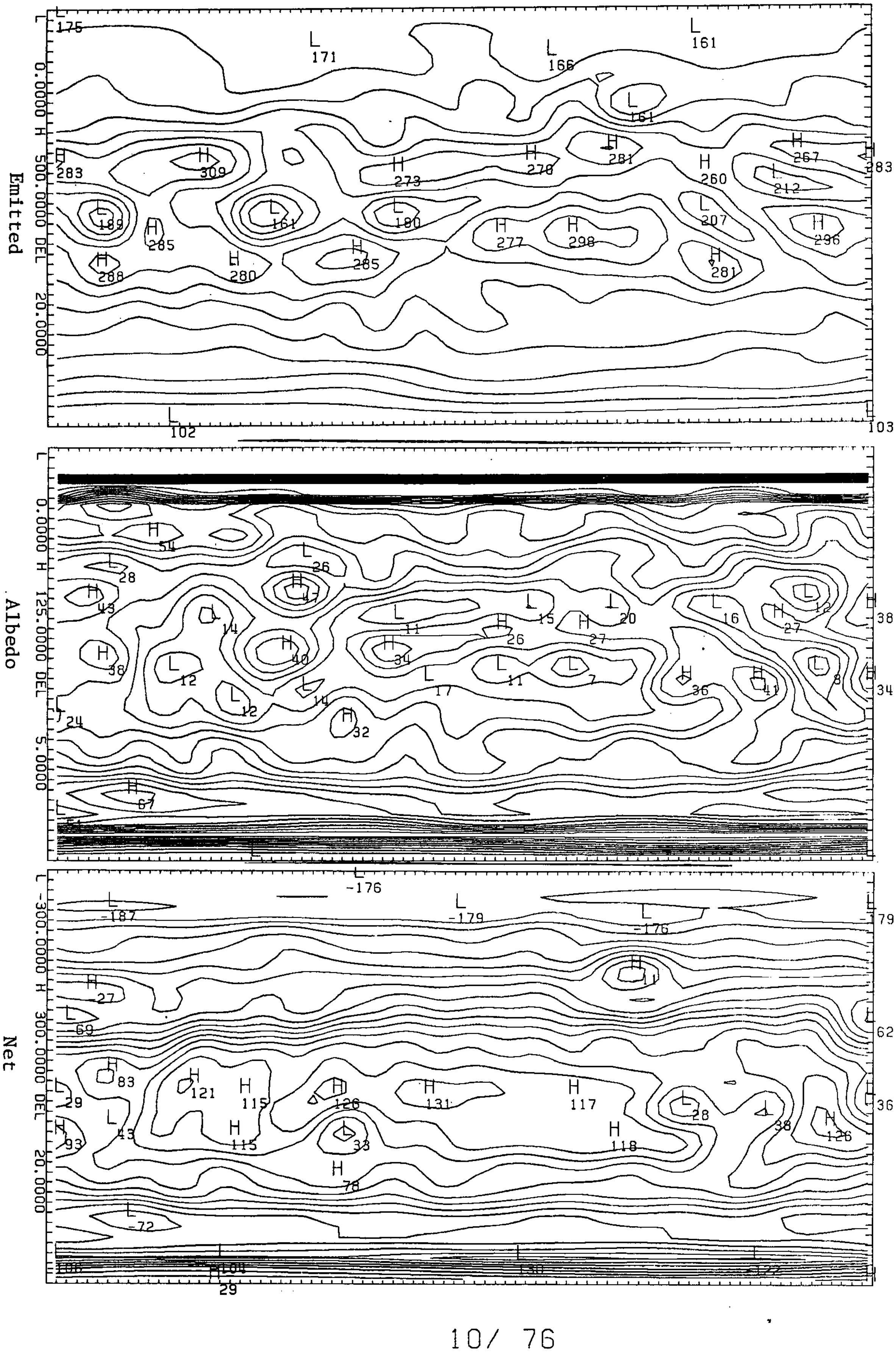
Emitted
0.0000 H 500.0000 DEL 20.0000
Albedo
0.0000 H 125.0000 DEL 5.0000
Net
-300.0000 H 300.0000 DEL 20.0000

10/ 76

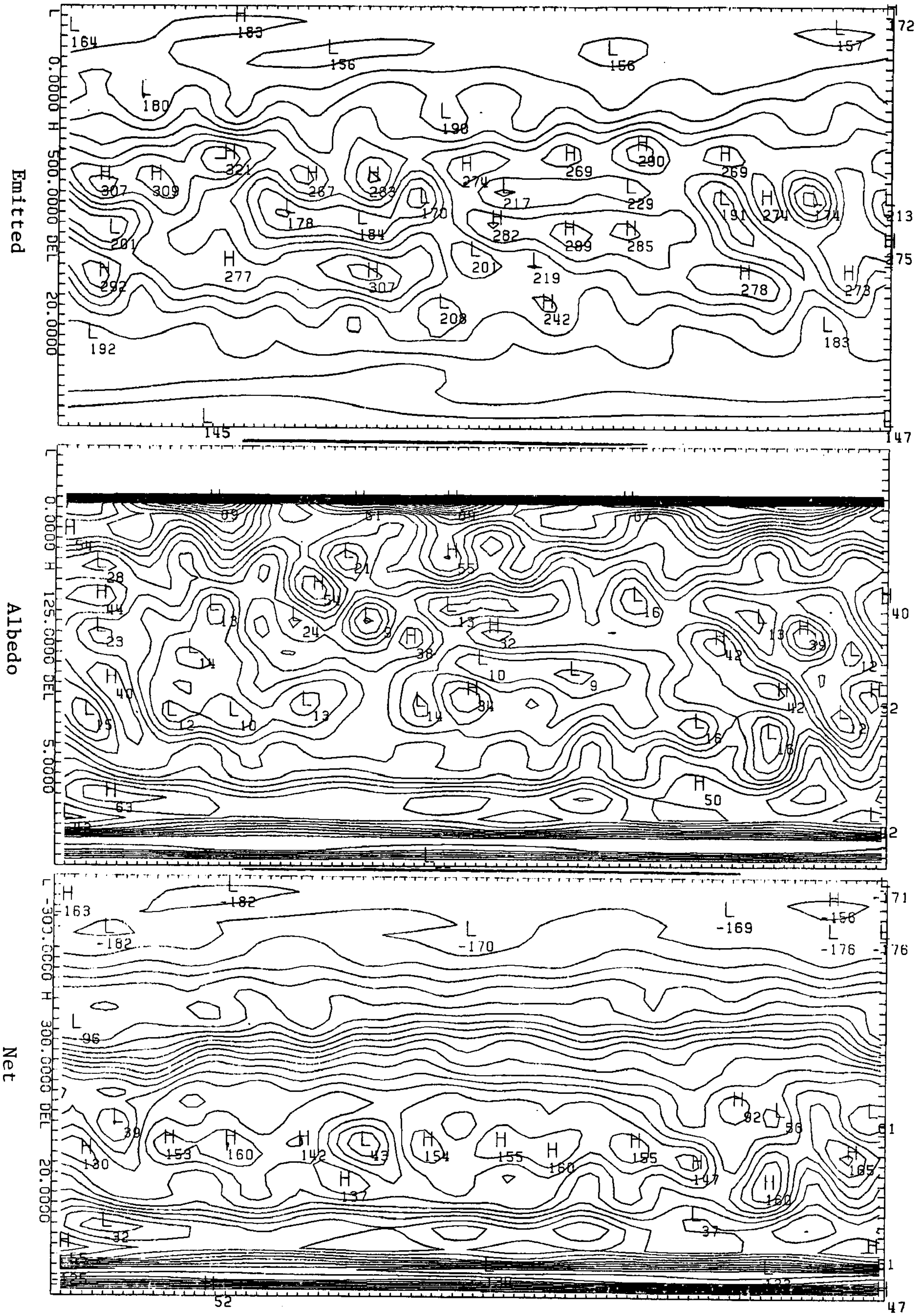
Emitted
0.0000 H 500.0000 DEL 20.0000
Albedo
0.0000 H 125.0000 DEL 5.0000
Net
-300.0000 H 300.0000 DEL 20.0000

11/ 75

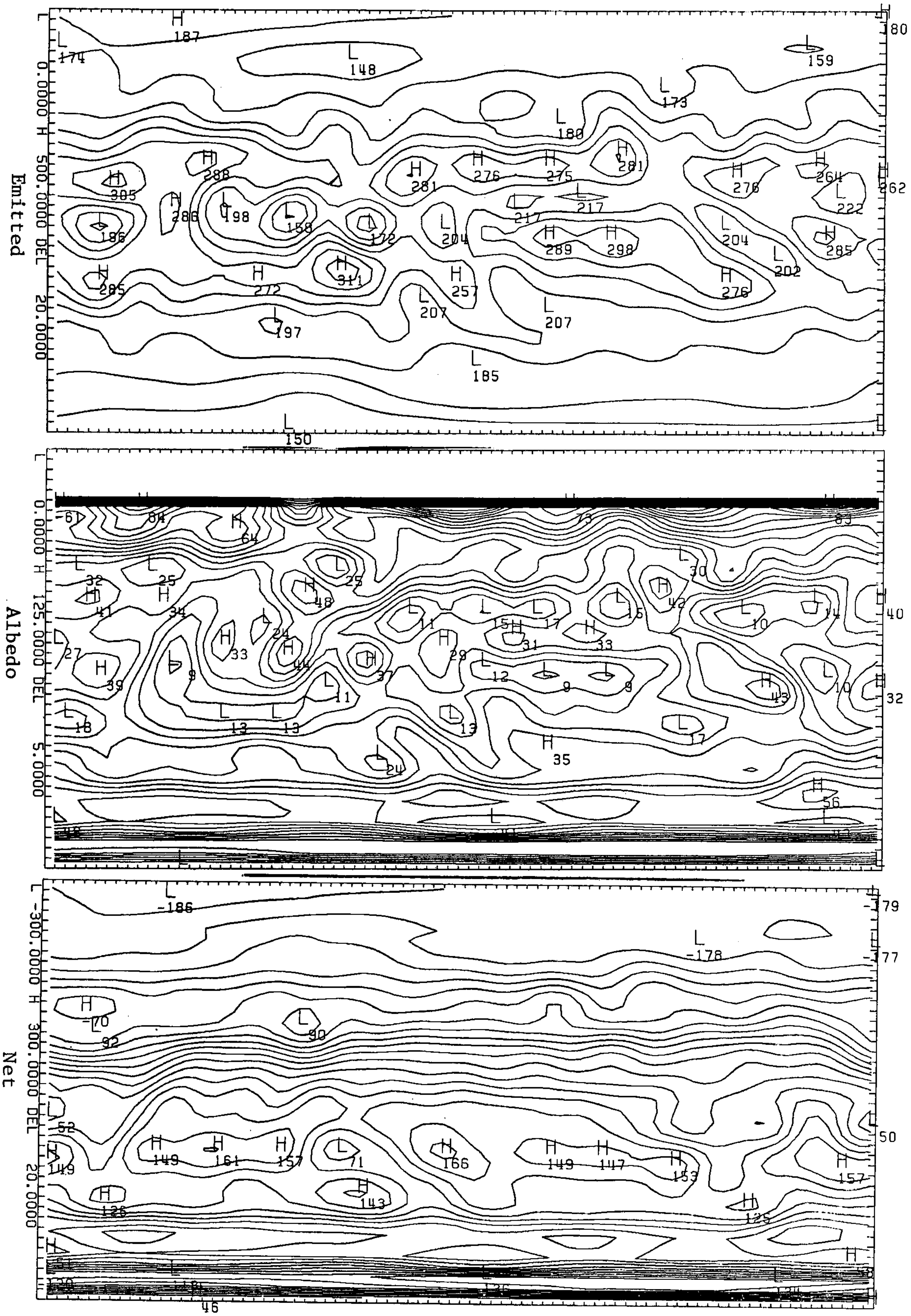
Emitted
0.0000 H 500.0000 DEL 20.0000
Albedo
0.0000 H 125.0000 DEL 5.0000
Net
-300.0000 H 300.0000 DEL 20.0000

11/ 76

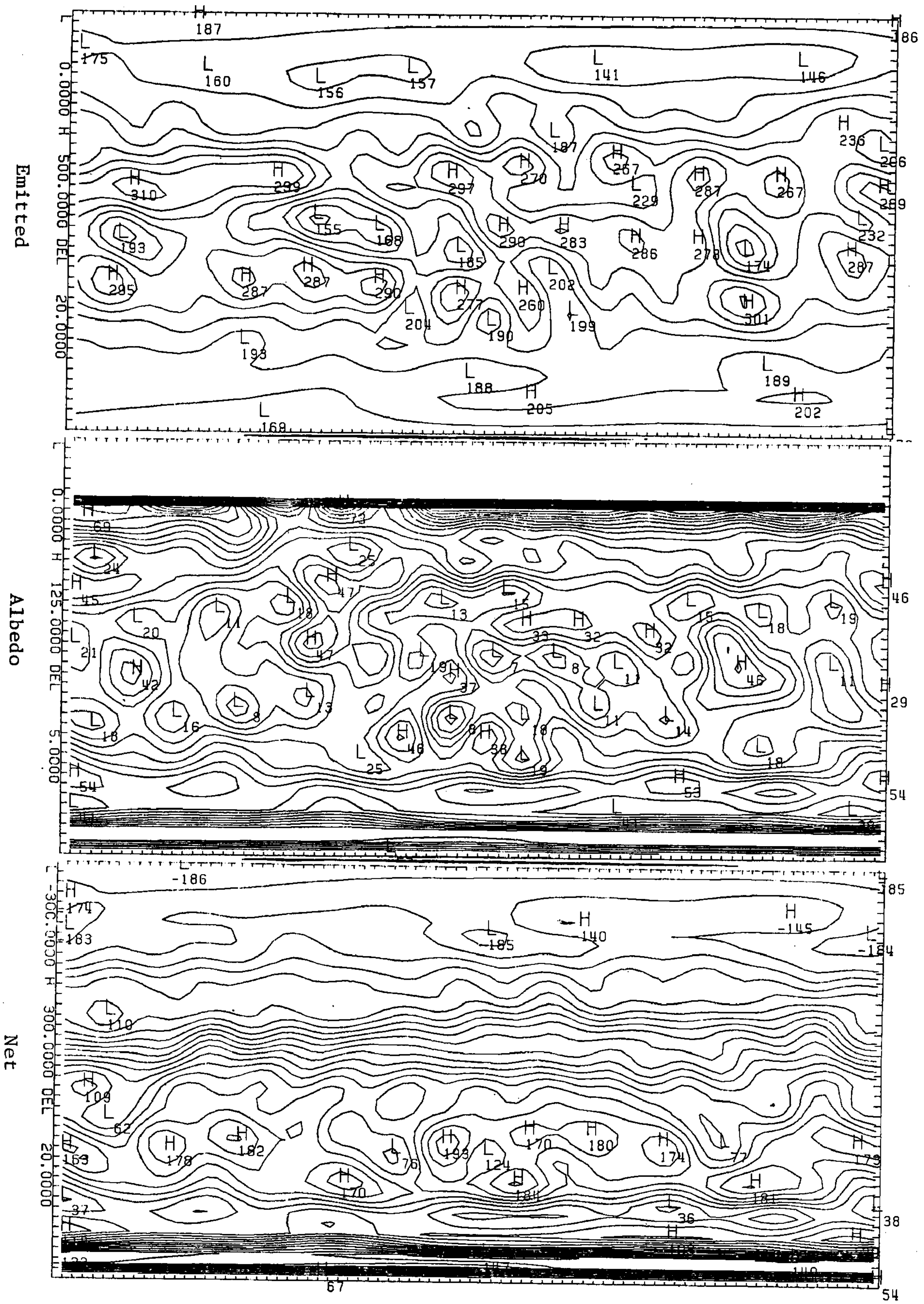

12/ 75

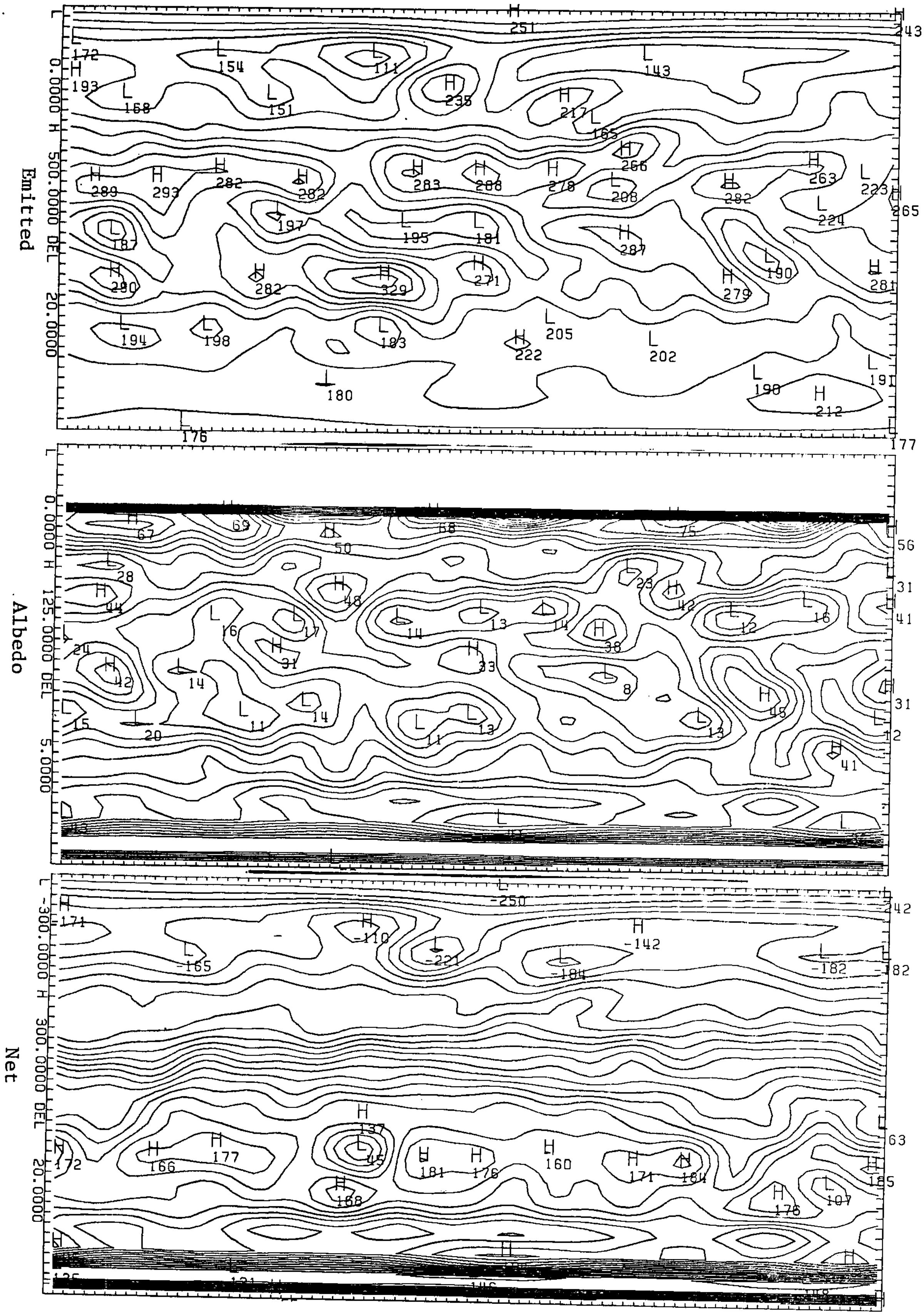
Emitted
0.0000 H 500.0000 DEL 20.0000
Albedo
0.0000 H 125.0000 DEL 5.0000
Net
-300.0000 H 300.0000 DEL 20.0000

12/ 76

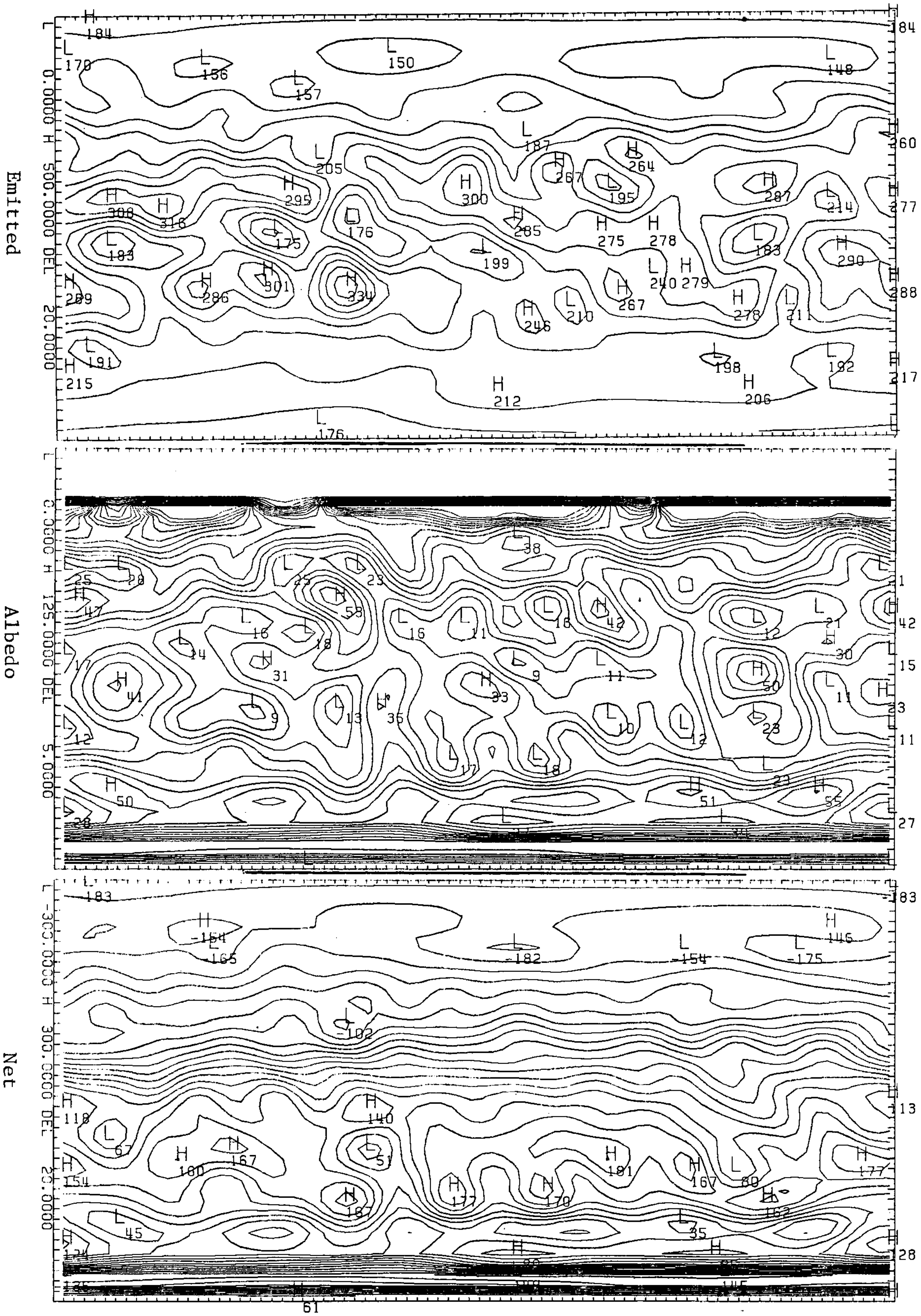
Emitted
0.0000 H 500.0000 DEL 20.0000
Albedo
0.0000 H 125.0000 DEL 5.0000
Net
-300.0000 H 300.0000 DEL 20.0000

1/ 76

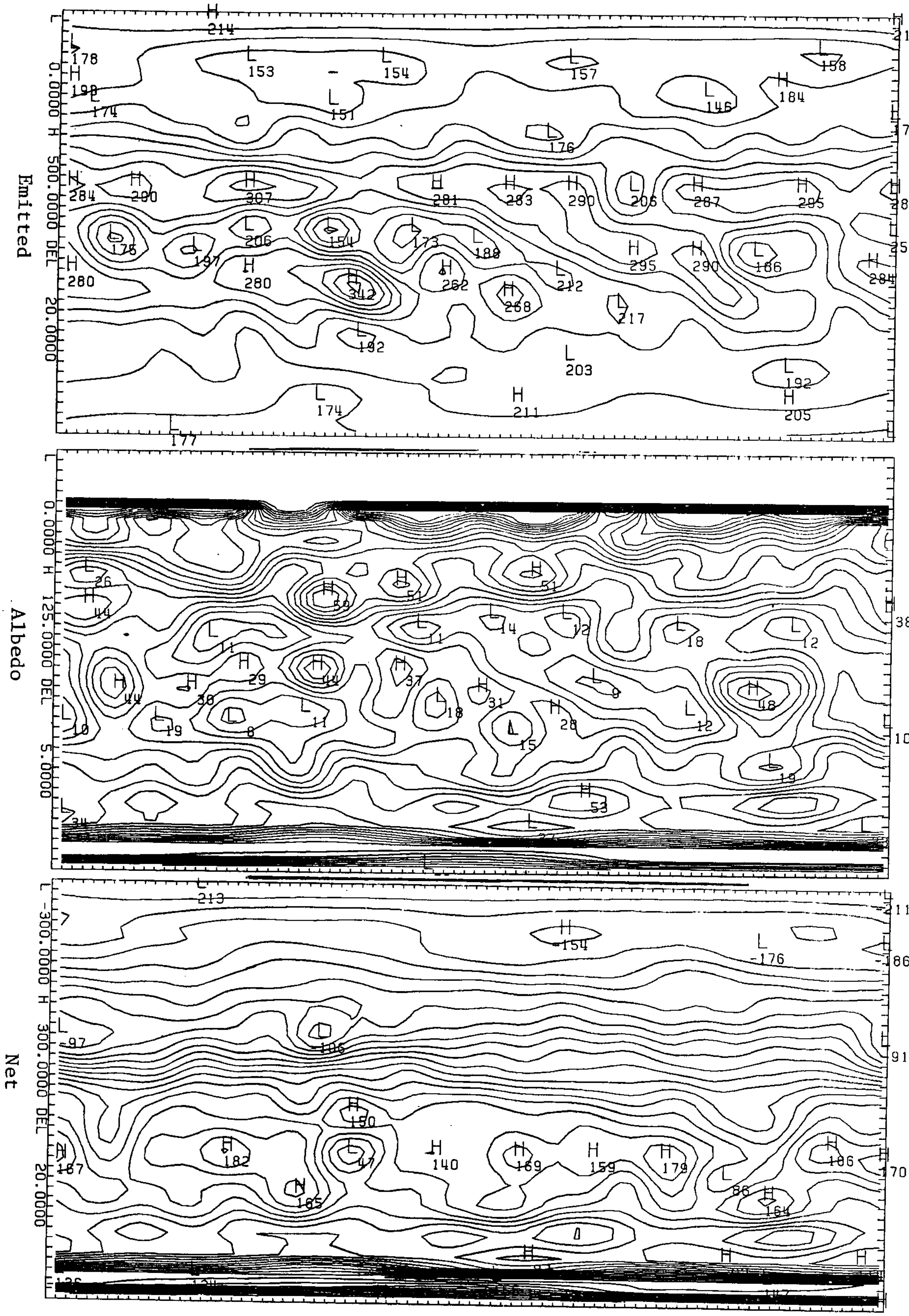
Emitted
0.0000 H 500.0000 DEL 20.0000
Albedo
0.0000 H 125.0000 DEL 5.0000
Net
-300.0000 H 300.0000 DEL 20.0000

1/ 77

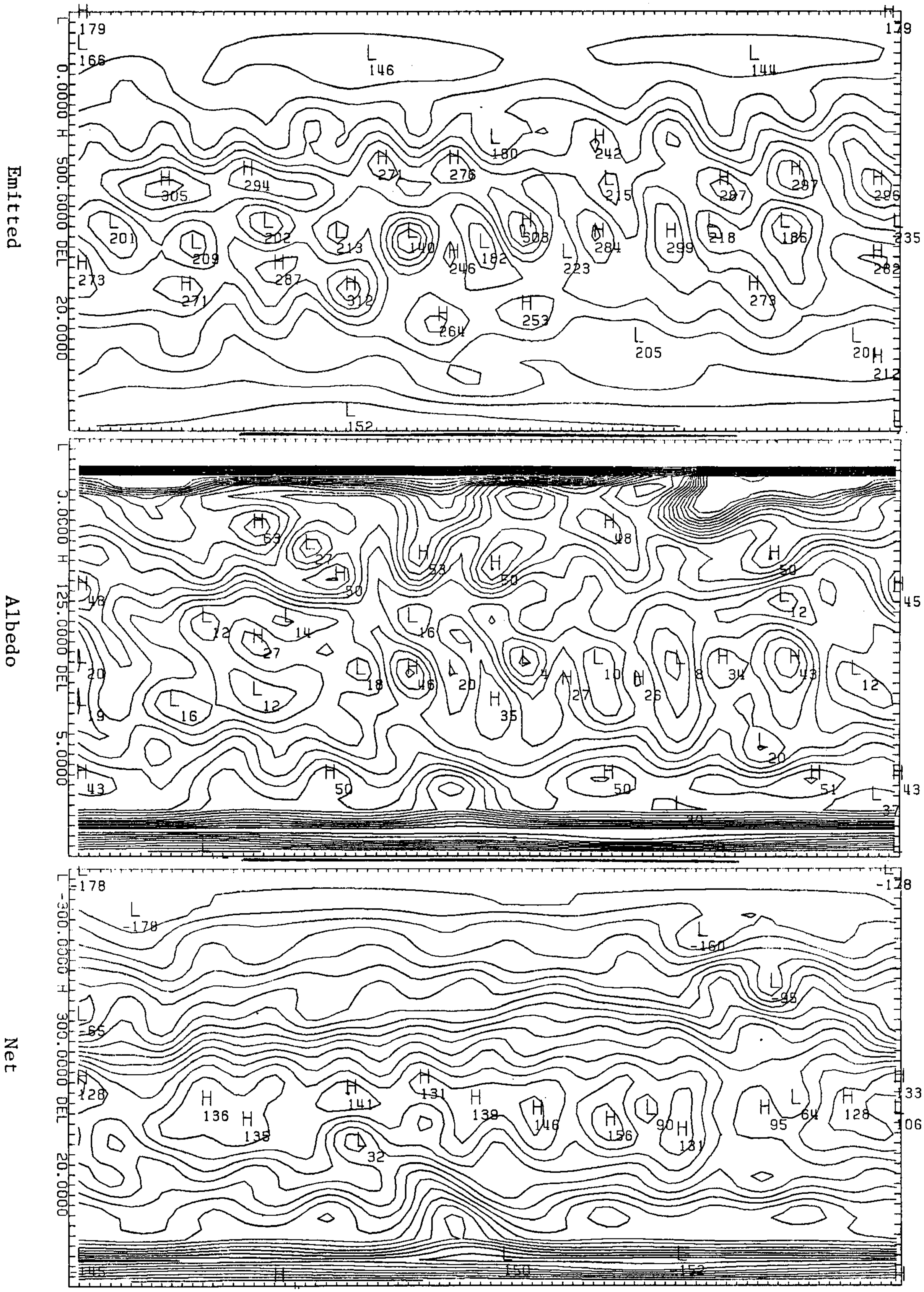
Emitted
0.0000 H 500.0000 DEL 20.0000
Albedo
0.0000 H 125.0000 DEL 5.0000
Net
-300.0000 H 300.0000 DEL 20.0000

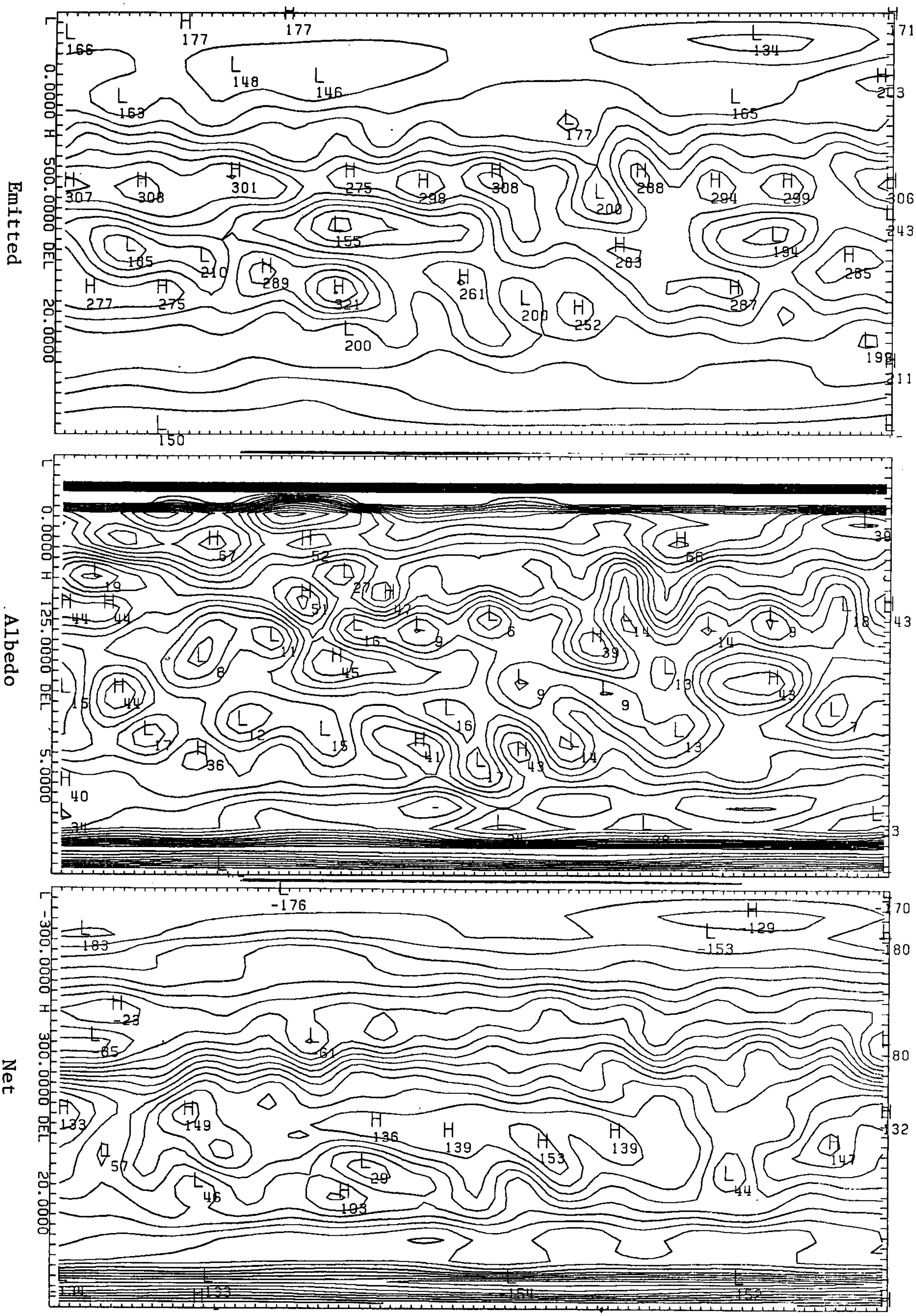
Emitted
0.0000 H 500.0000 DEL 20.0000
Albedo
0.0000 H 125.0000 DEL 5.0000
Net
-300.0000 H 300.0000 DEL 20.0000

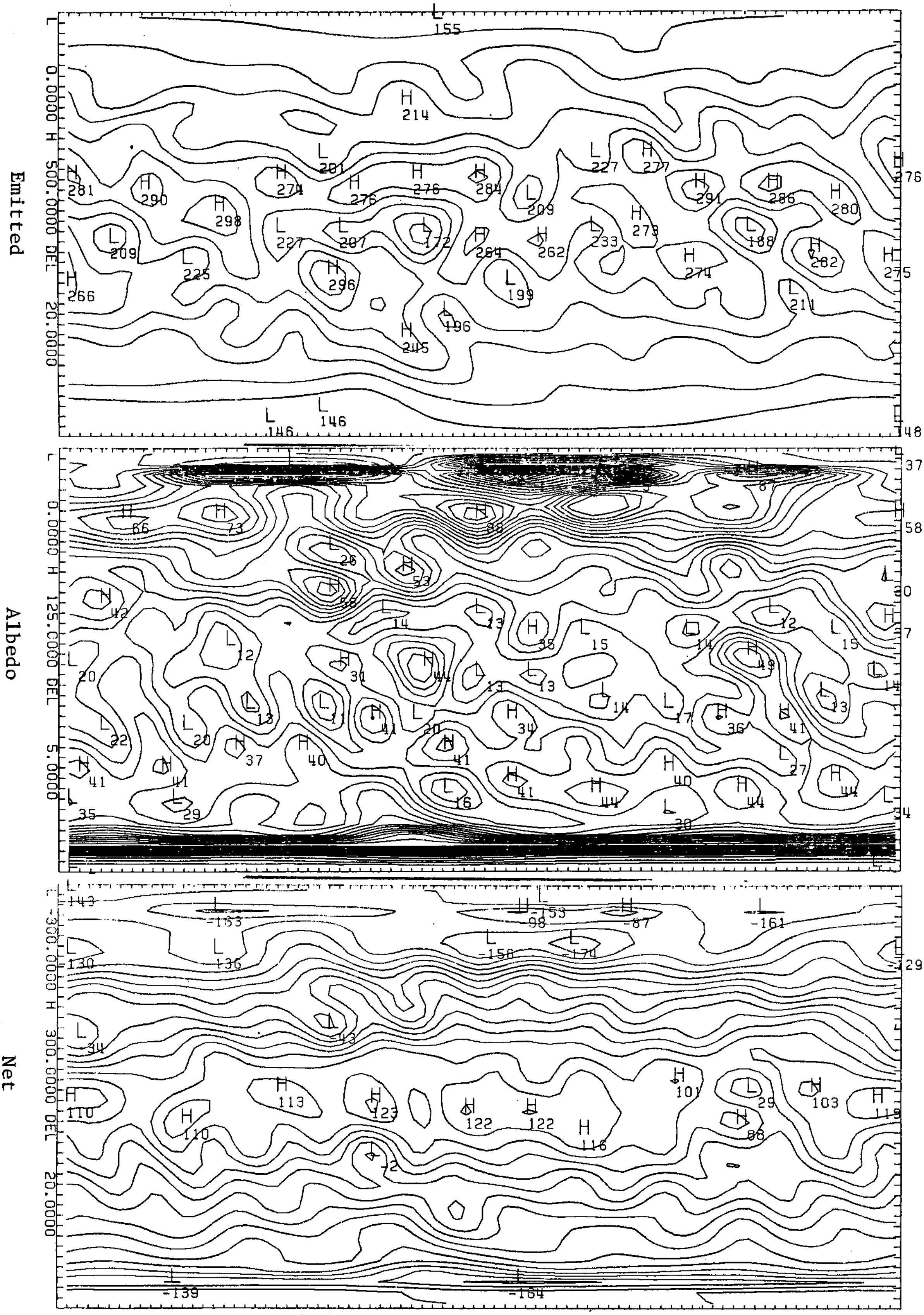
Emitted
0.0000 H 500.0000 DEL 20.0000
Albedo
0.0000 H 125.0000 DEL 5.0000
Net
-300.0000 H 300.0000 DEL 20.0000

3/ 76

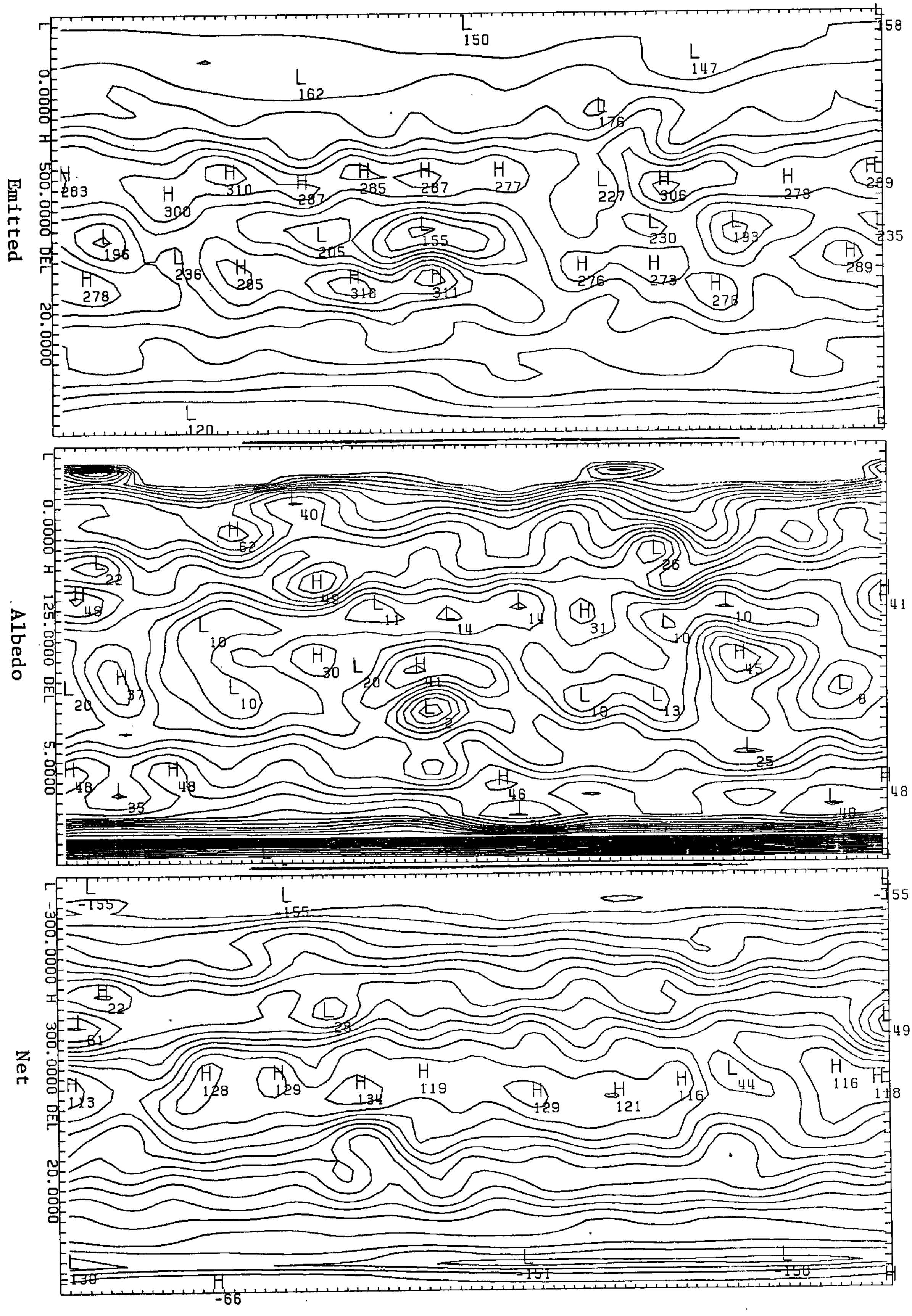
Emitted
0.0000 H 500.0000 DEL 20.0000
Albedo
0.0000 H 125.0000 DEL 5.0000
Net
-300.0000 H 300.0000 DEL 20.0000

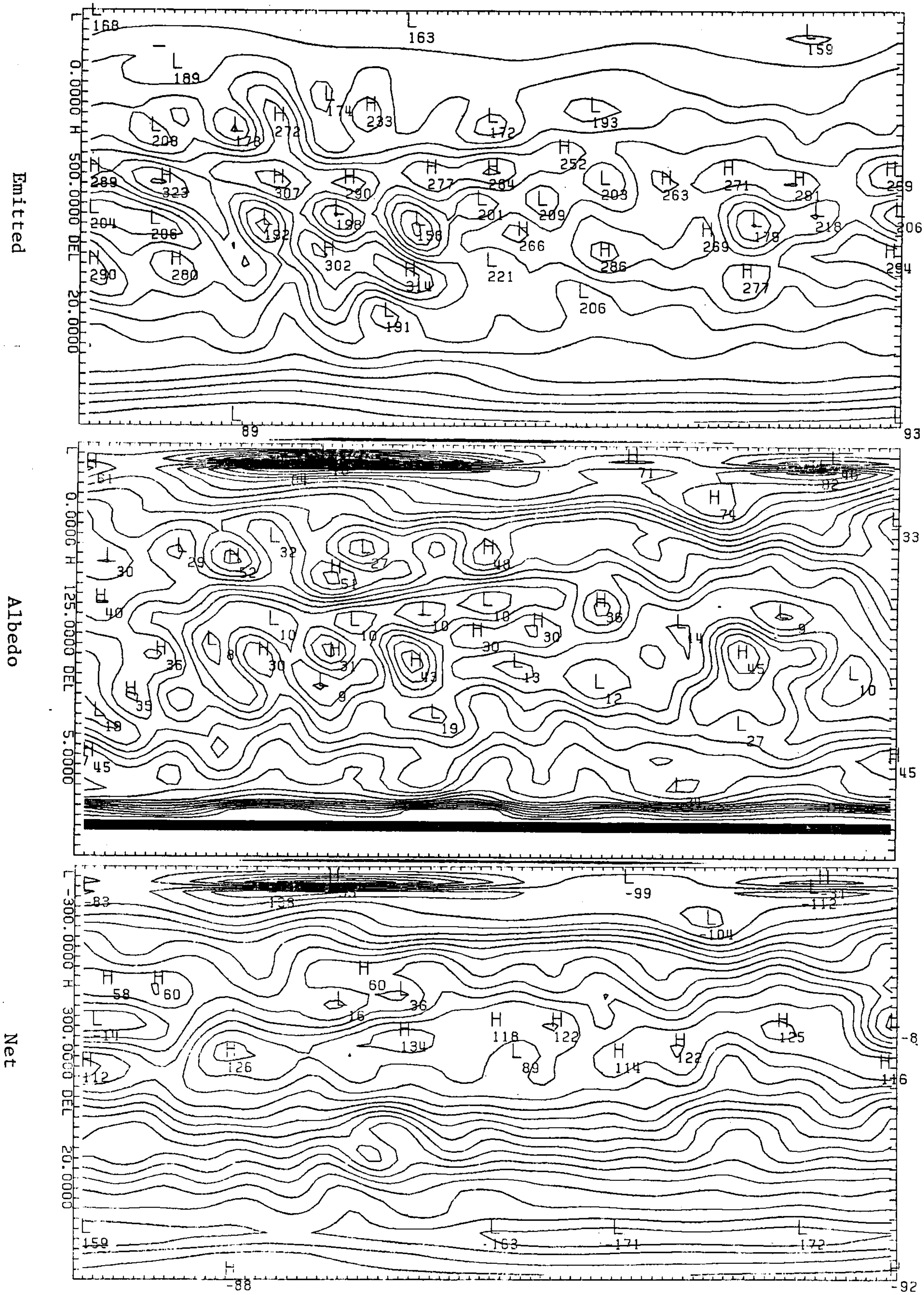
Emitted
0.0000 H 500.0000 DEL 20.0000
Albedo
0.0000 H 125.0000 DEL 5.0000
Net
-300.0000 H 300.0000 DEL 20.0000

4/ 76

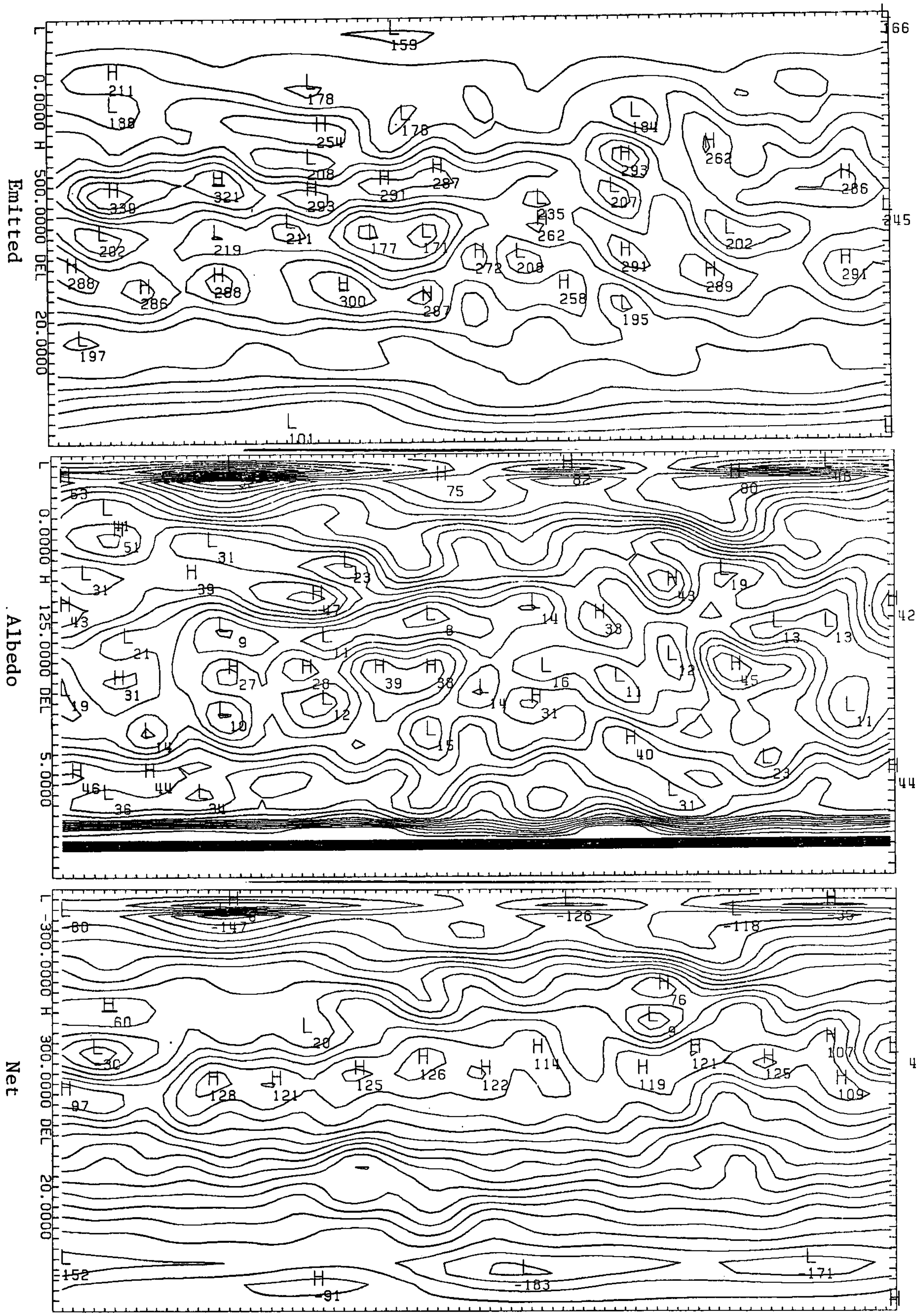
Emitted
0.0000 H 500.0000 DEL 20.0000
Albedo
0.0000 H 125.0000 DEL 5.0000
Net
-300.0000 H 300.0000 DEL 20.0000

4/ 77

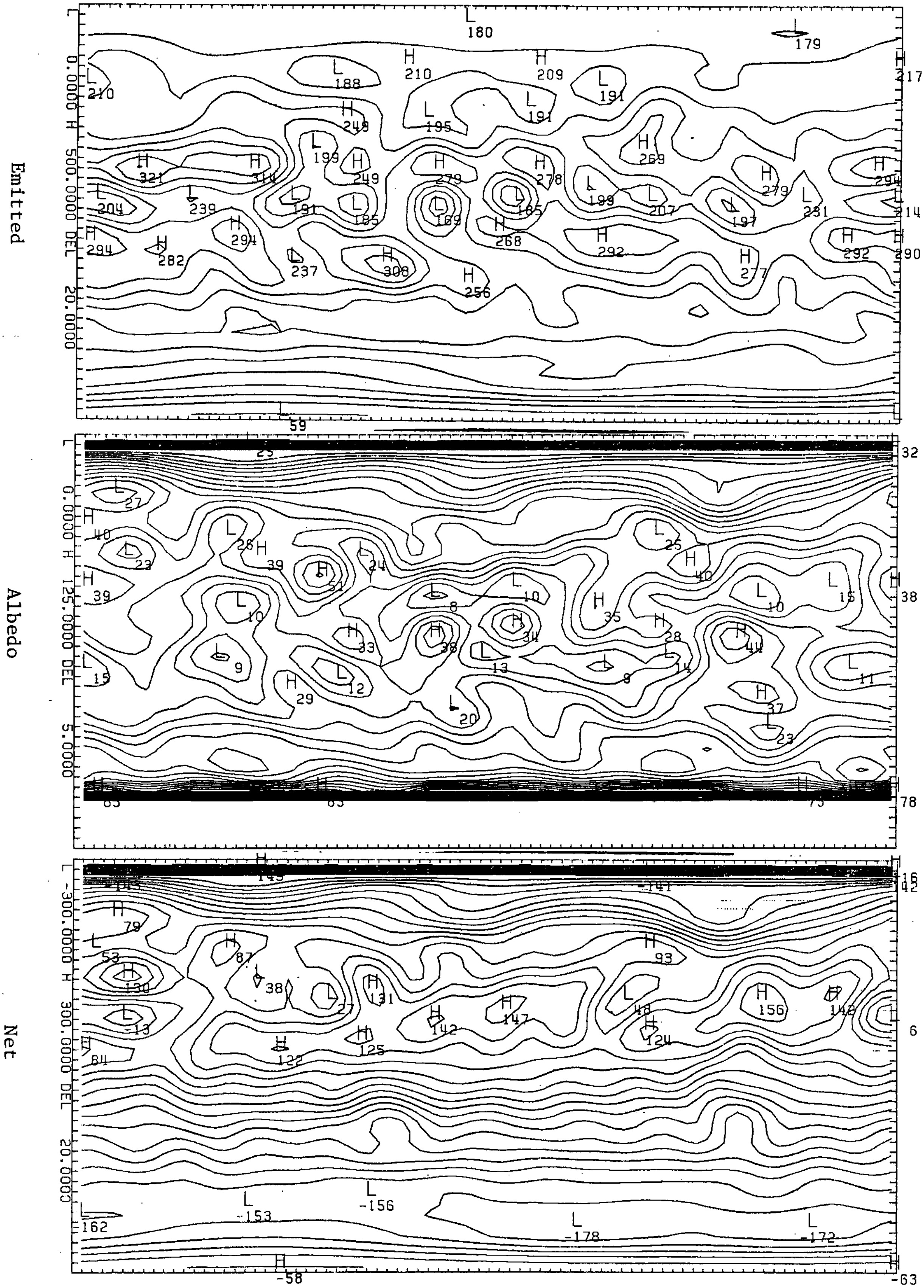
Emitted
0.0000 H 500.0000 DEL 20.0000
Albedo
0.0000 H 125.0000 DEL 5.0000
Net
-300.0000 H 300.0000 DEL 20.0000

5/ 76

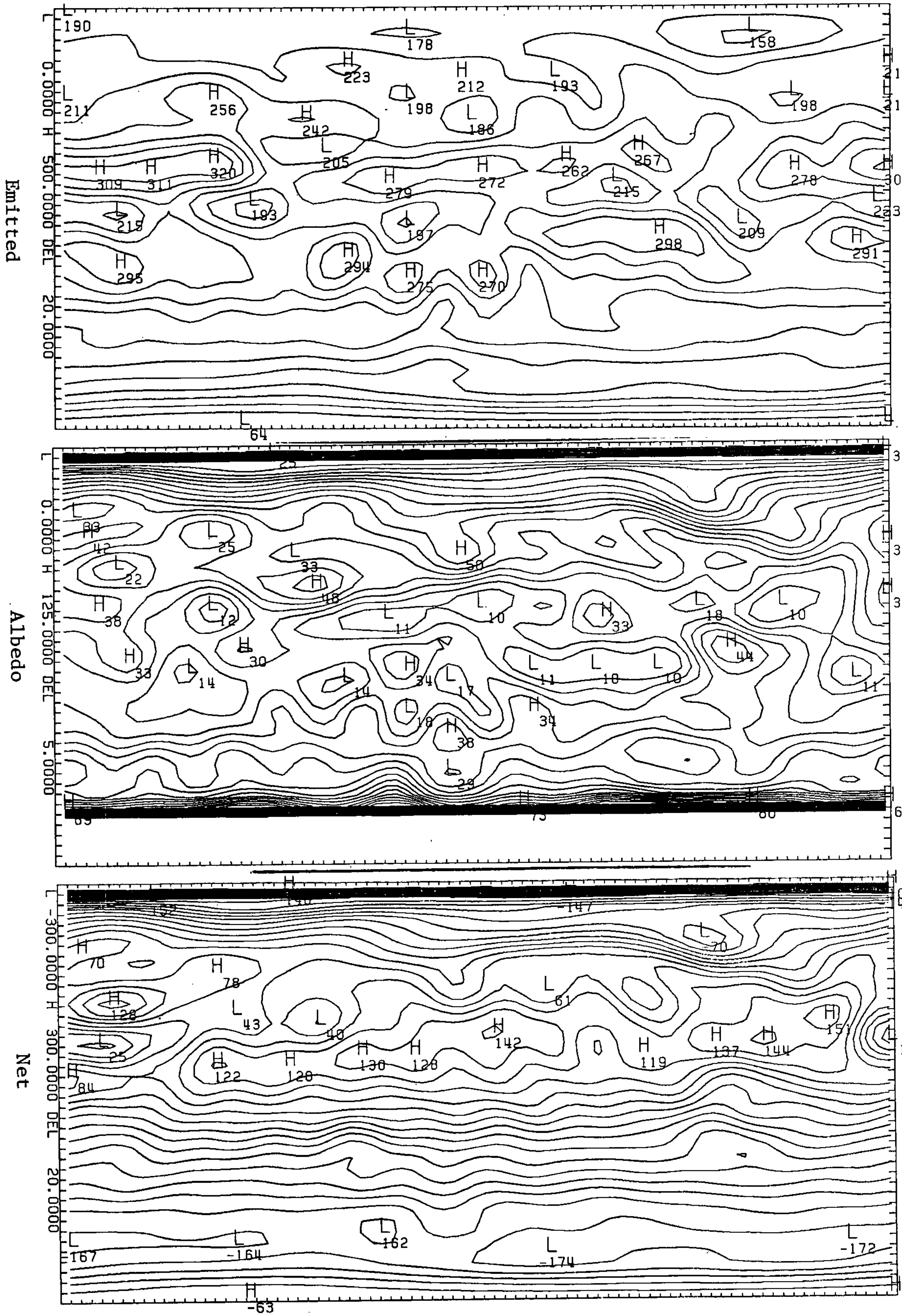
Emitted
0.0000 H 500.0000 DEL 20.0000
Albedo
0.0000 H 125.0000 DEL 5.0000
Net
-300.0000 H 300.0000 DEL 20.0000

5/ 77

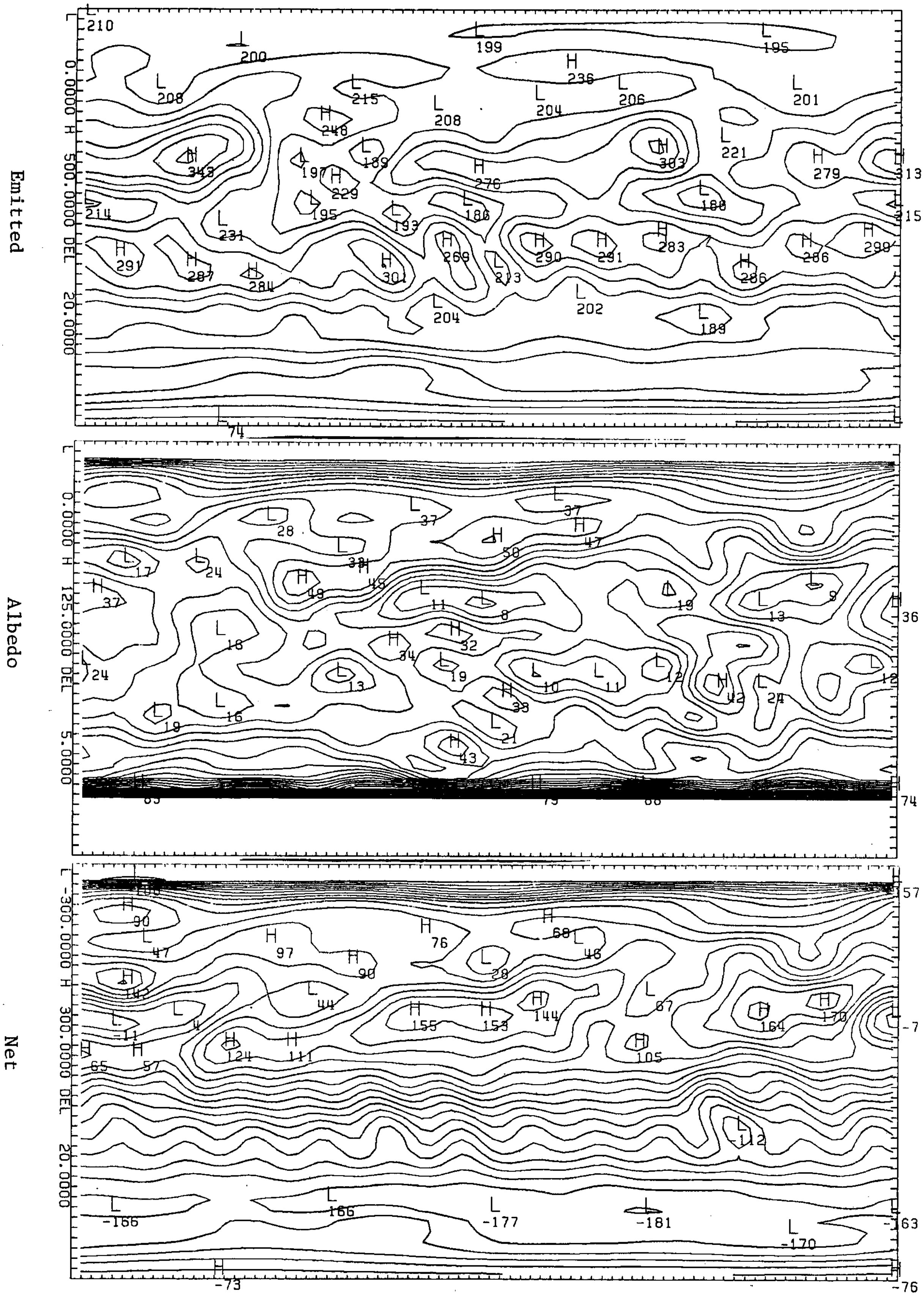
Emitted
0.0000 H 500.0000 DEL 20.0000
Albedo
0.0000 H 125.0000 DEL 5.0000
Net
-300.0000 H 300.0000 DEL 20.0000

6/ 76

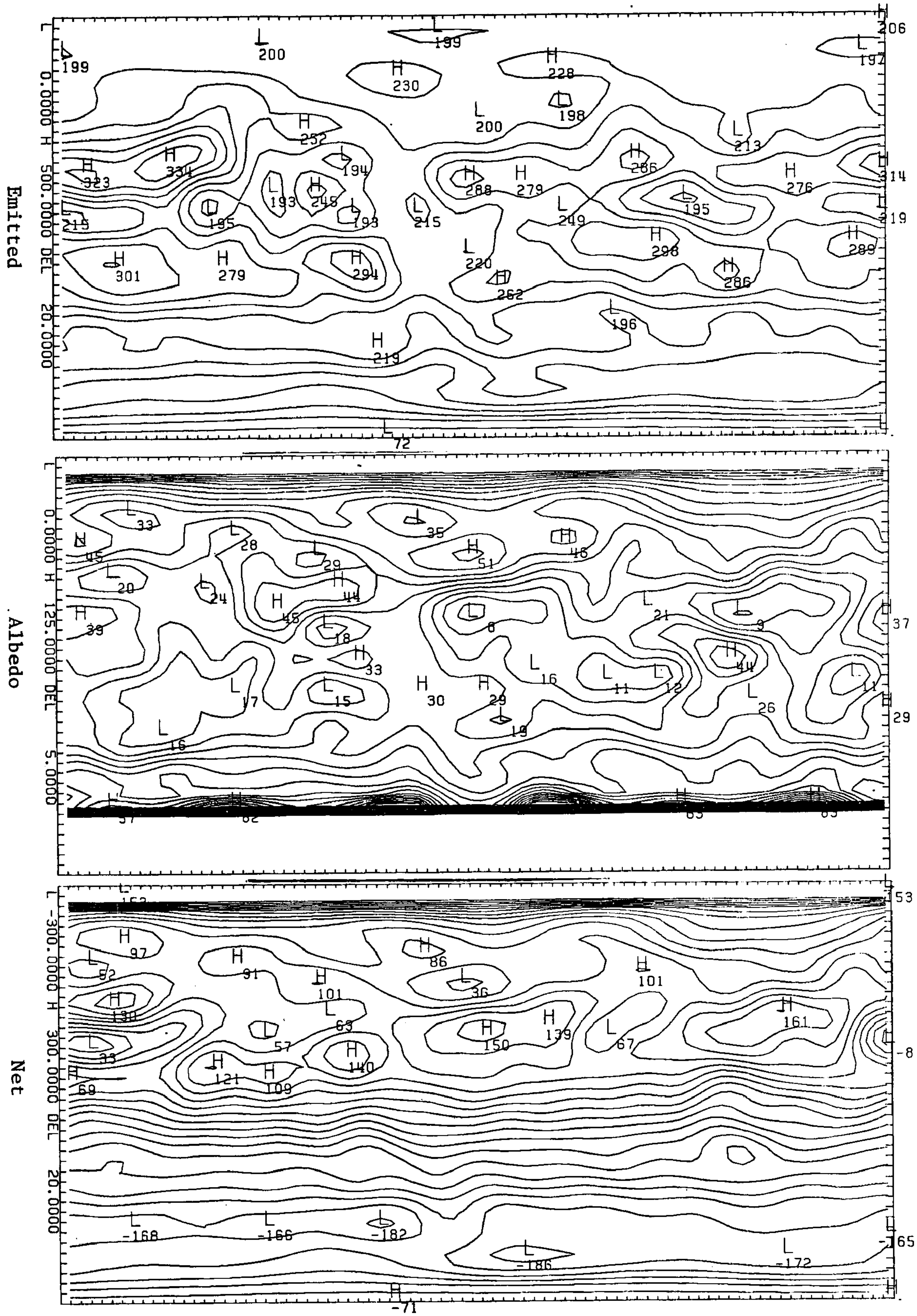
Emitted
0.0000 H 500.0000 DEL 20.0000
Albedo
0.0000 H 125.0000 DEL 5.0000
Net
-300.0000 H 300.0000 DEL 20.0000

6/ 77

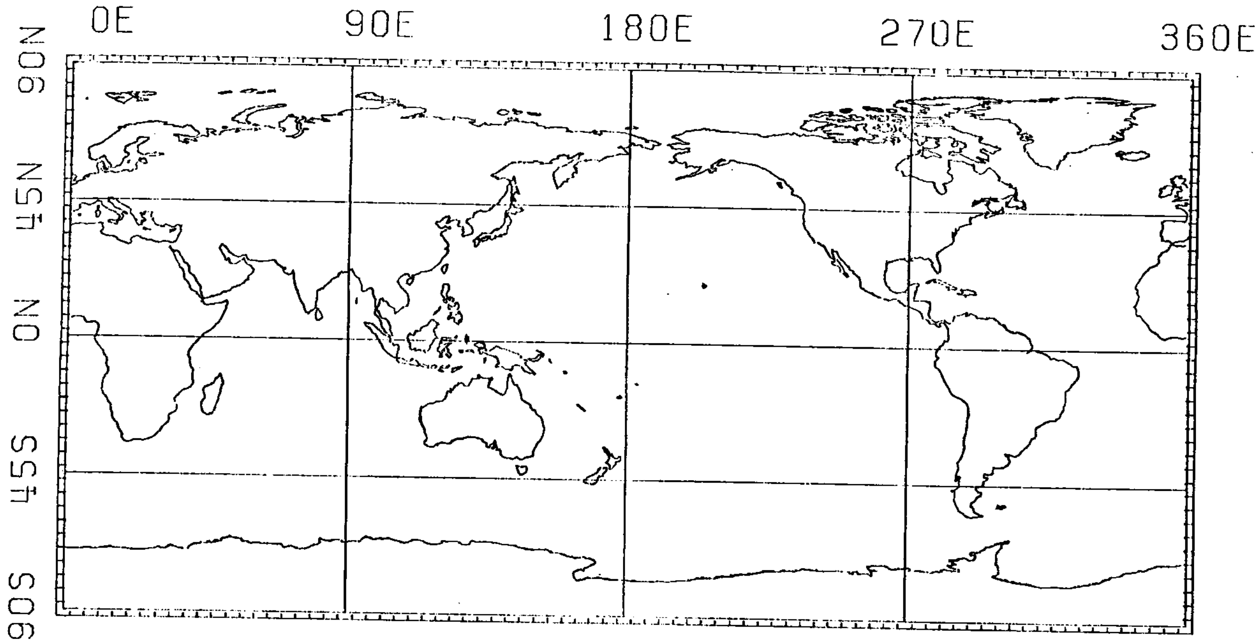
0E
90E
180E
270E
360E
90N
45N
0N
45S
90S

50272-101

REPORT DOCUMENTATION PAGE	1. REPORT NO.	2.	3. Recipient's Accession No.

4. Title and Subtitle

An Analysis of Two Years of Nimbus 6 Earth Radiation Budget Observations: July 1975 to June 1977

5. Report Date May, 1980

6.

7. Author(s)

G. G. Campbell and T. H. Vonder Haar

8. Performing Organization Rept. No. ATS Paper No. 320

9. Performing Organization Name and Address

Department of Atmospheric Science
Colorado State University
Fort Collins, CO 80523

10. Project/Task/Work Unit No.

11. Contract(C) or Grant(G) No.

(C) NAS5-22959

(G)

12. Sponsoring Organization Name and Address

National Aeronautics and Space Administration
600 Independence Ave., S.W.
Washington, D.C. 20233

13. Type of Report & Period Covered

14.

15. Supplementary Notes

16. Abstract (Limit: 200 words)

An independent analysis of Nimbus 6 Earth Radiation Budget measurements is presented for July 1975 to June 1977. Monthly mean maps of albedo, emitted exitance and net radiation were constructed from the individual satellite irradiance measurements from the wide field of view sensors. A recalibration was performed with reference to Nimbus 7 ERB, day-night comparisons, and removal of the trend in reflected data. Also, a resolution enhance scheme was used to improve the details in the maps, both on the emitted exitance and albedo estimates. The maps are then discussed in terms of zonal averages, land averages, ocean averages and variance emphasizing the year to year differences. For instance, substantial changes in emitted and albedo appear around the intertropical convergence zone for these two years. The largest variance in net radiation occurred along the north coast of the Pacific.

17. Document Analysis a. Descriptors

Earth Radiation Budget
Climate
Satellite Observations

b. Identifiers/Open-Ended Terms

c. COSATI Field/Group

18. Availability Statement:	19. Security Class (This Report)	21. No. of Pages
Unlimited release: Dept. of Atmos. Sci. Colorado State University Ft. Collins, CO 80523	Unclassified	86
	20. Security Class (This Page)	22. Price

(See ANSI-Z39.18) See Instructions on Reverse

OPTIONAL FORM 272 (4-77)
(Formerly NTIS-35)
Department of Commerce